



Georg Urstöger, Dipl.Ing.

Spectroscopic Investigations of Cellulosic Materials

Doctoral Thesis

to achieve the university degree of
Doktor der technischen Wissenschaften

submitted to

Graz University of Technology

Supervisor

Ao.Univ.-Prof. Mag. Dr.rer.nat. Robert Schennach

Institute of Bioproducts and Paper Technology

Co-supervisor: Univ.-Prof. Dipl.-Ing. Dr.techn. Ulrich Hirn

Graz, March 2020

Affidavit

I declare that I have authored this thesis independently, that I have not used other than the declared sources/resources, and that I have explicitly indicated all material which has been quoted either literally or by content from the sources used. The text document uploaded to TUGRAZonline is identical to the present thesis.

Date

Signature

Abstract

This doctoral thesis deals with the investigation of cellulosic materials with spectroscopic methods. Specifically I used Förster Resonance Energy Transfer (FRET) to investigate the interaction between cellulosic structures and Brillouin Microscopy to investigate the mechanical properties of cellulosic fibers.

The first part of this thesis is about the implementation and investigation of FRET spectroscopy and microscopy to apply this technique to cellulosic structures. Paper A therefore covers the systematic investigation of molecules regarding the feasibility to be used in a FRET experiment. The investigation showed which parameters need to be controlled and optimized to obtain a reliable measurement system. Paper B covers the investigation of the bonded region of paper fibers and model films using FRET microscopy. The research showed that using the developed technique it is not possible to investigate paper fibers. The most likely cause for the problems in the paper fibers is the used dyeing technique of the fibers. The dyeing procedure led to a bulk dyeing of the fibers which resulted in a poor signal to noise ratio. However we were also able to show that it is possible to investigate the interaction between model films using this technique.

The second part deals with Brillouin Spectroscopy and the application of this method to investigate cellulosic fibers. In the paper we were able to successfully quantify the storage and the loss modulus of viscose and bleached softwood Kraft pulp fibers and compare the results to similar measurements from different techniques. I believe that it will develop to be a viable method for future investigations of cellulosic materials.

Kurzfassung

Die vorliegende Doktorarbeit befasst sich mit der Untersuchung von Cellulosematerialien mittels spektroskopischen Methoden. Speziell wurde Förster Resonance Energy Transfer (FRET) verwendet, um die Wechselwirkung zwischen Cellulosestrukturen zu untersuchen, und Brillouin-Spektroskopie, um die mechanischen Eigenschaften von Cellulosefasern zu untersuchen.

Der erste Teil dieser Arbeit befasst sich mit der Implementierung und Untersuchung von FRET-Spektroskopie und -Mikroskopie, um diese Methode auf Cellulosestrukturen anzuwenden. Artikel A befasst sich daher mit der systematischen Untersuchung von Molekülen hinsichtlich der Verwendbarkeit in einem FRET-Experiment. Die Untersuchung ergab, welche Parameter gesteuert und optimiert werden müssen, um ein zuverlässiges Messsystem zu erhalten. Artikel B befasst sich mit der Untersuchung des gebundenen Bereichs von Papierfasern und Modellfilmen mittels FRET-Mikroskopie. Die Forschung hat gezeigt, dass es mit der entwickelten Technik nicht möglich ist, Papierfasern zu untersuchen. Die wahrscheinlichste Ursache für die Probleme bei den Papierfasern ist die verwendete Färbetechnik. Die Färbetechnik resultierte in einer durchgehenden Färbung der Fasern, was zu einem schlechten Signal-Rausch-Verhältnis führte. Jedoch konnte gezeigt werden, dass es möglich ist, die Wechselwirkung zwischen Modellfilmen mit dieser Technik zu untersuchen.

Der zweite Teil befasst sich mit Brillouin-Spektroskopie und der Anwendung dieser Methode zur Untersuchung von Cellulosefasern. In der Arbeit (Artikel C) konnten wir das Speicher- und das Verlustmodul von Viskose- und gebleichten Weichholz-Kraft-Zellstofffasern erfolgreich quantifizieren und die Ergebnisse mit Messungen aus verschiedenen aber ähnlichen Techniken vergleichen. Ich glaube daher, dass sich Brillouin Spektroskopie zu einer praktikablen Methode für zukünftige Untersuchungen von Cellulosematerialien entwickeln wird.

Acknowledgements

I would like to start by expressing my gratitude to my team of supervisors, namely Prof. Robert Schennach and Prof. Ulrich Hirn who have supported me throughout this dissertation. Not only did they consistently have open doors for professional issues but have also always had an open ear for personal questions which often triggered delightful and interesting conversations. I am very grateful for their guidance which helped me improve myself in many aspects of my life.

I would also like to thank the industrial partners for their support, none more so than Louis Saes, Gerhard Drexler and Ern Clevers who I had the opportunity to work with and had many interesting discussions with. A great thank you is due to my coauthors on the various publications, especially to Artem Kulachenko whose devotion to our joint paper at times felt as having a third supervisor.

I would like to thank the administrative team of the institute, namely Harald Streicher, Adelheid Bakhshi and Claudia Bäuml. Any questions about administrative task, experiments or IT issues that I had were always handled very professionally and with great speed. To the entire lab staff – thank you for your help and support with my experimental work.

I would like to thank the old PhD gang, Marina Jajcinovic, Wolfgang Fuchs, Lukas Jagiello, Rafael Giner Tovar and Jussi Lahti for a great time. Since most of them are already gone from the University I can honestly say that I miss the philosophical conversations we had during our coffee breaks. I really enjoyed every minute of it.

Additionally I would like to thank the Master students, Felix Hajek and Miltscho Andreev, and all the Bachelor Students that I supervised for their excellent work as well as all the people in the APV social room for the much needed and welcomed distractions during the coffee breaks.

The acknowledgments would not be complete without the mentioning of the IPZ gaming league. A group of fierce young students that do not shy away from competition nor do they take defeat lightly. The Friday afternoon sessions have been and will remain unforgettable.

I also want to thank my parents for their support during my studies- it enabled me to finish my studies successfully while still having a great time while studying.

Finally, I want to thank my girlfriend Marlene. There are no words to describe how thankful I am for your presence but I will still make a try. My life as it is right now would not be possible without you nor would I have a fraction of the joy that I am having now. You support me in every aspect of it and your presence simply makes me a better person.

Contents

Abstract	iii
Kurzfassung	iv
Acknowledgements	v
1. Part I: Förster Resonance Energy Transfer	1
1.1. Introduction	1
1.1.1. Förster Resonance Energy Transfer	2
1.2. Experimental	9
1.2.1. Materials	9
1.2.2. Ultraviolet–visible spectroscopy (UV-Vis)	10
1.2.3. Spectrofluorometry	11
1.2.4. Fluorescence Microscopy	13
1.2.5. How to calculate FRET - Inevitable Mathematics and Experimental Considerations	20
1.2.6. How to calculate FRET using a Microscope	24
1.2.7. Image Analysis Matlab Code	29
Bibliography	30
2. Paper A	33
3. Paper B	47
4. Part II: Brillouin Spectroscopy	62
4.1. Introduction	62
4.2. Brillouin Spectroscopy	63
4.2.1. Phonons	63
4.2.2. Material Constants of Fibers	66

Contents

4.2.3.	Measuring the speed of sound	68
4.2.4.	Brillouin Light Scattering Experiment	70
Bibliography		73
5. Paper C		74
A. Matlab Code for Image Analysis		88
A.1.	Script for Figure Import	88
A.2.	Function drawroi	89
A.3.	Function drawpolygons	90
A.4.	FRET Evaluation Script	92

List of Figures

1.1.	Jablonski diagram of fluorescence and FRET. A photon excites the donor molecule that has, in the proximity of an acceptor molecule, the possibility to transfer its energy by the FRET process. A requirement is that the acceptor has an appropriate electronic structure. The image was adapted from (Alex M Mooney - Own work, CC BY-SA 3.0, https://commons.wikimedia.org/w/index.php?curid=23197114).	3
1.2.	Efficiency of the energy transfer over the distance between the two molecules. The sensitivity of the transfer is limited to $1/2 R_0$ to $2 R_0$. When the Förster radius changes ($R_0 \rightarrow R_0^*$) due to e.g. changing environmental conditions the whole distance dependence changes of course as well.	5
1.3.	Schematic of the fluorescence spectra of the donor and acceptor dye. Also the effect of FRET and the necessary spectral overlap between the donor emission spectrum and the acceptor excitation spectrum is indicated. The images was adapted from Paper A.	7
1.4.	Molecules used for the FRET experiments.	10
1.5.	Schematic of the UV Vis spectroscopy (blue) and the fluorescence spectroscopy (red) setup.	11
1.6.	Typical measurement from a UV-Vis. a) Rawdata of the two molecules and the reference. b) calculated absorbance according to Eq. 1.4	12
1.7.	Fluorescence excitation and emission spectra of DCCH and FTSC a) covalently bonded to cellulose fibers and b) embedded in a pHema matrix.	13

List of Figures

1.8.	Filtersets used in the widefield microscopy in this thesis. The filters are labelled as Donor, Acceptor or FRET corresponding to what the filters should primarily measure. The fluorescence spectra in the background are the spectra of our dyes on fibers at pH 9.	15
1.9.	Spectra of the tungsten halogen lamp used in this thesis. The correction factors are calculated by integrating over the shaded areas that correspond to the excitation filters for the donor and acceptor.	16
1.10.	Quantum efficiency of the CMOS detector. Also the fluorescence emission spectra and the emission filters are shown. . .	18
1.11.	Schematic of a confocal laser scanning microscope. Reprinted with the permission of Carl Zeiss Microscopy GmbH, Jena . .	19
1.12.	FLIM measurement of DCCH and FTSC. From the semilogarithmic plot in b) one can clearly see that FTSC can be explained by a monoexponential decay while the DCCH needs a multiexponential approach.	21
1.13.	Schematic of the effect FRET has on the fluorescence emission spectra of a compatible FRET pair. a) shows the theoretical considerations such as the overlap integral J and the intensities without and with FRET. (same as Figure 1.3) b) is an actual measurement from this thesis.	22
1.14.	1) First fluorescence images using specific filter sets need to be aquired. In a second step 2) a region of interest (ROI) is drawn in the area where the both dyes can logically exhibit FRET. 3) The images of step 1) are used in an algorithm to calculate the FRET efficiency.	25
1.15.	Schematic on how the variables in the Gordon algorithms are aquired from the fluorescence microscopy images.	27
4.1.	One-dimensional monoatomic chain. The atoms with mass m are connected by springs with a spring constant κ . The distance between the atoms at rest is a	64
4.2.	Phonon dispersion relation for a monoatomic linear chain connected by springs. At low k (high wavelength limit) it can be seen that the dispersion is linear.	65

List of Figures

- 4.3. Schematic of the inelastic scattering process of light with the phonons of a thin film. 69
- 4.4. Schematic of a possible Brillouin Spectroscopy measurement (generic). The large center peak is also known as Rayleigh peak and stems from the elastic scattering of the incident light. As can be seen the measurements are symmetric around this center because the incident light can excite phonons and thereby lose some energy (Stokes branch) or the light can gain energy from the phonons (Anti-Stokes branch). Also it can be seen that due to the strong Rayleigh peak the measurement needs to be unmixed which is in spectroscopy usually done by Lorentzian distributions. The Brillouin peaks labelled as TA and LA correspond to the transverse acoustic and the longitudinal acoustic mode of the excitation. 71

1. Part I: Förster Resonance Energy Transfer as a tool to investigate the interaction between cellulosic surfaces

1.1. Introduction

In the 21st century this world, our collective civilisation, continues its laborious road to evolve into a society that will hopefully eventually be capable of populating this planet without depleting its resources. A critical aspect of this voyage is, in my opinion, the increased usage of biological materials that can be easily and ecologically recycled. One aspect of this is the strongly growing field of biopolymers and the usage of cellulosic products from plants to produce and build many of the products that we use in our daily lives. Another side is the search to create more efficient processes that decrease the amount of used materials or improve the energy consumption of the methods. This thesis is my humble contribution of humankind's goal to improve itself.

The production process of paper has been continuously improved for more than a century. Many consider that the scientific approach to study the properties of paper as a material was started by Derek Page in the 1960s. (D. H. Page & Tydeman, 1962; D. Page, 1969) However, in recent years the community investigating mechanical properties or fundamental properties of paper has decreased. With modern methods it is likely that we can improve our understanding of the basic principles responsible for many paper properties and subsequently tailor the production, saving a vast

1. Part I: Förster Resonance Energy Transfer

amount of resources in the process. Here, we make an attempt to improve the fundamental understanding of the interaction between cellulosic materials by Förster Resonance Energy Transfer (FRET).

Fluorescence Resonance Energy Transfer (sometimes also Förster Resonance Energy Transfer) or short FRET has been described by Theodor Förster in the 1940s. (Förster, 1948; Förster, 1949) The process involves two molecules, labelled donor and acceptor, being in close proximity. When the donor enters an excited state and other conditions, which will be discussed later, are fulfilled it can transfer its energy to the acceptor molecule. Measuring this interaction was the first part of this thesis with the ultimate goal to investigate the area of molecular contact between two cellulose fibers labelled separately with donor and acceptor molecules.

1.1.1. Förster Resonance Energy Transfer

In this section we will discuss the theory behind FRET and the practical approaches that are undertaken to measure this effect. After reading this section a reader will understand the theory behind the effect and the necessary conditions to measure it as I believe that a good understanding of the theory is needed to accurately interpret measured data.

Theory

As it was initially derived by Theodor Förster, FRET can be summed up by three major equations which will be shown a little later. The full derivatization can be found in chapter 3 of the book FRET - Förster Resonance Energy Transfer by Medintz and Hildebrandt. Here I will briefly explain the effect, the main equations and the important experimental parameters. The idea and much of the theory in the following section stems from the chapter of the aforementioned book. (Meer, 2013)

The FRET theory was developed with the idea that the interacting molecules, labelled donor and acceptor, can be thought of as free oscillating dipoles. In a nutshell the process works as depicted in Figure 1.1. An incoming photon (Fig.1.1 blue arrows) is absorbed by the donor molecule which is excited to

1. Part I: Förster Resonance Energy Transfer

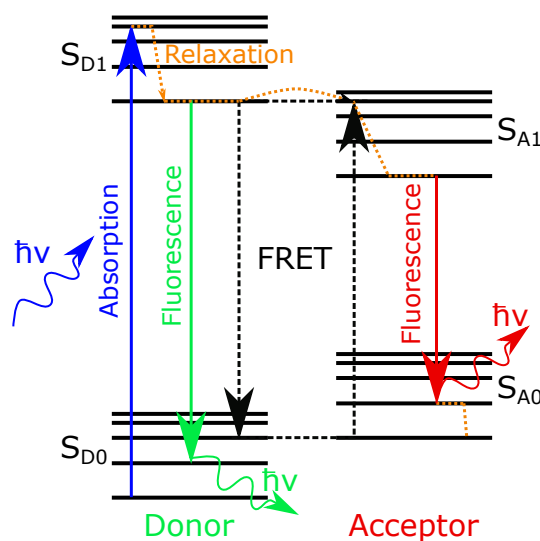


Figure 1.1.: Jablonski diagram of fluorescence and FRET. A photon excites the donor molecule that has, in the proximity of an acceptor molecule, the possibility to transfer its energy by the FRET process. A requirement is that the acceptor has an appropriate electronic structure. The image was adapted from (Alex M Mooney - Own work, CC BY-SA 3.0, <https://commons.wikimedia.org/w/index.php?curid=23197114>).

a higher energy level and exhibits an oscillating dipole. Subsequently, the donor in the excited state can get rid of some of its energy by relaxation processes. From the lowest excited state the donor can relax to its ground state by the emission of characteristic, fluorescent radiation (Fig. 1.1 green pathway). However, in the proximity of an acceptor molecule that has a compatible electronic structure the donor can transfer its energy, radiationless, via a dipole-dipole interaction to the acceptor. These two processes occur with a certain likelihood which depends primarily (among other quantities such as fluorescent lifetime or relative orientation of the dipoles) on the physical distance between the donor and the acceptor. If the acceptor is a fluorescent molecule it will eventually relax from its excited state to the ground state under the emission of a photon, corresponding to the acceptor's fluorescence emission spectrum (Fig. 1.1 red curve).

For FRET to be a possible transfer mechanism, the donor and the acceptor molecule need to have a compatible electronic structure as it is seen in

1. Part I: Förster Resonance Energy Transfer

Figure 1.1. There one can see that for FRET to occur some energy band of the acceptor must lie within the energy range of the donor band. For fluorescent molecules this can be guaranteed if the donor emission spectrum and the acceptor attenuation spectrum have an overlapping region. The efficiency of this energy transfer process can be written as

$$\eta_{FRET} = \frac{1}{1 + (r/R_0)^6} \quad (1.1)$$

where η is the transfer efficiency, R_0 is the Förster radius and r is the actual distance between the interacting molecules. With this equation it becomes clear why FRET can be used to measure the distances between molecules. The Förster radius is a constant property for two interacting molecules in a controlled environment. It is by definition the distance between the two molecules at which the efficiency of the energy transfer is 50 % as can be seen in Figure 1.2. In this figure one can also see that the sensitivity in which the distance between the two molecules can be determined is limited from $1/2 R_0$ to $2 R_0$. Below $1/2 R_0$ and above $2 R_0$ it is usually not possible to detect differences in the signal. This means that for quantitative analysis one needs to choose donor and acceptor such that their Förster radius falls within the desired range of sensitivity. However, if for the specific research question it is enough to get a binary signal of 1 meaning the molecules are interacting and 0 the molecules are not interacting, the specific range of the molecules might not be that crucial. In other words, if the qualitative information of exhibiting FRET or no FRET is sufficient for the experiment it is less important to choose the correct range.

The interaction of the donor and the acceptor molecule are described by a dipole dipole interaction. For the interaction to be modeled by this the ideal dipole approximation needs to hold. This approximation means that the distance between the dipoles is significantly larger than the size of the dipoles themselves. When the molecules come very close to each other this approximation breaks down and therefore the interaction cannot be described by a Förster behavior ($1/r^6$ behavior) anymore. In this close range, complex formation (Dexter transfer) or collision quenching can occur. In the long range limit the efficiency of the Förster Resonance is too low and it

1. Part I: Förster Resonance Energy Transfer

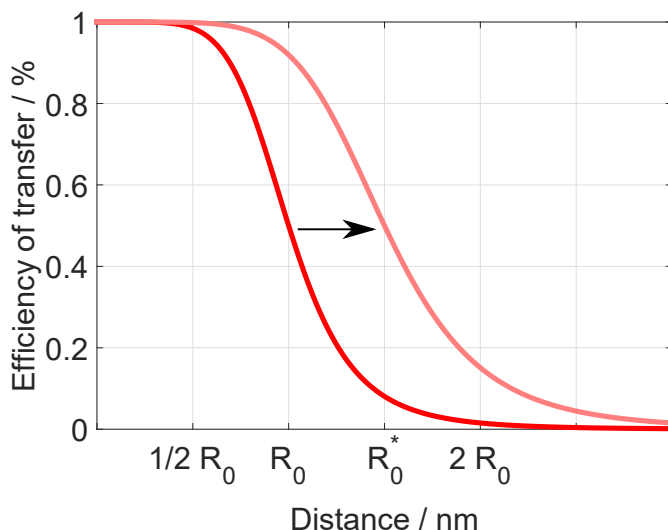


Figure 1.2.: Efficiency of the energy transfer over the distance between the two molecules. The sensitivity of the transfer is limited to $1/2 R_0$ to $2 R_0$. When the Förster radius changes ($R_0 \rightarrow R_0^*$) due to e.g. changing environmental conditions the whole distance dependence changes of course as well.

is more likely that simple emission and reabsorption of a photon emitted from the donor occurs. (Meer, 2013)

If the environment changes and this leads to a change in the spectroscopic properties of the molecules it will also lead to a different Förster radius as it is depicted in Figure 1.2. The change from $R_0 \rightarrow R_0^*$ leads to a shifted distance dependence of the system and if one is aiming for a quantitative analysis method this change can lead to a systematic error in the measurements. Therefore, this change needs to be taken into account for quantitative measurements. The Förster radius can be calculated by the following equation

$$R_0 = \left(\frac{9(\ln(10)) k^2 \Phi_D J}{128\pi^5 N_A n^4} \right)^{1/6} \quad (1.2)$$

where N_A is Avogadro's constant, k is an orientation factor describing the relative orientation of the dipoles, Φ_D is the quantum yield of the donor, n

1. Part I: Förster Resonance Energy Transfer

is the refractive index of the solvent (or investigated medium) and J is the overlap integral. The orientation factor k can be a quite important quantity but it has one major drawback. In the majority of cases it is not possible to measure it. In principle it can range from 0 to 4 but if the molecules can freely rotate and statistically assume every possible relative orientation in a sufficiently small time scale the average of the factor is $2/3$. (Meer et al., 2013) The overlap integral J is calculated according to Eq. 1.3

$$J = \int I_D(\lambda)\epsilon_A(\lambda)\lambda^4 d\lambda \quad (1.3)$$

Where I_D is the emission spectrum of the donor normalized to unity, ϵ_A is the molar attenuation coefficient of the acceptor and λ is the wavelength. The overlap integral and the effect FRET has on the fluorescence spectra can be seen in Figure 1.3. The intensity of the donor emission spectrum decreases ($I_D \rightarrow I_{DA}$) due to FRET because the donor gives some of its energy to the acceptor who gets excited. Due to this the acceptor emission intensity increases compared to the excitation of the pure acceptor ($I_A \rightarrow I_{AD}$).

Experimental Praxis and Choice of Molecules

In this section the practical approaches to measure FRET will be discussed. To establish a FRET system one needs to consider many experimental variables. First and foremost it should be mentioned that one needs to choose a pair of molecules that are well suited specifically for the underlying problem. This choice is quite important and might be the most important choice to make. Other experimental questions are: Which microscope do I use? what are the correct filter sets? How do I compute FRET from the data? All these questions will be answered in the next sections.

First lets discuss the choice of molecules. There are many aspects that need to be considered before deciding on a FRET pair however not all of them are of equal importance. The hard requirements of the molecules are as follows

- They need to be spectroscopically compatible, meaning that it must be theoretically possible for them to exhibit Förster transfer. This can be

1. Part I: Förster Resonance Energy Transfer

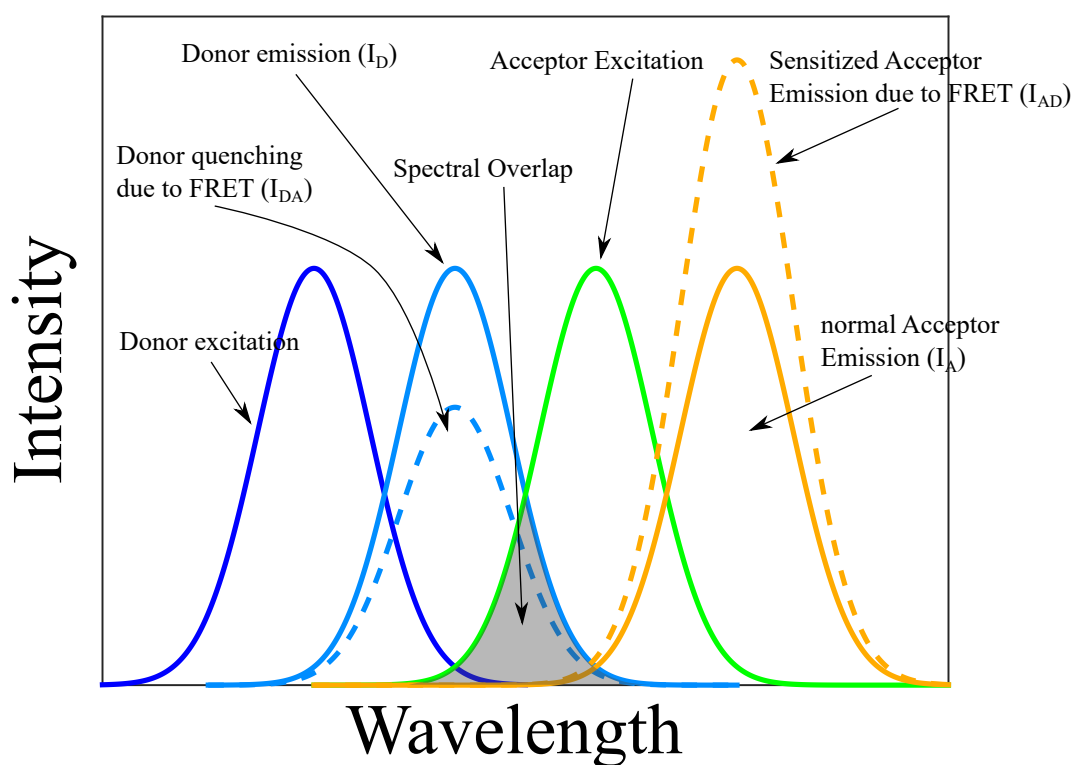


Figure 1.3.: Schematic of the fluorescence spectra of the donor and acceptor dye. Also the effect of FRET and the necessary spectra overlap between the donor emission spectrum and the acceptor excitation spectrum is indicated. The images was adapted from Paper A.

achieved by choosing a pair of molecules that show an overlap of the donor emission spectrum and the acceptor extinction coefficient such as in figure 1.3. The combination of these two properties is one part of the Förster radius (see equation 1.2)

- Another requirement (for many cases) is that they need to be able to react chemically in such a way that the resulting product is covalently linked to a desired structure. This covalent link guarantees that diffusion of the molecules can be neglected.

Second there are some more soft requirements that are not strictly necessary for FRET however they make ones life easier when performing the measurements.

1. Part I: Förster Resonance Energy Transfer

- The quantum yield (QY) of both, donor and acceptor, should be as high as possible. A high quantum yield of the donor is important as it is directly connected to the Förster radius and, therefore, has an influence on the sensitivity of the FRET pair. Additionally a high QY of the donor ensures that overall intensity of the signals are higher. This usually leads to better statistics and simpler image processing. For the same reason a high quantum yield of the acceptor is preferable as it makes it easier to detect the FRET signal.
- Although only the attenuation coefficient of the acceptor molecule is a relevant variable in the calculation of the Förster radius (equation 1.2) also the equivalent of the donor is relevant for the Förster signal as it will increase the brightness of the donor molecule (together with the QY).
- The chosen dyes should be stable under changing environments. This means that the spectroscopic properties of the molecules should not change too much when conditions such as pH of the investigated system or the used solvent changes. At the very least the change of the spectroscopic properties should be investigated if the environmental conditions are expected to change.

For measuring FRET one needs a setup to probe the spectroscopical properties of the investigated system. This can be achieved by using a spectrofluorometer or also in some cases by using a light microscope with appropriate filter sets, detector and light source. If it is accessible it is highly recommended to investigate the system with a second FRET method, ideally measuring a different aspect of the effect, as this can make a stronger case for the investigation.

If one wants to use FRET as a quantitative tool to determine the distance between the interacting molecules the Förster Radius of the pair needs to be determined according to Equation 1.2. This can be done in the following way. (Hildebrandt, 2013)

1. Measure the molar attenuation coefficient of the acceptor molecule. This is usually done by using a UV Vis spectrophotometer by recording a reference and a sample and subsequently calculating the attenuation coefficient by knowing the concentration and the path length. Care has to be taken that the inner filter effect does not decrease the intensity

1. Part I: Förster Resonance Energy Transfer

of the analyzed signal which leads to an error in the measurements. Deviations from the linear Beer-Lambert law can occur at quite low optical densities (OD) and therefore it is recommended to measure the coefficient with a peak ODs < 0.2 . This number is just a rough anchor and in reality one should perform a concentration series to see the development of the attenuation coefficient over concentration.

2. Measure the full fluorescence emission spectrum of the donor molecule. Although the spectrum is not as sensitive to the concentration as the attenuation coefficient also here one should take care not to use too high concentrations so the inner filter effect can be avoided. For the calculation the spectrum needs to be normalized by its area.
3. Measure the quantum yield (QY) of the donor. As described in Paper A this can be done by methods such as the relative method by relating the QY of the investigated molecule to a known QY of a reference molecule. Another possibility exists by measuring the QY with an absolute method. (Würth et al., 2013)
4. The resulting data is used in Eq. 1.2 and 1.3 to calculate the Förster radius.

1.2. Experimental

Additionally to the explanation of the experimental practices found in the published papers the utilized techniques will be explained in detail in the next few sections. Special focus will be given to the computational evaluation of the acquired fluorescence microscope images in order to obtain a fully corrected FRET signal.

1.2.1. Materials

The dyes used for the labelling and measurement of FRET were 7-(diethylamino)coumarin-3-carbohydrazide (DCCH) and Fluorescein-5-thiosemicarbazide (FTSC). The structure can be seen in Figure 1.4. Under the right environmental conditions the DCCH was employed as the donor and the FTSC as the acceptor. The reactive hydrazide and semicarbazide groups

1. Part I: Förster Resonance Energy Transfer

were used to attach the molecules to cellulosic structures. The labelling process can be found in Paper B.

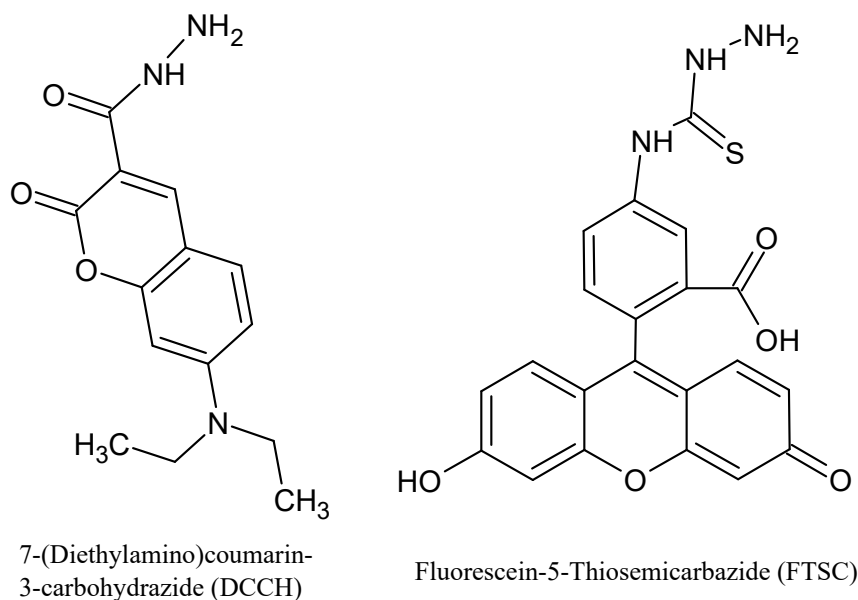


Figure 1.4.: Molecules used for the FRET experiments.

1.2.2. Ultraviolet–visible spectroscopy (UV-Vis)

This method is used to measure the molar attenuation coefficient of the dye molecules. The basic working principle can schematically be seen in Figure 1.5. Monochromatic light is directed through a cuvette holding the dye molecule (usually in solution) and the intensity of the light after the cuvette is detected. This is done for a reference (I_R) and the sample (I_S) and the two resulting spectra are recorded. In a next step Beer Lamberts law can be used to calculate the attenuation coefficient.

$$A = -\log\left(\frac{I_S}{I_R}\right) = \epsilon \cdot c \cdot l \quad (1.4)$$

With ϵ the molar attenuation coefficient, c the concentration of the molecules in the sample, l the length of the light path through the sample and A the

1. Part I: Förster Resonance Energy Transfer

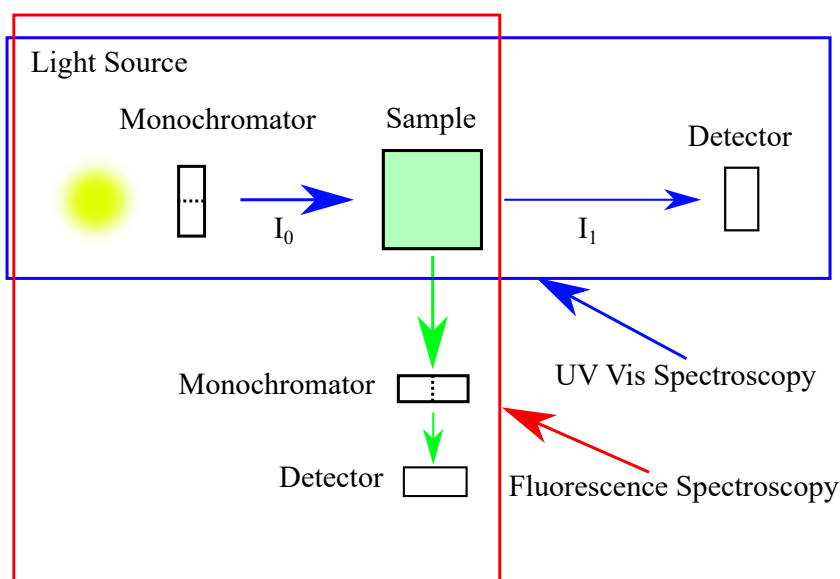


Figure 1.5.: Schematic of the UV Vis spectroscopy (blue) and the fluorescence spectroscopy (red) setup.

absorbance. Although knowing that the absorbance is a dimensionless quantity the unit optical density (OD) was established. Regarding these measurements it is important to mention that due to scattering and the inner filter effect deviations from the linear behavior of the absorbance can occur. This error can occur already at very low concentrations so it is therefore important to take it into consideration if one wants to accurately determine the molar attenuation coefficient. A quick concentration series can shine light on the magnitude of error for a molecule. The standard cuvette for UV-Vis has the dimensions of 1 x 1 cm but if one needs to go to a higher concentration special cuvettes are available (e.g. 1 x 0.1 cm). As an anchor the attenuation coefficient should be calculated from measurements with peak absorbances smaller than 0.2 OD ($A_{peak} < 0.2 \text{ OD}$).

1.2.3. Spectrofluorometry

Fluorometry is a similar technique to UV-Vis but measures light at an angle from the incident beam as seen in Figure 1.5. This makes it possible to not

1. Part I: Förster Resonance Energy Transfer

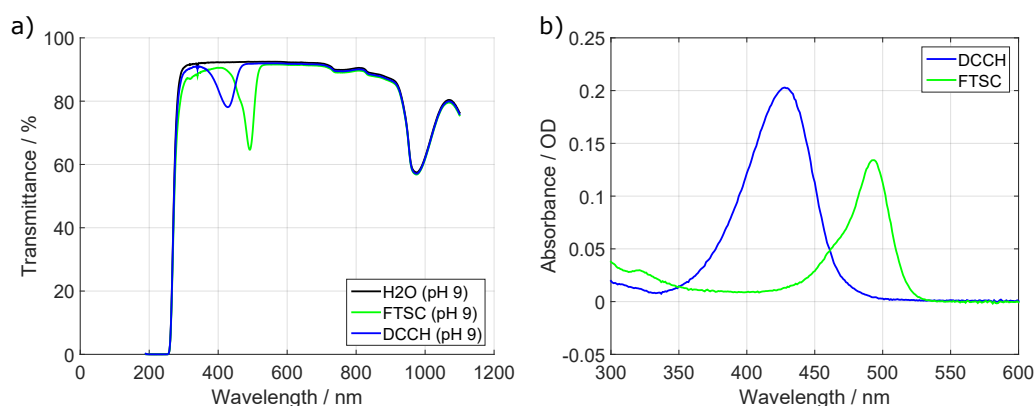


Figure 1.6.: Typical measurement from a UV-Vis. a) Rawdata of the two molecules and the reference. b) calculated absorbance according to Eq. 1.4

detect the incident light but only the light coming from the sample, which is the samples fluorescence. Also in this case the concentration in combination with the molar attenuation coefficient can play a big role as the inner filter effect can decrease the measured intensity significantly and in certain cases even not uniformly throughout the spectrum. In the standard setup the angle between the incident light and the detector is 90° . Some devices can measure at other angles (e.g. 15°) which can be useful for investigations of thin films or highly concentrated samples. A standard work on fluorescence about the theory as well as experimental considerations was written by (Lakowicz, 2006).

As can be seen in Figure 1.7 the emission and excitation spectra of the two dyes overlap to a certain extent. More specifically it is quite visible that the donor emission spectrum overlaps with the acceptor emission spectrum, in technical terms the donor emission bleeds into the acceptor emission and hence the term spectral bleedthrough (BT) was coined. This BT is the reason why the fluorescence emission spectra need to be unmixed in the case of measuring FRET in a spectrofluorometer and why intricate correction algorithms need to be applied in the case of fluorescence microscopy.

1. Part I: Förster Resonance Energy Transfer

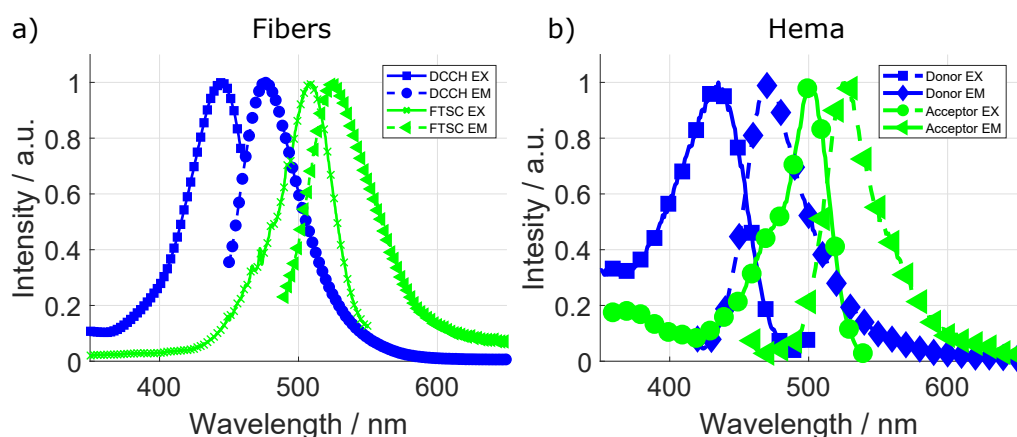


Figure 1.7.: Fluorescence excitation and emission spectra of DCCH and FTSC a) covalently bonded to cellulose fibers and b) embedded in a pHema matrix.

1.2.4. Fluorescence Microscopy

The methods described here to measure FRET are based on different aspects and implementations of fluorescence microscopy. Simple put the following principles are techniques to measure the fluorescence of a sample in a microscope. A light source is used to excite the fluorescent molecules in the sample. The re-emitted light is subsequently detected and analyzed. Often this is useful as it can provide spacial information additionally to the fluorescent information. However, due to the usage of filter sets the spectral information is usually reduced to a measured intensity over the whole filter. Especially when measuring FRET this can be a disadvantage as the spectral information is very valuable. In the following sections we will discuss some of the practical setups that are commonly used to determine FRET. The standard work of Lakowicz can provide further details and concepts that go beyond the scope of this thesis. And the following sections were therefore also developed with this book. (Lakowicz, 2006)

Widefield Microscopy

Fluorescent widefield microscopy is easy to implement since most laboratories have a microscope that can be equipped with fluorescent filter cubes.

1. Part I: Förster Resonance Energy Transfer

These filter cubes consist of one excitation filter, a dichroic mirror and an emission filter. The filter sets used in this thesis and how they correspond to the spectra of the employed dyes can be seen in Figure 1.8. The light from the lamp is first filtered to only select the light which corresponds to the excitation of the molecule while simultaneously minimizing the excitation of the other dye molecule. In the next step the filtered excitation light is directed to the sample using a dichroic mirror. The light hits the sample and results in characteristic fluorescence which can pass the dichroic mirror as it is of a higher wavelength. Subsequently a second filter is used to filter only part of the fluorescence signal that passes through the dichroic mirror. This filter is again optimized regarding signal intensity while keeping the spectral bleedthrough at a minimum.

When this method is used for quantitative analysis a few extra considerations regarding the lighting source and the detector need to be taken into account. On the one hand they concern the maximization of the detected light as in fluorescence microscopy the intensity is often low. On the other hand it is important to note that the relative differences in images collected using different filter sets can lead to a flawed image as will be shown in the next paragraph.

Now let's look at the choice of light source. Typical lighting sources employed in microscopy are tungsten halogen lamps, metal halide lamps, xenon or mercury arc lamps, LEDs or Lasers. LEDs and Lasers have the advantage of providing a high intensity but have the disadvantage of being expensive and not versatile as they emit light in a narrow range. Xenon lamps usually have lower illumination intensities than LEDs and Lasers however they provide a full spectrum. Over a wide range these spectra have a constant intensity output. Tungsten Halogen lamps have the advantage of being cheap and readily available. Their spectrum follows the one of a black body radiator as can be seen in Figure 1.9. A full discussion on the lighting sources is yet again provided by (Lakowicz, 2006).

The important consideration here is that when images recorded at different excitations are used for further calculations, correction factors need to be applied that correct for the different light intensities. The correction factors for the tungsten halogen lamp used in this thesis can be found in Table 1.1. If absolute numbers are important it is necessary to normalize the spectrum

1. Part I: Förster Resonance Energy Transfer

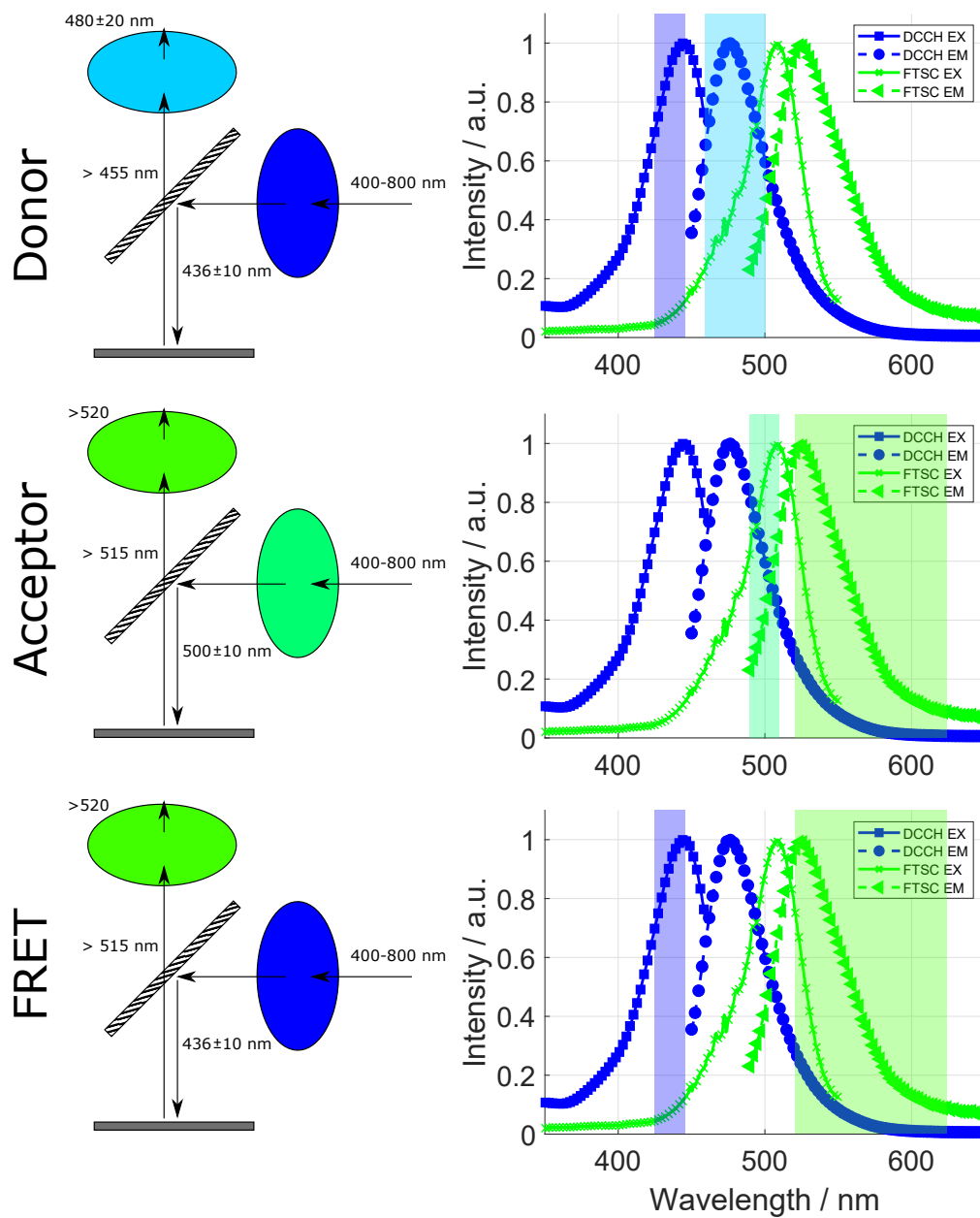


Figure 1.8.: Filtersets used in the widefield microscopy in this thesis. The filters are labelled as Donor, Acceptor or FRET corresponding to what the filters should primarily measure. The fluorescence spectra in the background are the spectra of our dyes on fibers at pH 9.

1. Part I: Förster Resonance Energy Transfer

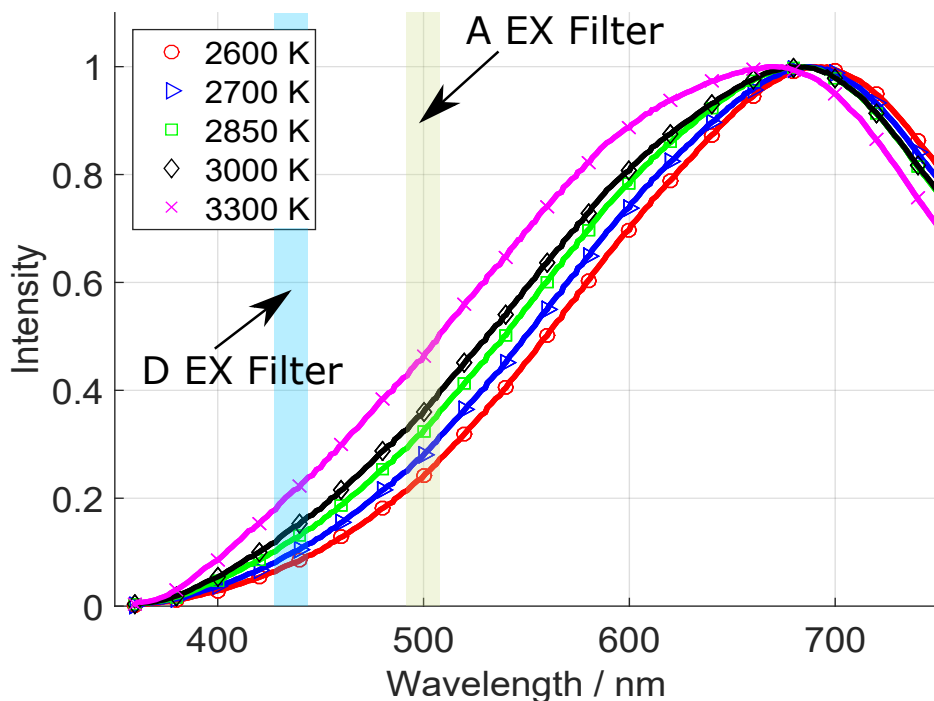


Figure 1.9.: Spectra of the tungsten halogen lamp used in this thesis. The correction factors are calculated by integrating over the shaded areas that correspond to the excitation filters for the donor and acceptor.

by its area. In our case the relative differences were enough and therefore we used spectra normalized by their peak intensities. The factors were subsequently calculated by the following equation.

$$c_{lamp} = \int_{f_l}^{f_u} I(\lambda) d\lambda \quad (1.5)$$

f_u and f_l are the upper and lower edge of the excitation filter. I is the spectrum of the used lamp.

Similarly the detector needs to be considered. The camera used here was a monochromatic CMOS detector from QI Imaging (Optimos). The detector

1. Part I: Förster Resonance Energy Transfer

Table 1.1.: Correction factors for the tungsten halogen lamp

Temperature	2600 K	2700 K	2850 K	3000 K	3200 K
Donor	1.6557	2.0630	2.5662	3.0023	4.4069
Acceptor	5.0972	5.9212	6.8566	7.6038	9.7691

efficiency together with the fluorescent emission spectra from the dyes and the filter sets can be seen in Figure 1.10.

For the correction of the detector the emission spectra of the fluorescent dyes must also be taken into account. The factor is calculated with the following equation.

$$c_{detector} = \frac{\int_{f_l}^{f_u} QE(\lambda) \cdot I_{EM}(\lambda) d\lambda}{\int_{f_l}^{f_u} I_{EM}(\lambda) d\lambda} \quad (1.6)$$

f_u and f_l are the upper and lower edge of the emission filter. QE is the quantum efficiency of the detector and I_{EM} is the emission spectrum of either donor or acceptor. In this case for every molecule there are two factors which leads to a total of 4 factors. The calculated factors can be seen in Table 1.2.

Table 1.2.: Correction factors for the detector

Spectra	Donor	Acceptor
Donor Filter	0.4618	0.4727
Acceptor Filter	0.5328	0.5353

The correction factors end up being quite similar which leads to a simpler correction procedure. If it was not like that it would lead to problems correcting the images in cases where a signal of both dyes occurs in the same image. It would not be possible to accurately correct this scenario without complex image processing.

1. Part I: Förster Resonance Energy Transfer

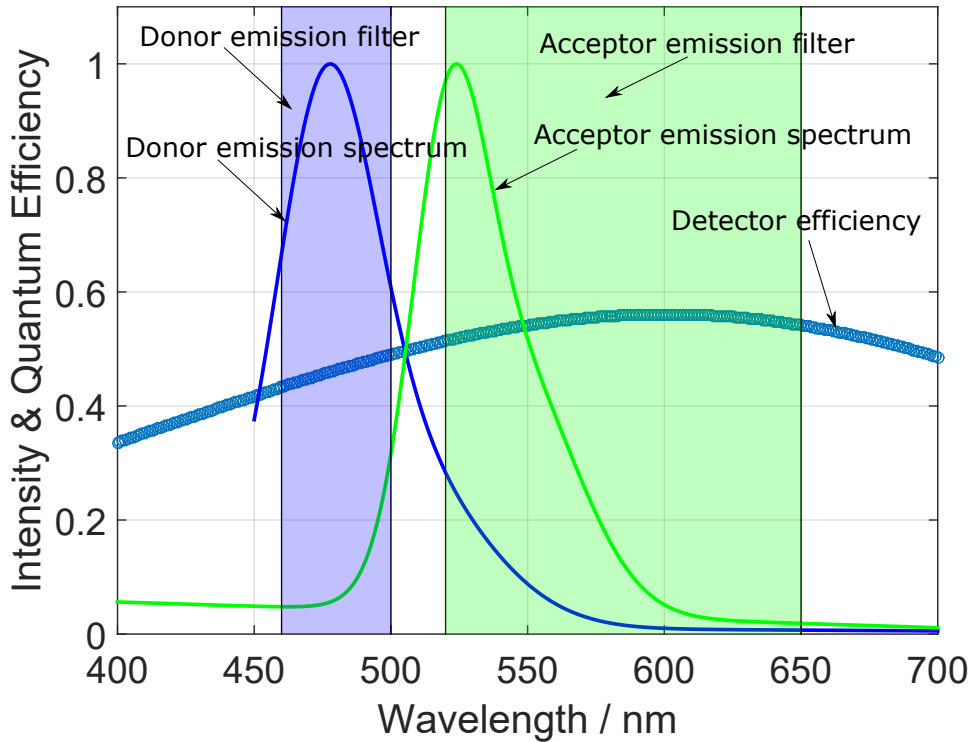


Figure 1.10.: Quantum efficiency of the CMOS detector. Also the fluorescence emission spectra and the emission filters are shown.

Confocal Laser Scanning Microscopy (CLSM)

In the context of this thesis a CLSM has the potential to improve the quality of the obtained fluorescent images. The basic setup of a CLSM can be seen in Figure 1.11. In principle a CLSM works the same way as a normal microscope however due to the introduction of two pinholes that only let a very small portion of the light pass the out of plane light can be greatly reduced. (Paddock, 1999) A laser that passes through a first pinhole is used to illuminate only a small part of the sample and the resulting light is then detected by a photomultiplier tube (PMT) after a second pinhole. The first pinhole is used to create a focus point on the sample which is subsequently moved to scan the whole sample and the second pinhole is used to get

1. Part I: Förster Resonance Energy Transfer

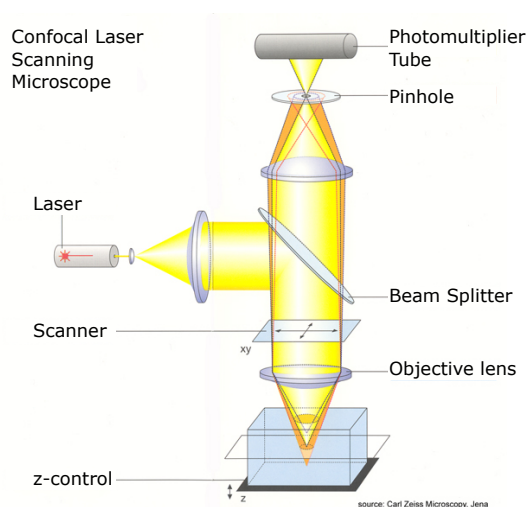


Figure 1.11.: Schematic of a confocal laser scanning microscope. Reprinted with the permission of Carl Zeiss Microscopy GmbH, Jena

depth information by eliminating the out of focus light.

The fact that in fluorescence microscopy the light intensity is often low is improved by using a photomultiplier tube (PMT) to detect the light and lasers to excite the samples. A PMT is a device that converts incoming photons to an electric signal and has a very high sensitivity. Additionally the intensity of the images can be increased by increasing the laser power. The usage of lasers often makes the first pinhole obsolete as the laser dot itself is already very small. An increased power needs to be used carefully though as a higher laser input leads to increased photobleaching of the fluorescent samples.

Modern CLSMs have a feature that allows them to automatically scan over different wavelengths thereby creating a spectrum of the measured area. This can be an advantage when one is trying to measure FRET as a clear shift could be seen in the spectra.

1. Part I: Förster Resonance Energy Transfer

Fluorescence Lifetime Imaging Microscopy (FLIM)

This method, which is described in (Lakowicz, 2006), measures the intensity of the fluorescence signal over time and allows the determination of molecule specific relaxation time. This relaxation time is often of interest because also the lifetime of a molecule is affected by FRET and an investigation like this can provide solid proof of energy transfer. The decrease of the fluorescence intensity N of an excited molecule at time t can be described as an exponential decay of the form

$$N(t) = N_0 e^{-t/\tau} \quad (1.7)$$

with N_0 being the initial intensity and τ the fluorescence lifetime. For systems that consist of more than one fluorescent molecule a monoexponential decay is not sufficient to model the data. It might occur that even only one molecule cannot be modelled by a monoexponential decay. This could be because it has more than one stable protonation state, different conformations or because the batch was not completely pure. In any case it is necessary to apply a multiexponential model as in the following equation

$$N(t) = \sum_i N_i(t) = \sum_i N_{i,0} e^{-t/\tau_i} \quad (1.8)$$

The measurements from the molecules DCCH (blue) and FTSC (green) can be seen in Figure 1.12. In a logarithmic display of the data, as in Figure 1.12b), one can immediately see that the FTSC can be modelled by a monoexponential curve while the DCCH needs a multiexponential model.

1.2.5. How to calculate FRET - Inevitable Mathematics and Experimental Considerations

This section focuses on how to calculate FRET from data obtained by the methods mentioned above. Most of the theory will again follow the book of Medintz and Hildebrandt. (Hildebrandt, 2013) The book contains more and deeper information on the effect itself, the necessary calculations and the

1. Part I: Förster Resonance Energy Transfer

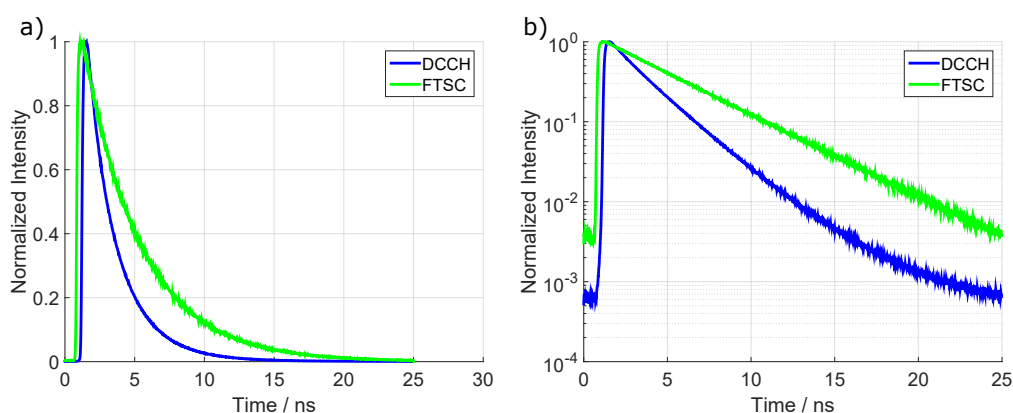


Figure 1.12.: FLIM measurement of DCCH and FTSC. From the semilogarithmic plot in b) one can clearly see that FTSC can be explained by a monoexponential decay while the DCCH needs a multiexponential approach.

interpretation of the data. Also there one can find many applications and case studies on how FRET was used to solve problems.

Förster Radius

For a quantitative FRET analysis the Förster radius (R_0) of the donor-acceptor pair needs to be determined first. It is also generally a good idea to determine this property as it can provide an anchor on whether the investigated FRET pair can be used in the experiment. E.g. if one expects to measure distances in the range of (8 – 16) nm it will be necessary to use a FRET pair with a Förster distance of at least 8 nm as the sensitivity of the method ranges only from $1/2 R_0$ to $2 R_0$.

The Förster Radius can be calculated with Eq. 1.2. The first measurement to achieve that is to measure the molar attenuation coefficient of the acceptor as described in section 1.2.2. In the next step the donor emission spectrum needs to be measured as described in section 1.2.3. With these properties measured the overlap integral can be calculated according to Eq. 1.3.

For our FRET pair this distance has been calculated for solutions in paper A but also for the cases of being embedded in pHema and covalently bonded to cellulose fibers in paper B.

1. Part I: Förster Resonance Energy Transfer

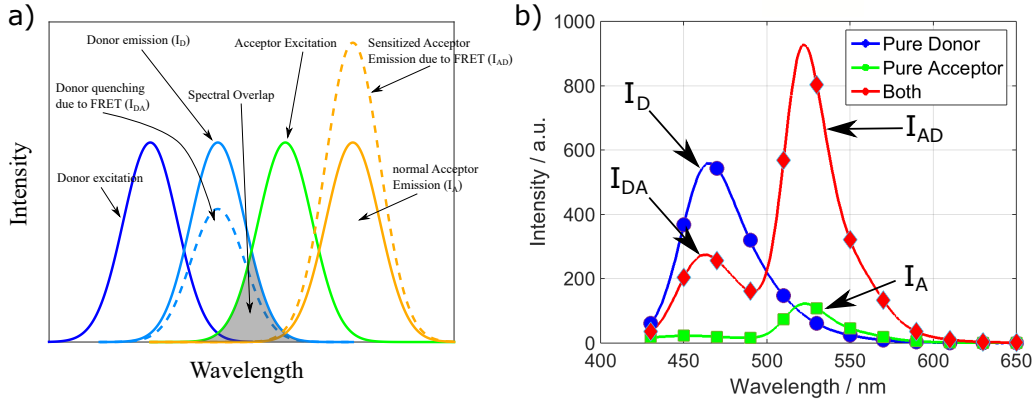


Figure 1.13.: Schematic of the effect FRET has on the fluorescence emission spectra of a compatible FRET pair. a) shows the theoretical considerations such as the overlap integral J and the intensities without and with FRET. (same as Figure 1.3) b) is an actual measurement from this thesis.

Donor Quenching

The first method to calculate a FRET efficiency measures the quenching of the donor efficiency due to FRET. After the excitation of the donor it transfers a part of its energy to an acceptor. This means that the donor emits less photons than it would without the acceptor being present. In other words it means that the donor intensity I_D is reduced to I_{DA} in the presence of the acceptor. Schematically this is shown in Figure 1.13a) and b).

To calculate the FRET efficiency η_{FRET} the following equation can be used

$$\eta_{FRET} = 1 - \frac{\Phi_{DA}}{\Phi_D} = 1 - \frac{\tau_{DA}}{\tau_D} = 1 - \frac{I_{DA}}{I_D} \quad (1.9)$$

with Φ being the quantum yield, τ the fluorescence lifetime and I the fluorescence intensity. Although donor quenching is not only an indication of FRET but even a necessary condition of the effect and can also be used to calculate the efficiency one needs to be careful as it is no sufficient proof of FRET because the donor can be deactivated by other means.

1. Part I: Förster Resonance Energy Transfer

Acceptor Sensitisation

The second method to calculate the FRET efficiency measures the increased emission of the acceptor. As shown in Figure 1.13 the transferred energy results in the acceptor being sensitized. In the presence of a donor the intensity of the acceptor signal increases from the pure signal I_A to I_{AD} . The efficiency is calculated by

$$\eta_{FRET} = \left(\frac{I_{AD} - I_A}{I_A} \right) \left(\frac{\epsilon_A}{\epsilon_D} \right) = \left(\frac{I_{AD}}{I_A} - 1 \right) \left(\frac{\epsilon_A}{\epsilon_D} \right) \quad (1.10)$$

with ϵ being the molar attenuation coefficient. Contrary to donor quenching, acceptor sensitisation is a clear sign of energy transfer and can therefore provide solid proof of FRET. The attenuation coefficient here is of course the coefficient at the excitation wavelength. In the case of filter sets and a microscope one has to think of a different method to calculate the ratio $\frac{\epsilon_A}{\epsilon_D}$. One possibility could be to calculate the average of the attenuation coefficient over the filter set limits.

Acceptor Photobleaching

The third method to determine the FRET efficiency measures and provides a strong case for FRET by measuring the intensity of the donor signal before and after photobleaching of the acceptor. It can be interpreted as the opposite of donor quenching with the difference of being aware of one more important circumstance, namely that the only change was that the acceptor was fully photobleached. The photobleaching results in the deactivation of the FRET pathway and the only way the donor can get rid of its energy is by its usual options, including fluorescence, hence the formerly quenched donor signal I_{DA}^{pre} increases to I_{DA}^{post} . In this case the efficiency is calculated by

$$\eta_{FRET} = 1 - \frac{I_{DA}^{pre}}{I_{DA}^{post}} \quad (1.11)$$

1. Part I: Förster Resonance Energy Transfer

Although this method has not been used in this thesis it is still worth mentioning as it is the simplest way, regarding setup and measurement, to measure FRET. Theoretically one only needs to measure the donor intensity (e.g. one filter set) and a strong enough light source to fully bleach the acceptor. It is important to realize that the unintended photobleaching of the donor (although photobleaching of the acceptor is desired) can lead to wrong results and needs to be accounted for.

Final considerations

With all of the above mentioned techniques it is possible to determine the FRET efficiency of a system. However there are some points that need to be considered in order to obtain accurate and reliable measurements. Independently of whether FRET is measured with a microscope or a spectrophotometer it is likely that the resulting spectra or intensity data will be flawed due to spectral bleedthrough (BT). BT occurs when the fluorescence spectra of the dyes overlap as it is the case for many FRET pairs and also the one used in this thesis. For our DCCH-FTSC FRET pair the overlap can be seen in Figure 1.7. As can be seen most spectra have an overlap to some degree. Hence these spectra or intensity values need to be unmixed in order to obtain a reliable measurement. How this is done with microscopic data will be discussed in detail in the next section. The spectral unmixing has been described in Paper A.

1.2.6. How to calculate FRET using a Microscope

The previous section explained how FRET is in principal calculated and how one can extract the relevant and corrected spectral data to calculate the FRET efficiency of the system. In the case of microscopic data the images also have to be corrected in a similar yet a little more complicated fashion.

It should be mentioned here that most of the calculations that were done in Matlab can also be performed in image processing software such as Fiji (formerly ImageJ). This software comes with ready made plugins for

1. Part I: Förster Resonance Energy Transfer

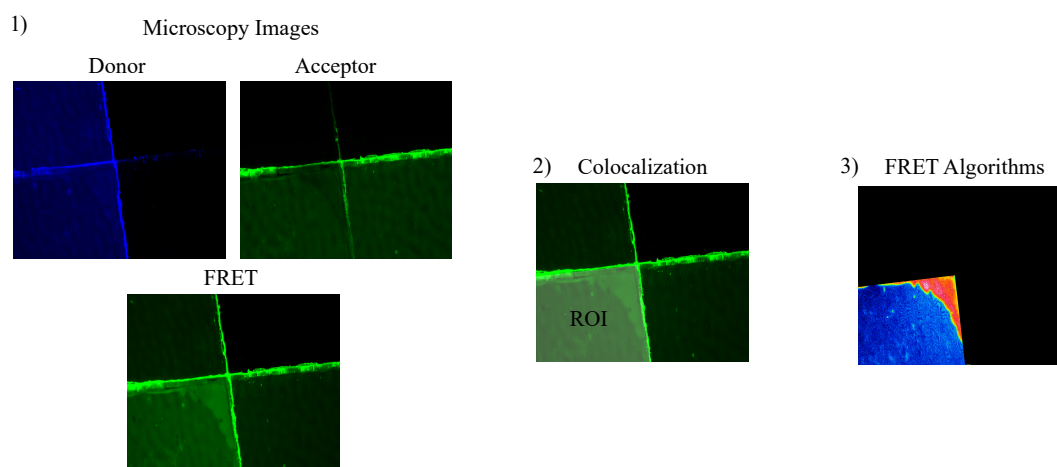


Figure 1.14.: 1) First fluorescence images using specific filter sets need to be acquired. In a second step 2) a region of interest (ROI) is drawn in the area where the both dyes can logically exhibit FRET. 3) The images of step 1) are used in an algorithm to calculate the FRET efficiency.

colocalization and also for the calculation of FRET and is in general very helpful when working with images.

Colocalization

Colocalization describes a process in fluorescence microscopy to check if two fluorophores occupy the same pixel. As FRET is an interaction between two fluorophores colocalization provides an excellent starting point for further evaluation. All the pixels in which only one of the dyes is present can be ruled out by logic.

The basic approach to colocalization makes use of the Pearson correlation coefficient as it was introduced to fluorescence microscopy by Manders et al. (E. M. Manders et al., 1992; E. M. M. Manders et al., 1993; Pearson & Henrici, 1896) Additionally to the Pearson coefficient Manders later introduced further coefficients, commonly labelled M1 and M2, which quantify the relative amount of colocalized fluorescent objects in channel 1 and 2, respectively. A further improvement of these intensity-correlation based methods was developed by Li et al. (Li et al., 2004) An automated method

1. Part I: Förster Resonance Energy Transfer

to detect an unbiased threshold was developed by Costes et al. (Costes et al., 2004) Finally a recent work showed that colocalization can be greatly improved by combining object-recognition with pixel-intensity-correlation. (Moser et al., 2017) Excellent overviews of the topic of colocalization can be found in (Bolte & Cordelières, 2006; Comeau et al., 2006)

Although in this work some of the above mentioned methods were tested in an in-house written Matlab routine, none of the tested methods (Pearson, Manders and Costes), were suitable for our application. Due to the inherent bleedthrough of our fluorescent molecules in the images the methods detected colocalization at positions that were not possible. Additionally it was shown (Paper B) that the FRET algorithms are sensitive to large intensity changes which often occur at the edges of objects.

Due to these problems we chose to abandon the idea of automated colocalization evaluation and decided to investigate our structures manually as by visual inspection and logic the colocalized area is uniquely defined. The resulting method consisted of manually redrawing the bonded area of the fiberbond and subsequently using an image erosion algorithm to uniformly decrease this area until we could be positive that we do not measure the edges of our samples.

Gordon Algorithm

Fluorescence microscopy images that are captured through filter sets are likely to be corrupted by spectral bleedthrough (BT). The origins of BT were already discussed in section 1.2.3. To still be able to obtain reliable results the corrupted images need to be corrected. Gordon et al. developed an algorithm to fully correct the images from spectral bleedthrough and obtain an objective measure for the FRET efficiency. In detail the method and the variables are described in the original paper. (Gordon et al., 1998)

In brief the algorithm uses images recorded with the different filter sets to obtain the corrected intensities and uses them to calculate the FRET efficiency. To keep track of the many different required measurements Gordon et al. constructed 2 and 3 letter variables for the equations. Figure 1.15 shows how the variables are defined in an actual FRET measurement.

1. Part I: Förster Resonance Energy Transfer

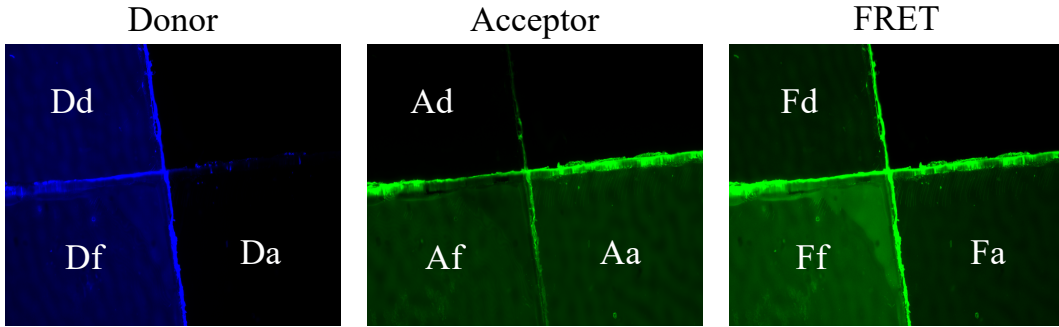


Figure 1.15.: Schematic on how the variables in the Gordon algorithms are acquired from the fluorescence microscopy images.

Three areas (pure donor (d), pure acceptor (a) and donor+acceptor (f)) are imaged by three filter set (Donor (D), Acceptor (A) and FRET (F)) which leads to 9 variables labelled by the filter set used and the investigated area. E.g. the pure donor investigated by the FRET filter set would be Fd. Gordon uses these measured two-letter variables to calculate the corrected three-letter variables such as Afa. e.g. Afa would be the signal from only the acceptor (a) in the area where both donor+acceptor are present (f) measured with the acceptor filter set (A). The following equations show how the efficiency is then calculated.

$$\overline{Afa} = \frac{Af - \left(\frac{Ad}{Fd}\right) \cdot Ff}{1 - \left(\frac{Fa}{Aa}\right)\left(\frac{Ad}{Fd}\right)} \quad (1.12)$$

$$FRET1 = \frac{(Ff - \left(\frac{Fd}{Dd}\right) \cdot Df - \overline{Afa} \cdot \left[\left(\frac{Fa}{Aa}\right) - \left(\frac{Fd}{Dd}\right) \cdot \left(\frac{Da}{Aa}\right)\right])}{G\left[1 - \left(\frac{Da}{Aa}\right) \cdot \left(\frac{Fd}{Dd}\right)\right]} \quad (1.13)$$

$$\overline{Dfd} = Df + FRET1 \cdot \left[1 - G \cdot \left(\frac{Da}{Aa}\right)\right] - \overline{Afa} \cdot \left(\frac{Da}{Aa}\right) \quad (1.14)$$

$$FRETN = \frac{FRET1}{\overline{Afa} \cdot \overline{Dfd}} \quad (1.15)$$

1. Part I: Förster Resonance Energy Transfer

Sensitized Emission Method

In some cases the filter sets and or the molecules can be chosen such that D_a and A_d become effectively 0. If this is the case Gordon showed that the following simple equation produces the same FRET efficiency as the "full" Gordon algorithm.

$$FRET_N = \frac{F_f - D_f \cdot \left(\frac{F_d}{D_d}\right) - A_f \cdot \left(\frac{F_a}{A_a}\right)}{G \cdot D_f \cdot A_f} \quad (1.16)$$

For these cases it is useful to not only use the sensitized emission method to evaluate the FRET efficiency but also the Gordon algorithm (Equation 1.15). As the image processing is done anyhow this provides a simple check if the algorithms were implemented correctly and if the measurements were interpreted correctly. If it is the case the two methods should provide the same results.

Xia Algorithm

Xia et al. (Xia & Liu, 2001) improved the algorithm from Gordon by normalizing the resulting FRET intensity $FRET_1$ by the square root of the product of the corrected pure donor and acceptor intensities as seen in the following equation.

$$N_{FRET} = \frac{FRET_1}{\sqrt{A_f a \cdot D_f d}} \quad (1.17)$$

Using this normalization has two advantages. First, using the geometric mean results in a more robust estimation against large concentration variations and provides a more realistic measurement when different concentrations are used. Second, using this normalization leads to a dimensionless FRET efficiency which is better comparable through different data sets.

1. Part I: Förster Resonance Energy Transfer

According to the Gordon algorithm also the sensitized emission method can be normalized this way leading to

$$FRETN = \frac{Ff - Df \cdot \left(\frac{Fd}{Dd}\right) - Af \cdot \left(\frac{Fa}{Aa}\right)}{G \cdot \sqrt{Df \cdot Af}} \quad (1.18)$$

1.2.7. Image Analysis Matlab Code

The code to analyze the resulting fluorescence images was added in the appendix. There are some parameters that I was not able to automatize hence the code needs to be run with care. Some parameters need to be adapted as described in the previous sections and also in the comments of the scripts.

Bibliography

- Bolte, S., & Cordelières, F. P. (2006). A guided tour into subcellular colocalization analysis in light microscopy. *Journal of Microscopy*, 224(3), 213–232. <https://doi.org/10.1111/j.1365-2818.2006.01706.x> (cit. on p. 26)
- Comeau, J. W. D., Costantino, S., & Wiseman, P. W. (2006). A Guide to Accurate Fluorescence Microscopy Colocalization Measurements. *Biophysical Journal*, 91(12), 4611–4622. <https://doi.org/10.1529/biophysj.106.089441> (cit. on p. 26)
- Costes, S. V., Daelemans, D., Cho, E. H., Dobbin, Z., Pavlakis, G., & Lockett, S. (2004). Automatic and Quantitative Measurement of Protein-Protein Colocalization in Live Cells. *Biophys J*, 86(6), 3993–4003. <https://doi.org/10.1529/biophysj.103.038422> (cit. on p. 26)
- Förster, T. (1948). Zwischenmolekulare Energiewanderung und Fluoreszenz. *Ann. Phys.*, 437(1-2), 55–75. <https://doi.org/10.1002/andp.19484370105> (cit. on p. 2)
- Förster, T. (1949). Experimentelle und theoretische untersuchung des zwischenmolekularen übergangs von elektronenanregungsenergie. *Zeitschrift für naturforschung A*, 4(5), 321–327 (cit. on p. 2).
- Gordon, G. W., Berry, G., Liang, X. H., Levine, B., & Herman, B. (1998). Quantitative Fluorescence Resonance Energy Transfer Measurements Using Fluorescence Microscopy. *Biophysical Journal*, 74(5), 2702–2713. [https://doi.org/10.1016/S0006-3495\(98\)77976-7](https://doi.org/10.1016/S0006-3495(98)77976-7) (cit. on p. 26)
- Hildebrandt, N. (2013). How to Apply FRET: From Experimental Design to Data Analysis. In *FRET – Förster Resonance Energy Transfer* (pp. 105–163). John Wiley & Sons, Ltd. <https://doi.org/10.1002/9783527656028.ch05>. (Cit. on pp. 8, 20)
- Lakowicz, J. R. (2006). *Principles of Fluorescence Spectroscopy* (3rd ed.). Springer US. <https://doi.org/10.1007/978-0-387-46312-4>. (Cit. on pp. 12–14, 20)

Bibliography

- Li, Q., Lau, A., Morris, T. J., Guo, L., Fordyce, C. B., & Stanley, E. F. (2004). A Syntaxin 1, Gao, and N-Type Calcium Channel Complex at a Presynaptic Nerve Terminal: Analysis by Quantitative Immunocolocalization. *J. Neurosci.*, 24(16), 4070–4081. <https://doi.org/10.1523/JNEUROSCI.0346-04.2004> (cit. on p. 25)
- Manders, E. M., Stap, J., Brakenhoff, G. J., Driel, R. v., & Aten, J. A. (1992). Dynamics of three-dimensional replication patterns during the S-phase, analysed by double labelling of DNA and confocal microscopy. *Journal of Cell Science*, 103(3), 857–862. Retrieved September 18, 2019, from <https://jcs.biologists.org/content/103/3/857> (cit. on p. 25)
- Manders, E. M. M., Verbeek, F. J., & Aten, J. A. (1993). Measurement of co-localization of objects in dual-colour confocal images. *Journal of Microscopy*, 169(3), 375–382. <https://doi.org/10.1111/j.1365-2818.1993.tb03313.x> (cit. on p. 25)
- Meer, B. W. v. d. (2013). Förster Theory. In *FRET – Förster Resonance Energy Transfer* (pp. 23–62). John Wiley & Sons, Ltd. <https://doi.org/10.1002/9783527656028.ch03>. (Cit. on pp. 2, 5)
- Meer, B. W. v. d., Meer, D. M. v. d., & Vogel, S. S. (2013). Optimizing the Orientation Factor Kappa-Squared for More Accurate FRET Measurements. In *FRET – Förster Resonance Energy Transfer* (pp. 63–104). John Wiley & Sons, Ltd. <https://doi.org/10.1002/9783527656028.ch04>. (Cit. on p. 6)
- Moser, B., Hochreiter, B., Herbst, R., & Schmid, J. A. (2017). Fluorescence colocalization microscopy analysis can be improved by combining object-recognition with pixel-intensity-correlation. *Biotechnol J*, 12(1). <https://doi.org/10.1002/biot.201600332> (cit. on p. 26)
- Paddock, S. W. (1999). Confocal Laser Scanning Microscopy [Publisher: Future Science]. *BioTechniques*, 27(5), 992–1004. <https://doi.org/10.2144/992750V01> (cit. on p. 18)
- Page, D. H., & Tydeman, P. (1962). A new theory of the shrinkage, structure and properties of paper. In *The formation and structure of paper* (pp. 397–425). (Cit. on p. 1).
- Page, D. (1969). A theory for the tensile strength of paper. *Tappi*, 52, 674–681 (cit. on p. 1).
- Pearson, K., & Henrici, O. M. F. E. (1896). VII. Mathematical contributions to the theory of evolution.—III. Regression, heredity, and panmixia. *Philosophical Transactions of the Royal Society of London. Series A, Con-*

Bibliography

- taining Papers of a Mathematical or Physical Character, 187*, 253–318. <https://doi.org/10.1098/rsta.1896.0007> (cit. on p. 25)
- Würth, C., Grabolle, M., Pauli, J., Spieles, M., & Resch-Genger, U. (2013). Relative and absolute determination of fluorescence quantum yields of transparent samples. *Nat Protoc*, 8(8), 1535–1550. <https://doi.org/10.1038/nprot.2013.087> (cit. on p. 9)
- Xia, Z., & Liu, Y. (2001). Reliable and global measurement of fluorescence resonance energy transfer using fluorescence microscopes. *Biophys J*, 81(4), 2395–2402. Retrieved November 5, 2018, from <https://www.ncbi.nlm.nih.gov/pmc/articles/PMC1301710/> (cit. on p. 28)

2. Paper A

RESEARCH ARTICLE

Spectroscopic Investigation of DCCH and FTSC as a potential pair for Förster Resonance Energy Transfer in different solvents

Georg Urstöger^{1,2}, Andreas Steinegger³, Robert Schennach^{2,4}, Ulrich Hirn^{1,2*}

1 Institute for Paper, Pulp and Fiber Technology, Graz University of Technology, Graz, Austria, 2 CD-Laboratory for Fiber Swelling and Paper Performance, Graz University of Technology, Graz, Austria, 3 Institute of Analytical Chemistry and Food Chemistry, Graz University of Technology, Graz, Austria, 4 Institute of Solid State Physics, Graz University of Technology, Graz, Austria

* ulrich.hirn@tugraz.at

Abstract

Two molecules, 7-(diethylamino)coumarin-3-carbohydrazide (DCCH) and fluorescein-5-thiosemicarbazide (FTSC) were investigated in different solvents, under varying pH conditions regarding their spectroscopic properties for the usage as a Förster Resonance Energy Transfer (FRET) pair to study the molecular interaction between cellulosic surfaces. All the relevant spectroscopic properties to determine the Förster distance were measured and the performance as a FRET system was checked. From the results, it is clear that the environmental conditions need to be accurately controlled as both, but especially the FTSC dyes are sensitive to changes. For high enough concentrations positive FRET systems were observed in DMF, DMSO, H₂O, THF and alkaline DMF. However due to the low quantum yield of the unmodified DCCH throughout the investigated parameter range and the strong environmental dependency of FTSC, both dyes are not preferable for being used in a FRET system for studying interaction between cellulosic surfaces.

OPEN ACCESS

Citation: Urstöger G, Steinegger A, Schennach R, Hirn U (2020) Spectroscopic Investigation of DCCH and FTSC as a potential pair for Förster Resonance Energy Transfer in different solvents. PLoS ONE 15 (2): e0228543. <https://doi.org/10.1371/journal.pone.0228543>

Editor: Warren Batchelor, Monash University, AUSTRALIA

Received: August 22, 2019

Accepted: January 17, 2020

Published: February 11, 2020

Peer Review History: PLOS recognizes the benefits of transparency in the peer review process; therefore, we enable the publication of all of the content of peer review and author responses alongside final, published articles. The editorial history of this article is available here: <https://doi.org/10.1371/journal.pone.0228543>

Copyright: © 2020 Urstöger et al. This is an open access article distributed under the terms of the [Creative Commons Attribution License](https://creativecommons.org/licenses/by/4.0/), which permits unrestricted use, distribution, and reproduction in any medium, provided the original author and source are credited.

Data Availability Statement: All relevant data are within the paper and its Supporting Information files.

Introduction

Förster Resonance Energy Transfer (FRET) is a technique mainly used to determine the distance between a so-called donor and an acceptor molecule. Developed by Theodor Förster in the 1940s, FRET has evolved to a standard investigation technique in cellular biology to study the interactions between protein molecules, in the usage of biomarkers or for building sensors. [1–3]

The theory of the physical effect is based on the electromagnetic interaction between a donor and an acceptor molecule. An incident photon excites the donor molecule which can transfer its energy, by a non-radiative interaction, to the acceptor. In principle, there are other interaction mechanisms but Förster could show that in the near field range (approx. 1–20 nm) the dominant energy transfer mechanism is Förster transfer. The efficiency of the transfer depends on the proximity of the two molecules and is in principle determined by the Förster Radius (R_0). This quantity is specific for every Donor-Acceptor pair and gives the range within

Funding: The authors thank the Austrian Federal Ministry of Economy, Family and Youth and the Austrian National Foundation for Research, Technology and Development for their financial support. Also the industrial partners Mondi, Canon Production Printing, SIG Combibloc and Kelheim Fibres are acknowledged.

Competing interests: The authors have declared that no competing interests exist.

which the distance can be quantified. Beyond this range, which is about $\frac{1}{2} R_0$ – $2 R_0$, it may still be possible to qualitatively determine whether the molecules do or do not interact. Closer than the lower limit the energy transfer mechanism is called Dexter transfer.[4,5]

While many people already use this technique as a standard analyzing tool in life sciences, others strive to develop further applications.[6,7] However, in all cases it is crucial to have a deep and thorough understanding of the employed dyes and the system that is under investigation. We present here a detailed analysis of 7-(diethylamino)coumarin-3-carbohydrazide (DCCH) and fluorescein-5-thiosemicarbazide (FTSC) in different solvents, under varying pH conditions regarding their spectroscopic properties for the usage as a FRET pair. The two chromophores were used by Thomson et al. to detect an interaction between paper fibers.[8,9], which is a promising approach to quantify the nanometer-scale contact area available for adhesion between the fiber surfaces [22].

The following brief introduction to the most prominent equations in Förster Theory were taken from chapter 3 of the book, FRET–Förster Resonance Energy Transfer, From Theory to Applications, written by Prof. Van der Meer and is based partly on the original papers of Förster.[3,10,11] The efficiency of the energy transfer (η_{eff} [-]) is given by Eq (1):

$$\eta_{\text{eff}} = \frac{1}{1 + \left(\frac{r}{R_0}\right)^6} \tag{1}$$

Where r [nm] stands for the distance between the donor and acceptor and R_0 [nm] stands for the Förster radius of the donor-acceptor pair. The Förster radius or distance can be calculated via Eq (2):

$$R_0^6 = \frac{9 \ln 10}{128 \Pi^5 N_A} (k^2 n^{-4} Q_0 J) \tag{2}$$

Where N_A [mol⁻¹] is Avogadro’s constant, k [-] is the orientation factor, n [-] is the index of refraction of the medium, Q_0 [-] is the quantum efficiency of the donor in the absence of FRET and J [M⁻¹cm⁻¹λ⁴] is the overlap integral which is calculated with Eq (3):

$$J = \int f_D(\lambda) \epsilon_A(\lambda) \lambda^4 d\lambda \tag{3}$$

Where f_D [a.u.] is the area normalized fluorescence intensity of the donor, ϵ_A [M⁻¹cm⁻¹] is the attenuation coefficient of the acceptor and λ [nm] is the wavelength.

By measuring the transfer efficiency one can calculate the distance between the Donor and Acceptor once the Förster radius for the system has been determined. Practically, this can be done by different methods which can be implemented in either microscopy setups or measured by spectrophotometry, which was used in this paper. Regardless of the measurement method, a FRET signal can be detected by different aspects of the effect. Two prominent ones are the donor quenching (data provided in the [S1 File](#)) which measures the decrease of the donor fluorescence due to FRET; or the acceptor sensitisation method which measures the increase of the acceptor fluorescence due to FRET. While donor quenching is an indication for FRET, one cannot be certain of it as there are other mechanisms such as concentration quenching that can deactivate the excited Donor. Acceptor sensitisation on the other hand provides a compelling argument for FRET as the acceptor fluorescence can only be increased by some sort of energy transfer. To be certain of the resulting data many people have developed equations that correct the efficiency for all possible cross talk situations.[12,13] To quantify the FRET efficiency using a spectrophotometer it is necessary to spectrally unmix the detected

emission curves. Then the FRET efficiency η [-] can be calculated by

$$\eta_{\text{eff}} = \left(\frac{I_{AD}}{I_A} - 1 \right) * \frac{\epsilon_{\text{Acceptor}}}{\epsilon_{\text{Donor}}} \quad (4)$$

Where I_{AD} [a.u.] and I_A [a.u.] are the fluorescence emission intensities of the acceptor in the presence and in the absence of donor, respectively. $\epsilon_{\text{Acceptor}}$ [$M^{-1}cm^{-1}$] and ϵ_{Donor} [$M^{-1}cm^{-1}$] are the molar attenuation coefficients of the acceptor and the donor molecule at the used excitation wavelength, respectively.

The fluorescence quantum yield of a molecule is the probability of an excited state to be deactivated by fluorescence rather than by another, non-radiative mechanism. The quantum yield can be measured via the usage of a known fluorescence standard by Eq 4,

$$Q_{F(x)} = Q_{F(s)} \frac{A_s F_x n_x^2}{A_x F_s n_s^2} \quad (5)$$

where Q_F [-] stands for the fluorescence quantum yield, A [OD] is the absorbance at the excitation wavelength, F [a.u.] is the area under the corrected emission curve and n [-] is the refractive index of the medium. The indices x and s refer to the unknown and the standard sample, respectively. Another possibility to measure the quantum yield is with the absolute method. [14–18]

The molar attenuation coefficient (ϵ [$M^{-1}cm^{-1}$]) is connected to the absorbance by Beer Lamberts Law (Eq 6)

$$A = \epsilon c l \quad (6)$$

Where A [OD] is the absorbance defined as the negative decadic logarithm of the measured transmittance, c [mol/L] is the concentration of the solution and l [cm] is the length of the light path. Correctly measured the attenuation coefficient tells you how well a substance absorbs light at a certain wavelength independent of concentration or geometrical considerations.

This paper focuses on the stepwise determination of spectral properties (excitation/emission spectra, attenuation Coefficient, quantum yield) needed to calculate the Förster radius and the subsequent investigations of mixtures to determine whether an energy transfer can be observed or not, and under which conditions the system works well. Ultimately this method will be adapted for measuring adhesion between surfaces and to understand a complicated system like that groundwork such as this is necessary. For a related system it was shown that a good FRET response was achievable.[10,11]

Experimental

Materials

The dyes 7-(diethylamino)coumarin-3-carbohydrazide (DCCH, Purity 95%, CAS: 100343-98-4), fluorescein-5-thiosemicarbazide (FTSC, Purity 99%, CAS: 76863-28-0) and the standard fluorescein sodium salt were bought from Santacruz Biotechnology (Dallas, Texas, USA). Coumarin 30 was bought from (Sigma Aldrich) The solvents N,N-dimethylformamide (DMF), dimethyl sulfoxide (DMSO), Tetrahydrofuran (THF), and Acetonitril were purchased from VWR (Vienna, Austria). All chemicals were used without further purification.

Sample preparation and methods

The volume of the cuvette for all measured solutions was 2 ml. In the case of the capillary a volume of 2 ml was prepared and thoroughly mixed. To investigate the influence of the pH value on the properties the pH of the solutions was adjusted by adding 12 μL triethylamine to the 2 ml solution of H_2O , DMF and DMSO. To accordingly adjust the pH in THF 10-times the volume of triethylamine was used (120 μL). The pH values of the systems are reported in the [S1 File](#).

The absorbance was measured with a VARIAN CARY, UV-vis spectrophotometer. To minimize the inner filter effect and deviations from Beer-Lamberts law the optical density of the transmission measurements never exceeded 0.5 OD. Fluorescence spectra were recorded on a FluoroLog 3 spectrofluorometer from Horiba Scientific equipped with a R2658 photomultiplier from Hamamatsu.

FRET experiments were performed with concentrations of molecules of 0.1 mM and 1 mM in two different ways. For the lower concentration experiments were conducted using standard optical glass 10 mm precision cuvettes from Hellma Analytics, with the Fluorolog. Additionally, FRET experiments were conducted using a capillary due to the need to go to higher concentrations. The spectra of those experiments were measured with a RF-5301PC, spectrofluorophotometer from Shimadzu. Using a capillary was necessary to avoid the inner filter effect which occurs at higher concentrations. All FRET experiments were performed using a ratio of 1:1 between the molecules. Equipment used for Fluorometry or UV/Vis was spectroscopy grade and cleaned rigorously between measurements. Also, care was taken to minimize the exposure of the solutions to ambient light to avoid photobleaching.

As a reference for the quantum yield measurements coumarin 30 in acetonitril and fluorescein sodium salt in 0.1 M NaOH were used with reported quantum yields of 0.55 and 0.95, respectively.[19,20] The quantum yields for the fluorescein compound in DMF, DMSO and THF were determined by the absolute method using a Quanta- ϕ integrating sphere-based set-up from Horiba Scientific connect to the Fluorolog 3 spectrophotometer. The concentration of the solutions was chosen such that the absorbance in the UV-vis is as large as close as possible but still below 0.05 OD ($\lambda_{\text{max}} \leq 0.05 \text{ OD}$). This way one can be sure that the inner filter effect does not influence the result. The method was taken from Würth et al. [18]

Since the dyes should eventually be used embedded in a matrix or bound to cellulosic surfaces measurements of the quantum yields of the dyes in Poly(2-hydroxyethyl methacrylate) (pHema thin films) and chemically bound to paper fibers (paper sheets) were also included. The production of the thin films and the dyeing of the paper fibers can be found in Urstöger et al.[21] The quantum yields were measured by the absolute method either directly of the thin films or of a small sheet of paper produced with alkaline (pH 9, NaOH) water.

To test if a modification of the dyes can improve the QY, DCCH was modified using an acetylation reaction. DCCH was dissolved by weighting 1 mg of DCCH into 500 μl of THF. Subsequently 10 μl of Triethylamine and 10 μl acetyl chloride were added to the solution. Thin layer chromatography (TLC) was used to determine if the reaction was finished. The solution was filtered with a Chromafil XTRA PTFE 0.45 μm filter. Before measuring the QY of the solution the pH was adjusted using TEA to match the unmodified version.

Results and discussion

Molar attenuation coefficient

As a key spectroscopical property, the attenuation coefficient tells you how well a substance absorbs light at a certain wavelength. On the one hand this quantity is important as it is

directly connected to the Förster Radius (Eq 2) by the overlap integral (Eq 3) which in the end determines at which distances the method will be applicable. On the other hand in combination with the quantum yield, the molar attenuation coefficient also determines how well the donor will provide energy for the transfer process. This means that for the acceptor a high attenuation coefficient is beneficial as the excitation of this energetic transition becomes more likely. Generally a higher molar attenuation coefficient is desirable however, under some circumstances it could be beneficial to have a lower coefficient e.g. in the case where a high concentration of molecules is needed but due to the high molar attenuation coefficient the solution becomes hard to measure due to the inner filter effect. In such a case a lower molar attenuation coefficient could be better. Therefore, this property is not only important for the calculation of the Förster radius but is also very relevant as a property itself.

As can be seen in Fig 1 the coefficient can vary quite drastically depending on the solvent as well as on the pH value. In the case of DCCH, one can see in Fig 1A that, without any base, the peak of the absorption band shifts with different solvents ranging from 412 to 427 nm. They also shift in intensity up to a factor of 2.5. When a base is added (Fig 1B) the shift in position becomes smaller and the spectra become more similar. The intensity in DMF and THF gets smaller when adding base while the intensity in DMSO stays almost constant and in H₂O it increases slightly. The maximum of the spectra shifts towards higher wavelengths by 5–13 nm. The FTSC curves in Fig 1C and 1D can be analyzed in a similar fashion. Without any base the attenuation coefficient of FTSC in all solvents except for water is extremely low. In water, we still get a sufficient absorbance while in other solvents it is almost zero throughout the complete spectrum. However, when a base is added to the system the intensity increases strongly while the position of the maximum and the shape of the curve also changes. The shift in position is quite high and lies between 47–56 nm. This trend is also seen by others and is likely to be attributed to variations in the protonation states of fluorescein.[22,23] In H₂O the maximum coincides with the NaOH reference while the DMF and DMSO samples show a distinct redshift. Adding the same amount of base to THF did not yield any change and even the 10-fold amount resulted only in little change. An important feature of these graphs is the increasing attenuation coefficient of FTSC in both, neutral and alkaline, conditions from 300 to 350 nm. The measurement in this region is tricky as the solvents start to absorb in that range as well. However, we believe that this is a real feature because an excitation in this range also appears in the fluorescence measurements.[23,24]

Quantum yield

The quantum yields were determined by the relative method and the absolute method described in the methods. A high quantum yield of the donor is worth striving for as it gives the donor the opportunity to provide more energy for the transfer process. Also, it is directly connected to the Förster distance via Eq 2. As can be seen in Table 1 the quantum yield can vary significantly depending on solvent and pH value. However, the QY of DCCH was generally low compared to FTSC. To check if the reason for the low QY of the molecules is the hydrazide group a chemical modification of DCCH was performed. The molecule was modified by adding acetyl chloride and triethylamine to the THF solution which results in an acetylation of the hydrazide group to create a hydrazine. The reaction scheme can be seen in Fig 2. As can be seen in Table 1 the quantum yield increased by more than a factor of 4. The QY for the fluorescein compound in DMF, DMSO and THF were measured absolutely and can be seen in Table 1. In all three solvents, the QY becomes very low most likely due to the reason that fluorescein is present in its lactone form which is known for having a very low QY. [25] Additionally in Table 1 the QY of the dyes incorporated in different structures like Poly

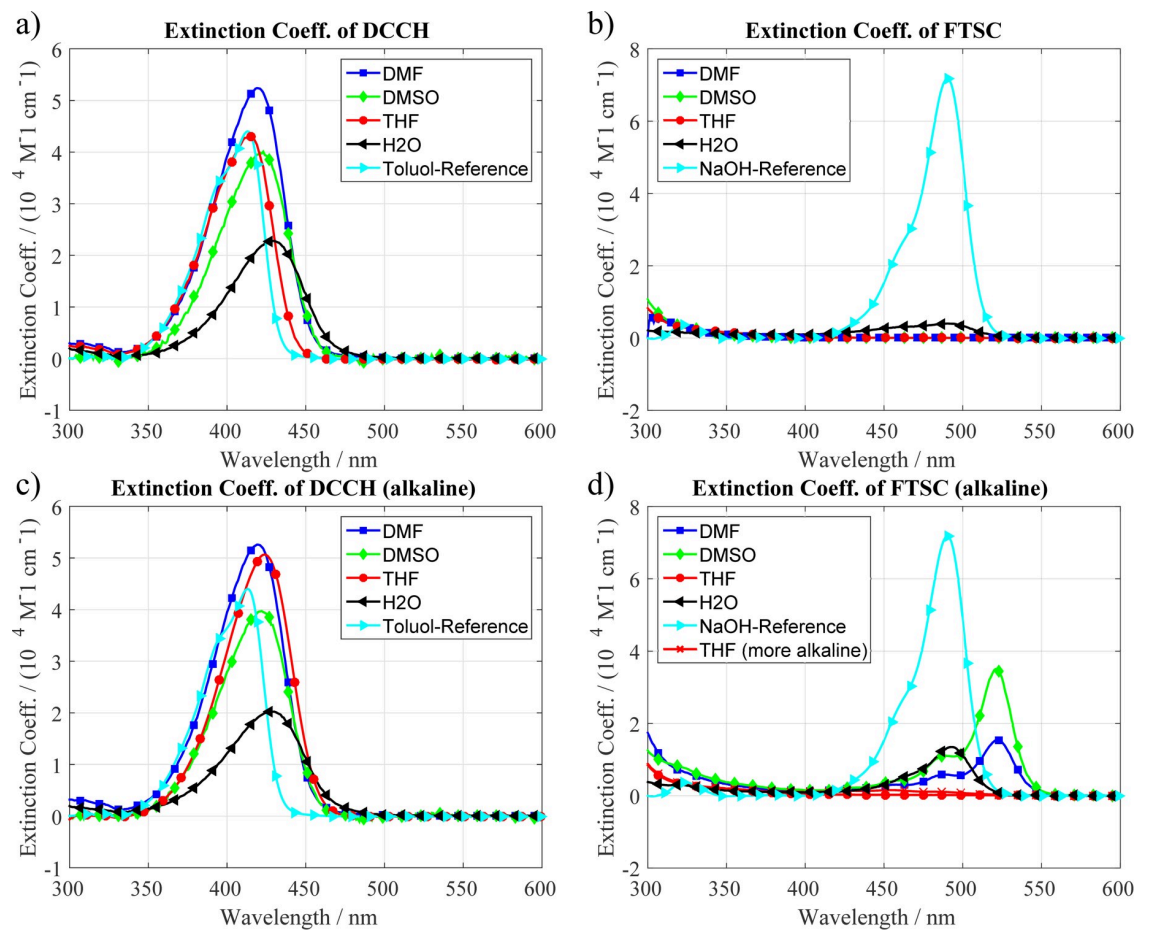


Fig 1. Molar attenuation coefficient of DCCH and FTSC at different pH conditions and in various solvents. a,b) Attenuation Coefficient of DCCH. The coefficients vary up to a factor of approx. 2.5 in the various solvents but do not show much change due to pH except for THF. The Toluol labeled sample represents the measurement of the reference molecule Coumarin 30 for the quantum yield (QY) measurements. c,d) Attenuation coefficient of FTSC. NaOH is the measurement of Fluorescein Sodium Salt needed as a reference for the QY of FTSC. c) One can see that the absorbance of FTSC is almost fully quenched in DMF, DMSO and THF in the visible range. In H₂O the performance is a little better. d) Going to alkaline conditions increases the attenuation coefficient in most solvents.

<https://doi.org/10.1371/journal.pone.0228543.g001>

(2-hydroxyethyl methacrylate) (pHema) and paper fibers was investigated. In the case of pHema the dyes were physically mixed in alkaline conditions into the pHema matrix. In the case of DCCH this increases the QY significantly by almost a factor of 5 whereas it decreases for the FTSC. An increase of quantum yields of dyes has been reported due to the immobilization of chemical groups.[26] The FTSC appears to be slightly quenched in the matrix. In the

Table 1. Quantum yield [-] of DCCH and FTSC for different solvents and pH value. The QY was determined by a relative measurement. Repeated measurements yielded an error of 20%.

Solvent Dye	H ₂ O	DMF	DMSO	THF	THF modified	pHema	Paper Fibers
DCCH	0.01	0.01	0.00	0.04	-	-	-
DCCH alkaline	0.01	0.02	0.01	0.04	0.19	0.14	0.23
FTSC	0.51	0.23	0.16	0.20	-	-	-
FTSC alkaline	0.23	0.26	0.10	0.29	-	0.12	0.41

<https://doi.org/10.1371/journal.pone.0228543.t001>

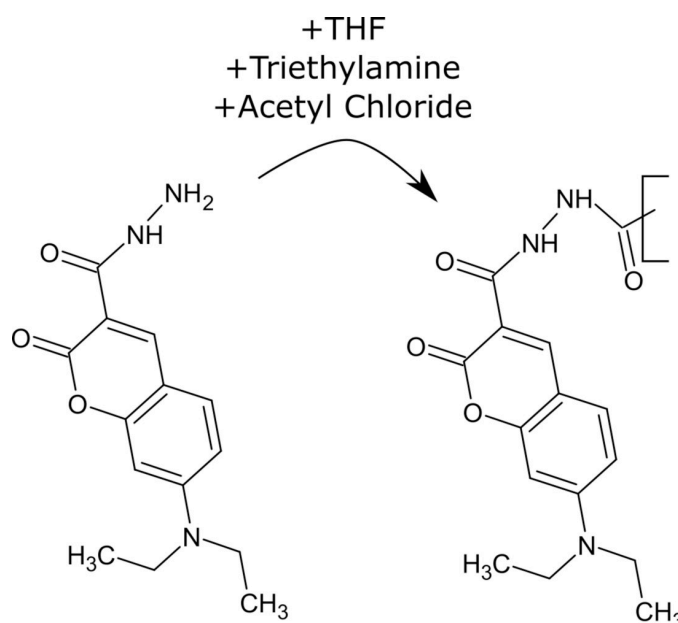


Fig 2. Chemical modification of the hydrazide group by acetylation with acetyl chloride. The resulting hydrazine increases the QY of the Coumarin by a factor of 5.

<https://doi.org/10.1371/journal.pone.0228543.g002>

case of the paper fibers the dyes were chemically bonded into the fiber matrix which lead to a strong increase in the QY which is likely a combination of the increase due to modification of the molecule and the immobilization effect described earlier. The dyeing is explained in the paper of Urstöger et al. [21]

Fluorescence spectra

Further important spectroscopic quantities for FRET are the fluorescence excitation and emission spectra of the molecules. They can be seen in Figs 3 and 4. Under the condition that the excitation spectra of the respective acceptor do not vary too much from the attenuation coefficient one can here nicely see the spectral overlap that is a necessary condition for FRET as seen in Eqs 2 and 3.

In Fig 3A and 3C the spectra of DCCH and FTSC in H₂O, in neutral, and in alkaline conditions are plotted. Compared to the attenuation Coefficient the excitation spectra of DCCH are in both cases shifted to the blue by about 10 nm. For FTSC, the maxima of the excitations coincide with the maxima of the attenuation Coefficients. In Fig 3C and 3D the spectra of the molecules in THF can be seen. The most prominent feature in this data is the strong blue shift of the FTSC excitation and emission spectrum. In THF the EX/EM peaks appear at 330 and 390 nm, respectively. This leads to a switch in the roles concerning a FRET application. In neutral THF the FTSC, shifts so strongly to the blue that it now takes on the role of the donor while the DCCH stays roughly the same and becomes the acceptor. The resulting spectra of FTSC in alkaline THF were low in intensity which is the reason why they appear quite noisy in the normalized graphs. We believe this is mainly due to the very low attenuation coefficient. Also the systems exhibit many excitation peaks which are likely due to varying amount of fluorescein in different protonation states.[23] The excitation spectra of DCCH in THF are consistent with the attenuation coefficient measurements of Fig 1. In Fig 4 the spectra of the molecules in DMF and DMSO can be seen. Due to the similarity of the solvents regarding many of their

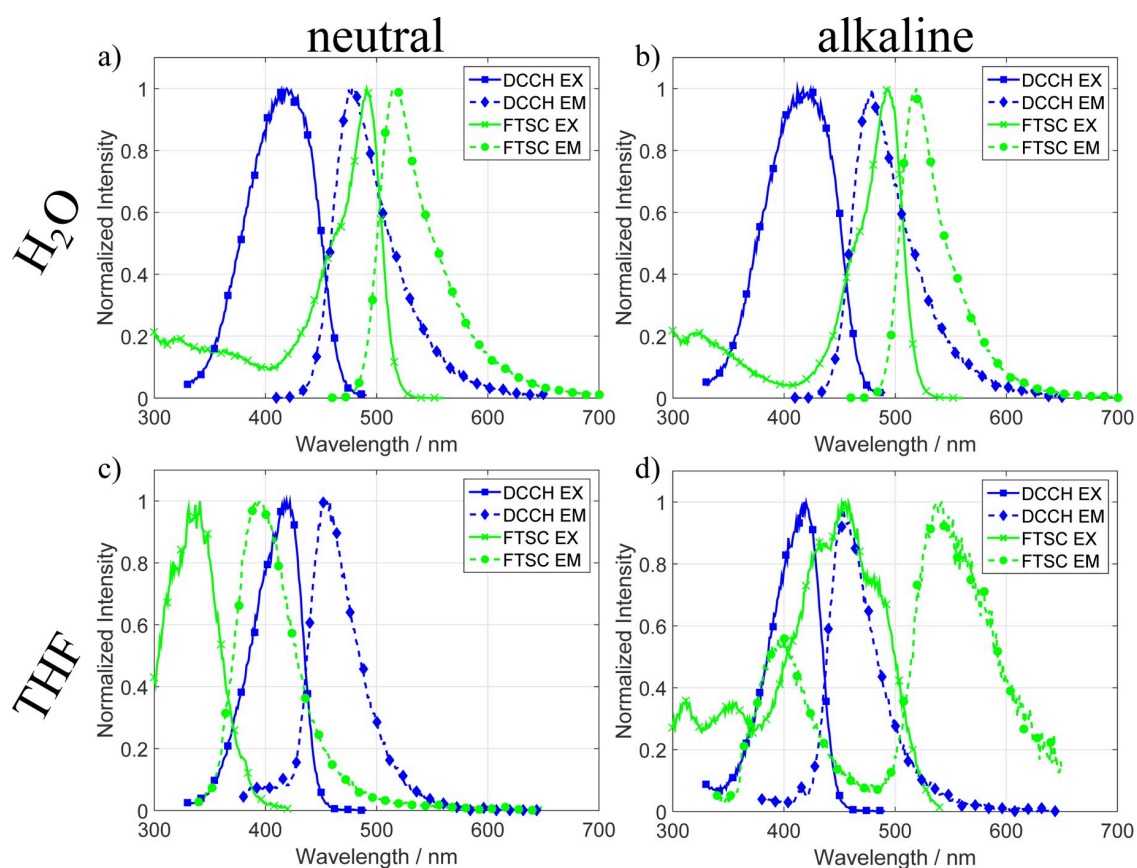


Fig 3. Normalized excitation and emission spectra of DCCH and FTSC in different solvents and pH values. In a) and b) one can see the spectra in water under neutral and alkaline conditions. One important feature in c) and d) is that in the neutral solution the FTSC spectra shift strongly (130–150 nm) into the blue compared to the H₂O spectra. In the alkaline solution the spectra shift back to the red and exhibit many side excitations.[22].

<https://doi.org/10.1371/journal.pone.0228543.g003>

properties, the investigated spectra look quite similar. However, compared to H₂O and THF there are many differences. First one can see in Fig 4A and 4C the same trend as in THF, namely that the FTSC EX/EM shifts so far to the blue that it takes on the role of acceptor. Compared to each other the excitation and emission spectra of FTSC in DMF and DMSO in neutral as well as in alkaline conditions look very similar. With the one difference that in DMF, FTSC exhibits an additional emission at 410 nm. The excitation spectra also look very similar to each other and also correlate to the attenuation coefficient measurements. DCCH shows a different behavior. First, the emission spectrum of the molecule is only weakly affected by the solvent or the pH conditions of the system. Second, the excitation changes quite strongly. Especially in DMF the excitation spectrum exhibits suddenly two excitations at 370 and 450 nm from which the 450 nm excitation is also much narrower than all the other recorded ones. In alkaline conditions (Fig 4B and 4D) both spectra exhibit an excitation peak at approx. 390 nm while the emission maximum is around 460 nm.

One explanation for the shifting spectra of FTSC is again the well-known pH dependence of the molecule.[23] Different protonation levels shift the electronic structure in such a way that a different transition becomes more probable. This is especially visible in the cases of THF, DMF and DMSO in which the shift of the maxima ranges up to 180 nm. Another effect on the spectra is caused by the interaction with the solvents themselves. Depending on the

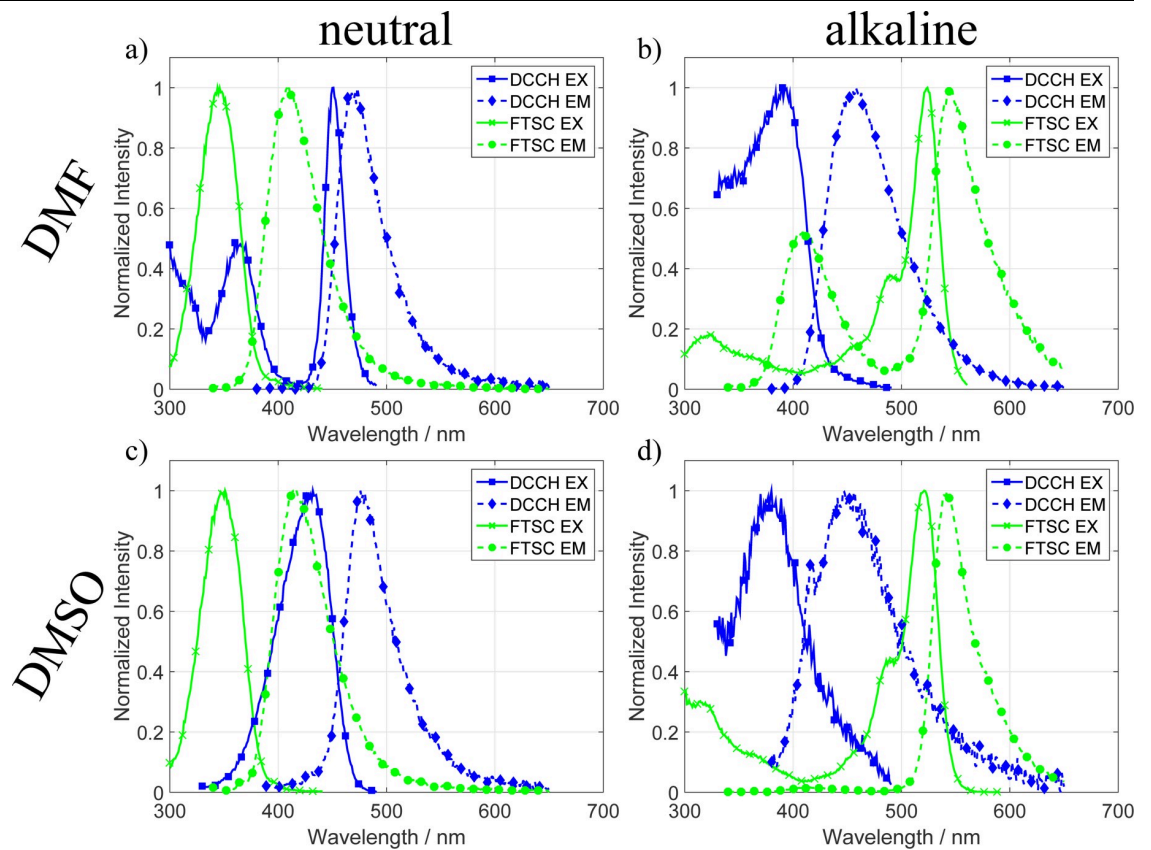


Fig 4. Normalized excitation and emission spectra of DCCH and FTSC in different solvents and pH values. In a) and b) one can see the spectra in DMF. Here the FTSC EX/EM shifts to 340/410 nm in the neutral case and shifts back to higher wavelengths (520/540 nm) in alkaline conditions where it additionally exhibits a second emission at 410 nm. The DCCH main excitation becomes narrower and a second excitation at 370 nm appears in the neutral state. Going to alkaline conditions shifts the DCCH spectra into the blue. c) and d) show the spectra in DMSO. The spectra for FTSC look quite similar as in DMF with the exception of the missing additional emission at 410 nm in the alkaline state. The DCCH spectra for the alkaline conditions are similar while in the neutral state the excitation spectrum shifts a few nm into the blue and the spectra become wider.

<https://doi.org/10.1371/journal.pone.0228543.g004>

polarity and the strength of the interaction of the solvent molecules with the dyes the peaks can shift, change their width or even exhibit additional peaks. The combination of the two investigated dyes in one solvent determines to a large extent whether the dyes are compatible when they are used as a FRET pair.

Förster distance

Having all the necessary data for the calculation measured, the Förster distances given by Eq 2 depending on pH and solvent were calculated. As can be seen in Table 2 the radius can range from 1.82 to 3.10 nm. The different radii can be put into two groups depending on which molecule, DCCH or FTSC, takes on the part of the donor in the FRET pair. In Table 2, this has

Table 2. Förster distance in nm of the DCCH and FTSC pair in dependence of solvent and pH value. The D and the F in the Table represent whether DCCH or FTSC took the role of the Donor in the combination, respectively. The other molecule was the acceptor.

Solvent pH	H ₂ O	DMF	DMSO	THF
Neutral	D 2.5 ± 0.6	F 3.1 ± 0.7	F 2.9 ± 0.7	F 2.9 ± 0.7
With base	D 2.9 ± 0.7	D 3.0 ± 0.7	D 2.6 ± 0.6	D 1.8 ± 0.5

<https://doi.org/10.1371/journal.pone.0228543.t002>

been marked with a D or an F depending whether DCCH or FTSC takes the part of the Donor, respectively. The variation in the Förster radius has an influence on the application of a chosen FRET pair to investigate the interaction between molecules. Depending on the solvent and on the pH value the distance dependence of the Förster transfer will be different. This means that a chosen FRET pair might work in one solvent or pH but fail under changing conditions. This is true whether FRET is qualitatively or quantitatively used to investigate a system. Qualitatively, this means that an interaction might not be detected due to a too far distance. If FRET is used to quantitatively study the interaction between molecules a changing Förster distance needs to be considered when performing the calculations as it can be a source of error.

FRET system

In this section we show under which of the previously discussed systems we were able to observe a Förster transfer and which conditions did not. The key difference in the two experimental series seen in Figs 5 and 6 was the concentration of the dyes in the solvents. In the first trial (Fig 5) all the measurements were performed with concentrations of 0.1 mM. With these concentrations we were only able to get a FRET signal using DMF and DMSO.

As mentioned in the experimental section it is possible to go to higher concentrations while avoiding the inner filter effect by using a capillary. By doing this we were able to detect in 3 more of the 8 investigated systems a FRET signal. The positive systems can be seen in Fig 6.

In total, we were able to get a FRET signal in 5 of the 8 investigated systems. The quantified parameters can be seen in Table 3. Interestingly 3 of the 5 positive systems, namely in THF, DMF and DMSO, were achieved with the FTSC molecule taking on the role of the Donor although the initial thought was to use it as the acceptor. It was also under these conditions that the FRET efficiency was the highest. A Table with the performed calculations of the FRET efficiencies can be found in the S1 File. By comparing the values in Table 3 it becomes obvious that the highest FRET efficiencies were achieved when both, the quantum yield of the donor and the molar attenuation coefficient of the acceptor, were large.

One of the most compelling techniques to investigate FRET systems would be fluorescence lifetime imaging (FLIM) which measures the FRET efficiency by the decrease of the characteristic lifetime the donor has due to the presence of acceptor molecules. Unfortunately, the

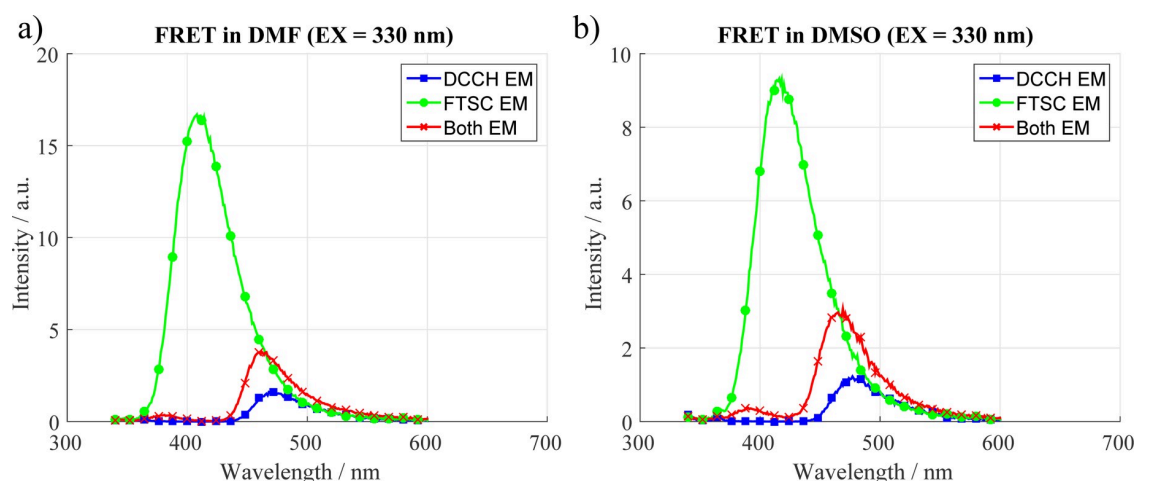


Fig 5. Fluorescence measurements with a concentration of 0.1 mM. When the dyes are mixed together the FTSC fluorescence is quenched and the DCCH fluorescence is enhanced which is a clear sign of FRET.

<https://doi.org/10.1371/journal.pone.0228543.g005>

authors did not have access to FLIM although we encourage future readers to use the technique additionally to others as it is such a valuable tool to investigate the FRET response of a system. Due to the underlying investigation it was possible to develop an already published method to investigate interactions between surfaces by measuring the adhesion between pHema thin films dyed with DCCH and FTSC. [21]

Conclusions

In this work, 7-(diethylamino)coumarin-3-carbohydrazide (DCCH) and fluorescein-5-thiosemicarbazide (FTSC) were investigated regarding their respective spectral properties in different solvents and under changing pH conditions with the goal of finding an optimal Förster Resonance Energy Transfer (FRET) pair. DCCH and FTSC do not appear to perform well in FRET experiments. On the one hand this is due to the strong dependence of the environment of the FTSC and on the other hand due to the low quantum yield of DCCH. Additionally, the FTSC is almost completely quenched (molar attenuation coefficient) when dissolved in DMF, DMSO or THF. After a chemical modification of DCCH it could be shown that the quantum yield improves significantly which leads to a better dye performance. The Förster Radii for different environmental conditions were determined and it was shown that they are slightly affected by solvent and pH. Therefore, for measuring and quantifying FRET one needs to carefully and meticulously determine and control the environmental influences and conditions under which

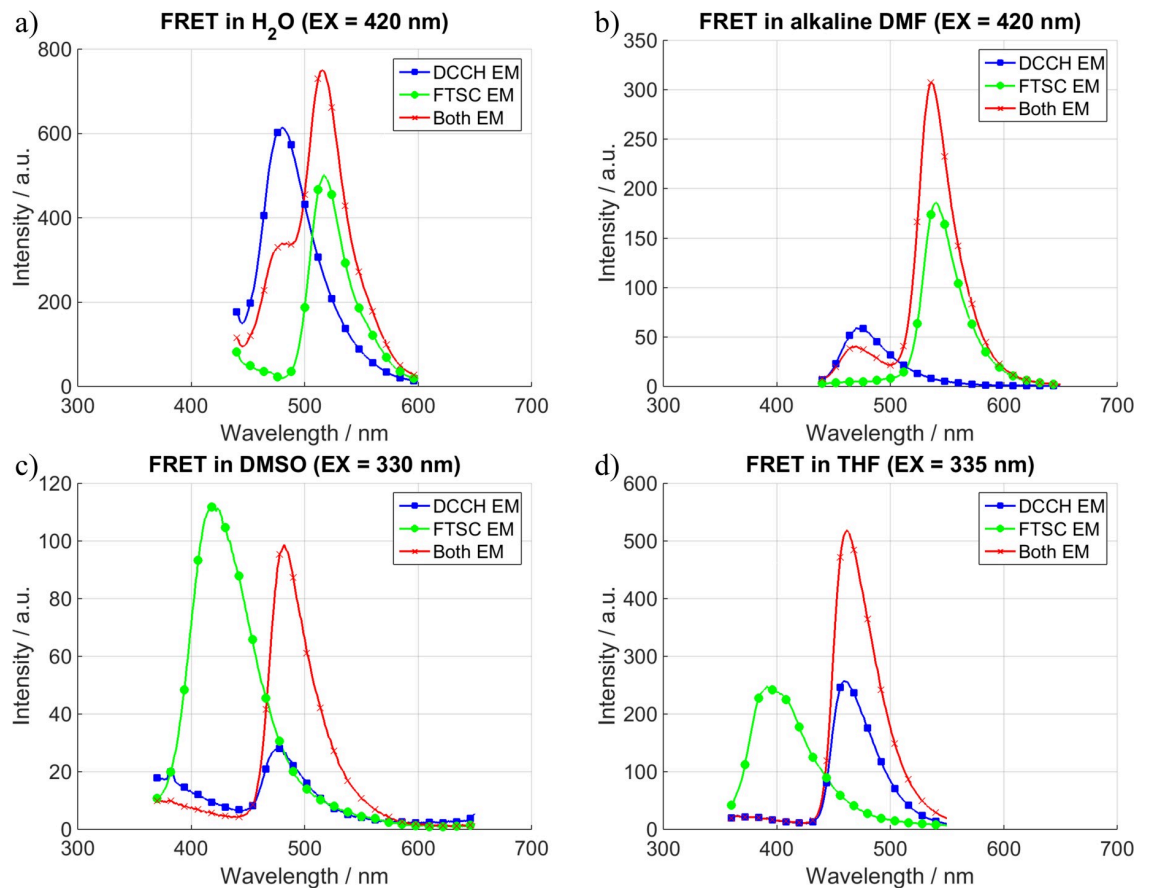


Fig 6. FRET measurements using a capillary and thus going to higher concentrations. Due to the higher concentration a FRET signal is also detected under other conditions. (Conc. H₂O = 0.15 mM, conc. Other = 1 mM).

<https://doi.org/10.1371/journal.pone.0228543.g006>

Table 3. Comparison between relevant parameters and the resulting FRET signal. The reported attenuation coefficient is the area under the measured curve and the provided FRET efficiency stems from acceptor sensitisation (Eq 4). The results for donor quenching can be found in the S1 File.

Solvent	Donor Molecule	Attenuation Coefficient Acceptor [$M^{-1} cm^{-1}$]	QY Donor [-]	R_0 [nm]	FRET Efficiency / [%]
H ₂ O	DCCH	3.1E+5	0.01	2.5	3
H ₂ O alkaline	DCCH	5.9E+5	0.01	2.9	0
DMF	FTSC	2.9E+6	0.23	3.1	73
DMF alkaline	DCCH	7.2E+5	0.02	3.0	2
DMSO	FTSC	2.2E+6	0.16	2.9	15/22*
DMSO alkaline	DCCH	1.4E+6	0.01	2.6	0
THF	FTSC	2.3E+6	0.2	2.9	9
THF alkaline	DCCH	2.5E+4	0.04	1.8	0

*15/22 corresponds to the efficiency in the lower (0.1 mM) and higher (1 mM) concentrated solutions, respectively.

<https://doi.org/10.1371/journal.pone.0228543.t003>

one wants to measure an interaction. Finally, it was observed in three cases that the initially intended donor (DCCH) and acceptor (FTSC) switched their role in the case of certain environmental conditions (DMF, DMSO, THF). In these cases, the FRET efficiency was the highest because these systems had the highest quantum yield of the donor and the highest molar attenuation coefficient of the acceptor. These investigations of the FRET systems in solution were later adapted to measure adhesion between pHEMA films. [21]. Cellulosic surfaces, however, are developing full adhesion only when they are in contact during drying from the water swollen state[27]. The investigated system therefore is, due to the instability of its fluorescence characteristics in water, only partly suited to study the adhesion between cellulosic surfaces.

Supporting information

S1 File.
(DOCX)

Author Contributions

Conceptualization: Ulrich Hirn.

Funding acquisition: Ulrich Hirn.

Investigation: Georg Urstöger, Andreas Steinegger, Robert Schennach, Ulrich Hirn.

Methodology: Andreas Steinegger, Robert Schennach, Ulrich Hirn.

Supervision: Robert Schennach, Ulrich Hirn.

Writing – original draft: Georg Urstöger, Robert Schennach, Ulrich Hirn.

Writing – review & editing: Georg Urstöger, Robert Schennach, Ulrich Hirn.

References


1. Chang Q, Sipior J, Lakowicz JR, Rao G. A Lifetime-Based Fluorescence Resonance Energy Transfer Sensor for Ammonia. *Analytical Biochemistry*. 1995 Nov 1; 232(1):92–7. <https://doi.org/10.1006/abio.1995.9955> PMID: 8600839
2. Chiu Y-L, Chen S-A, Chen J-H, Chen K-J, Chen H-L, Sung H-W. A Dual-Emission Förster Resonance Energy Transfer Nanoprobe for Sensing/Imaging pH Changes in the Biological Environment. *ACS Nano*. 2010 Dec 28; 4(12):7467–74. <https://doi.org/10.1021/nn102644u> PMID: 21082810
3. Th Förster. Zwischenmolekulare Energiewanderung und Fluoreszenz. *Ann Phys*. 1948 Jan 1; 437(1–2):55–75.
4. Dexter DL. A Theory of Sensitized Luminescence in Solids. *The Journal of Chemical Physics*. 1953 May 1; 21(5):836–50.

5. Knox RS. Förster's resonance excitation transfer theory: not just a formula. *J Biomed Opt.* 2012; 17(1):0110031–6.
6. Rowland CE, Brown CW, Medintz IL, Delehanty JB. Intracellular FRET-based probes: a review. *Methods Appl Fluoresc.* 2015 Oct 29; 3(4):042006. <https://doi.org/10.1088/2050-6120/3/4/042006> PMID: 29148511
7. Sukhanova A, Susha AS, Bek A, Mayilo S, Rogach AL, Feldmann J, et al. Nanocrystal-Encoded Fluorescent Microbeads for Proteomics: Antibody Profiling and Diagnostics of Autoimmune Diseases. *Nano Lett.* 2007; 7(8):6.
8. Thomson CI, Lowe RM, Ragauskas AJ. Imaging cellulose fibre interfaces with fluorescence microscopy and resonance energy transfer. *Carbohydrate Polymers.* 2007 Jul 2; 69(4):799–804.
9. Thomson CI, Lowe RM, Ragauskas AJ. First characterization of the development of bleached kraft softwood pulp fiber interfaces during drying and rewetting using FRET microscopy. *Holzforschung.* 2008; 62(4):383–388.
10. Förster T. Energy migration and fluorescence. *JBO, JBOPFO.* 2012 Feb; 17(1):011002.
11. Meer BW van der. Förster Theory. In: *FRET—Förster Resonance Energy Transfer* [Internet]. Wiley-Blackwell; 2013 [cited 2018 Aug 1]. p. 23–62. Available from: <https://onlinelibrary.wiley.com/doi/abs/10.1002/9783527656028.ch03>
12. Berney C, Danuser G. FRET or No FRET: A Quantitative Comparison. *Biophysical Journal.* 2003 Jun 1; 84(6):3992–4010. [https://doi.org/10.1016/S0006-3495\(03\)75126-1](https://doi.org/10.1016/S0006-3495(03)75126-1) PMID: 12770904
13. Gordon GW, Berry G, Liang XH, Levine B, Herman B. Quantitative Fluorescence Resonance Energy Transfer Measurements Using Fluorescence Microscopy. *Biophysical Journal.* 1998 May; 74(5):2702–13. [https://doi.org/10.1016/S0006-3495\(98\)77976-7](https://doi.org/10.1016/S0006-3495(98)77976-7) PMID: 9591694
14. Greenham NC, Samuel IDW, Hayes GR, Phillips RT, Kessener YARR, Moratti SC, et al. Measurement of absolute photoluminescence quantum efficiencies in conjugated polymers. *Chemical Physics Letters.* 1995 Jul 14; 241(1):89–96.
15. Pålsson L-O, Monkman AP. Measurements of Solid-State Photoluminescence Quantum Yields of Films Using a Fluorimeter. *Advanced Materials.* 2002 May 17; 14(10):757–8.
16. Porrès L, Holland A, Pålsson L-O, Monkman AP, Kemp C, Beeby A. Absolute Measurements of Photoluminescence Quantum Yields of Solutions Using an Integrating Sphere. *J Fluoresc.* 2006 Mar 1; 16(2):267–73. <https://doi.org/10.1007/s10895-005-0054-8> PMID: 16477506
17. Williams ATR, Winfield SA, Miller JN. Relative fluorescence quantum yields using a computer-controlled luminescence spectrometer. *The Analyst.* 1983; 108(1290):1067.
18. Würth C, Grabolle M, Pauli J, Spieles M, Resch-Genger U. Relative and absolute determination of fluorescence quantum yields of transparent samples. *Nat Protoc.* 2013 Aug; 8(8):1535–50. <https://doi.org/10.1038/nprot.2013.087> PMID: 23868072
19. Brouwer AM. Standards for photoluminescence quantum yield measurements in solution (IUPAC Technical Report). *Pure and Applied Chemistry.* 2011; 83(12):2213–2228.
20. Senthilkumar S, Nath S, Pal H. Photophysical Properties of Coumarin-30 Dye in Aprotic and Protic Solvents of Varying Polarities. *Photochemistry and Photobiology.* 2004 Jul 1; 80(1):104–11.
21. Urstöger G, Simoes MG, Steinegger A, Schennach R, Hirn U. Evaluating the degree of molecular contact between cellulose fiber surfaces using FRET microscopy. *Cellulose.* 2019 Aug 1; 26(12):7037–50.
22. Klonis N, Sawyer WH. Spectral properties of the prototropic forms of fluorescein in aqueous solution. *Journal of Fluorescence.* 1996 Sep; 6(3):147–57. <https://doi.org/10.1007/BF00732054> PMID: 24227203
23. Sjöback R, Nygren J, Kubista M. Absorption and fluorescence properties of fluorescein. *Spectrochimica Acta Part A: Molecular and Biomolecular Spectroscopy.* 1995 Jun; 51(6):L7–21.
24. Raikar US, Renuka CG, Nadaf YF, Mulimani BG, Karguppikar AM, Soudagar MK. Solvent effects on the absorption and fluorescence spectra of coumarins 6 and 7 molecules: Determination of ground and excited state dipole moment. *Spectrochimica Acta Part A: Molecular and Biomolecular Spectroscopy.* 2006 Nov; 65(3–4):673–7.
25. Krafft GA, Sutton WRandall, Cummings RT. Photoactivable fluorophores. 3. Synthesis and photoactivation of fluorogenic difunctionalized fluoresceins. *Journal of the American Chemical Society.* 1988 Jan; 110(1):301–3.
26. Rouhani F, Morsali A, Retailleau P. Simple One-Pot Preparation of a Rapid Response AIE Fluorescent Metal–Organic Framework. *ACS Appl Mater Interfaces.* 2018 Oct 24; 10(42):36259–66. <https://doi.org/10.1021/acsami.8b12404> PMID: 30259725
27. Hirn U, Schennach R. Fiber-fiber bond formation and failure: mechanisms and analytical techniques. In: *Proceedings of the 16th fundamental research symposium, Oxford.* 2017. p. 839–64.

3. Paper B



Evaluating the degree of molecular contact between cellulose fiber surfaces using FRET microscopy

Georg Urstöger · Monica G. Simoes · Andreas Steinegger · Robert Schennach · Ulrich Hirn 

Received: 15 April 2019 / Accepted: 17 June 2019 / Published online: 26 June 2019
© The Author(s) 2019

Abstract The degree of molecular contact, i.e. the contact area on the nanometer scale, between paper fibers is crucial for the van-der-Waals and hydrogen bond adhesion between the fibers and thus for the fiber-fiber bond strength. We apply Förster resonance energy transfer (FRET) to investigate the degree of contact in the distance range of 1–10 nm between pulp fiber bonds and between thin films. The FRET system with DCCH and FTSC as fluorescence dyes has been validated for spectrophotometry and for local imaging with widefield microscopy, using pHema thin films. Bonding between thin films can be detected with this

system, however it has not been possible to achieve a significant FRET signal between bonded pulp fibers. Therefore, we conclude that in principle it is possible to quantify the degree of contact between two surfaces on the nanometer scale with the investigated FRET system. For further work on pulp fibers we recommend an exclusively surface active dyeing, as bulk dyeing massively deteriorates the signal to noise ratio which is likely the reason for the low FRET signal found in this work.

Electronic supplementary material The online version of this article (<https://doi.org/10.1007/s10570-019-02575-x>) contains supplementary material, which is available to authorized users.

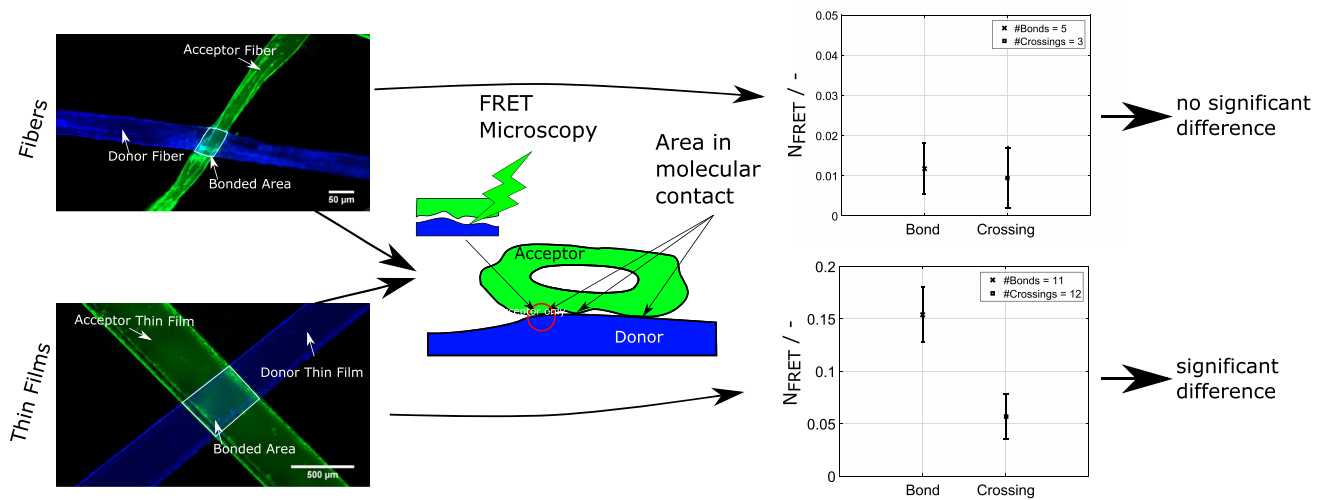
G. Urstöger · M. G. Simoes · U. Hirn (✉)
Institute of Paper-, Pulp- and Fibre Technology TU Graz,
Inffeldgasse 23, 8010 Graz, Austria
e-mail: ulrich.hirn@tugraz.at

A. Steinegger
Institute of Analytical Chemistry and Food Chemistry TU
Graz, Stremayrgasse 9/II, 8010 Graz, Austria

R. Schennach
Institute of Solid State Physics TU Graz, Petersgasse 16/2,
8010 Graz, Austria

G. Urstöger · R. Schennach · U. Hirn
CD Laboratory for Fiber Swelling and Paper Performance,
Inffeldgasse 23, 8010 Graz, Austria

Graphic Abstract



Keywords Adhesion · FRET · Contact mechanics · Förster resonance energy transfer · Cellulose fibers

Introduction

The strength of a paper sheet crucially depends on the strength of the adhesion between the bonded paper fibers. The fiber surfaces are not covalently bonded, still they exhibit adhesion between each other due to hydrogen bonding, van der Waals forces and Coulomb interaction (Lindström et al. 2005; Hirn and Schennach 2015). For hydrogen and van der Waals bonding the surfaces have to be closer than approximately 1 nm. The contact area on the nanometer scale between the surfaces thus is in direct proportion to the adhesion between the surfaces (Persson 2003; Persson et al. 2004). This contact area on the nanometer scale is often termed “real contact area” or “area in molecular contact” (AIMC).

Measuring the area in molecular contact using imaging techniques is difficult as illustrated in Fig. 1. Regions that appear to have full contact at a given imaging resolution turn out to be only partially bonded when imaged using a higher imaging resolution (Yang et al. 2008). Hence the area in molecular contact between two surfaces appears smaller and smaller as the resolution of the imaging technique increases. In order to provide relevant results for adhesion the bonding area has to be evaluated on the sub-nanometer scale (Hirn and Schennach 2017).

A detailed review on the different approaches to measure area in molecular contact in fiber-fiber bonds can be found in the work of Hirn et al. (2013). Different imaging methods have been applied like polarized light microscopy (Kappel et al. 2010) or X-ray tomography (Sormunen et al. 2019). Both techniques are not able to resolve the bonding region in the nanometer range. Transmission electron microscopy (Asunaa and Steenberg 1958) is close to the relevant optical resolution, however the sampling area becomes so small that this method is also not suitable to provide quantitative results. Another approach to measure AIMC are adsorption based methods. The idea here is e.g. to dye fiber fiber bonds, then break the bonds and look which fraction of the bonding area is colored (Torgnysdotter et al. 2007), implying that the uncolored areas have previously been bonded. Similarly BET nitrogen absorption on paper sheets is used as an indicator for AIMC, e.g. Haselton (1954). The problem with these methods also becomes visible in Fig. 1. Unbonded areas can be surrounded by bonded regions, making them inaccessible for the adsorbent (dye or nitrogen). Adsorption based methods thus are also not able to quantify the AIMC.

Our approach to measure this area is Förster Resonance Energy Transfer Microscopy (FRET). The working principles of FRET are schematically explained in Fig. 2. It is based on the electromagnetic interaction (dipole-dipole interaction) between two dyes, a donor and an acceptor molecule (Förster 1948). When the donor dye molecule is excited two things

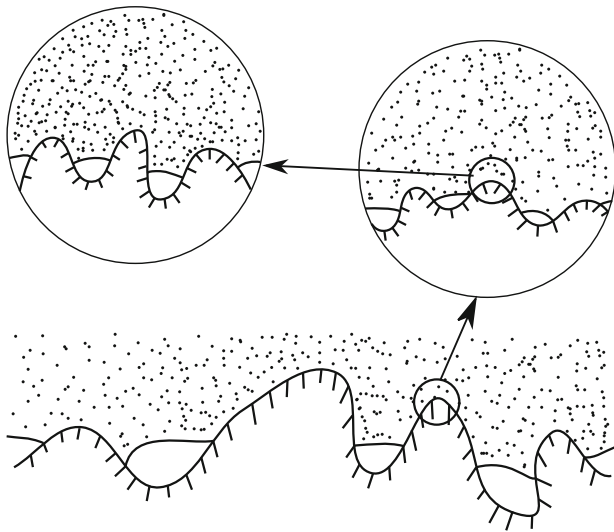


Fig. 1 Two surfaces in physical contact investigated under increasing magnification. As the magnification increases one can see that less area is in contact. Adapted from Persson et al. (2004)

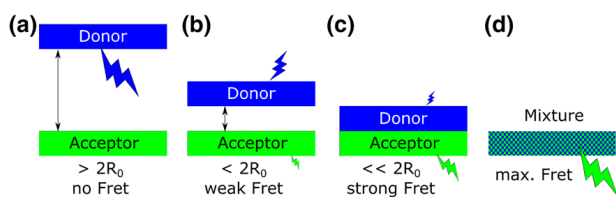


Fig. 2 Explanation of the FRET effect. A FRET signal occurs if the distance between the dye molecules is smaller than $2R_0$ (Förster Radius). In the cases **a–c** either surface is dyed with donor or acceptor dye, respectively. In this study the surfaces will be paper fibers (or polymer films). The donor dye is excited with light. As the donor and acceptor molecules between the surfaces come closer the acceptor fluorescence (FRET signal) increases and the donor fluorescence decreases. For a mixture of the dyes **d** a maximum FRET signal is observed

can happen. If an acceptor molecule is close the donor transfers its energy, by a non-radiative interaction, to the acceptor (Fig. 2c). The acceptor molecule is then emitting a photon, showing FRET fluorescence. The key point is that this FRET energy transfer, and the subsequent fluorescence of the acceptor molecule, only takes place if the donor and acceptor dye are close enough to each other, i.e. below 12 nm (Meer 2013). If there is no acceptor molecule close to the donor molecule, the donor emits a photon (Fig. 2a). The key prerequisite for FRET is that the fluorescence spectra of donor and acceptor are different but have a spectral overlap (see Fig. 4). By exciting the donor dye and recording the spectrum of the light emitted from the

sample the amount of energy transferred to the acceptor dye can be measured. Also it should be mentioned here that additionally to the distance of the dyes also the orientation of the dipoles plays a role in the efficiency of the transfer.

For our work we are exploiting FRET to measure the degree of molecular contact between pulp fibers (and also between polymer thin films). The basic principle is sketched in Fig. 2a–c. There, one can see two blocks labelled donor and acceptor. These blocks stand for paper fibers where one fiber is dyed with the donor molecule and the other one with the acceptor molecule. A FRET signal is only possible if the distance between these two surfaces becomes sufficiently small. Hence in this work we were using FRET to investigate the degree of bonding between paper fibers and model thin films. The key reason why FRET is a suitable technique for measuring the AIMC is that it operates on the relevant size scale for van-der-Waals and hydrogen bonding, i.e. a signal is only obtained if the two surfaces have a distance below 12 nm. If the surfaces are further apart than the critical distance $2R_0$ there is no FRET signal and only donor fluorescence (Fig. 2a). When the surfaces get closer there is an increasingly high acceptor fluorescence (i.e. FRET signal) with simultaneously decreasing donor fluorescence (b, c). When mixing the dyes together, e.g. in a polymer film, we obtain a very strong FRET signal, compare Fig. 2d. This configuration is used as a positive control as a mixture of molecules (with the same concentration as for the samples) provides an upper limit for the possible FRET intensity.

Literature reports qualitative work on FRET applied to fiber fiber bonds (Thomson et al. 2007, 2008a, b). In this work we are providing a quantitative investigation on FRET as a tool to measure the degree of nanoscale contact in fiber to fiber bonds. It will be demonstrated that with the employed technique it is not possible to measure a valid FRET signal between paper fibers. Nevertheless, it will also be shown that the proposed setup is a working FRET system, which will be demonstrated using pHema thin films.

Experimental

Förster resonance energy transfer (FRET)

The following brief introduction to Förster Theory was taken from the book by B.W. Van der Meer (Meer 2013) and is based partly on the original papers by Förster. The efficiency of the energy transfer between donor and acceptor dye depends on the distance between the two molecules, and is in principle determined by the Förster Radius (R_0). The Förster Radius can be calculated for every combination of donor and acceptor molecules as can be seen in the supplementary information (Table S1). R_0 is specific for every donor-acceptor pair in a particular system. The efficiency of the energy transfer (η_{eff}) between donor and acceptor is given by Eq. 1:

$$\eta_{eff} = \frac{1}{1 + \left(\frac{r}{R_0}\right)^6} \quad (1)$$

where r stands for the distance between the donor and acceptor and R_0 stands for the Förster radius of the donor-acceptor pair. Practically, the FRET efficiency can be measured by different methods which can be implemented in either microscopy setups or measured by spectrophotometry, both of which were used in this paper.

Regardless of the measurement method, a FRET process can be detected by different aspects of the effect. FRET changes the Donor emission intensity (Donor quenching), the acceptor emission intensity (Acceptor sensitisation), the lifetime of donor fluorescence (Lifetime measurements) and the polarization of the light (Anisotropy measurements). Here we used two of the more common methods to measure FRET, namely donor quenching (DQ) and acceptor sensitisation (AS). Donor quenching measures the decrease of the donor fluorescence due to FRET. Acceptor sensitisation measures the increase of the acceptor fluorescence due to FRET. While DQ is an indication for FRET, one cannot be certain of it, as there are other mechanisms such as concentration quenching that can deactivate the excited donor. AS on the other hand provides conclusive evidence for FRET as the acceptor fluorescence can only be increased by some sort of energy transfer (Meer 2013). An excellent review about implementation and the pitfalls of the technique is provided by Broussard et al. (2013). One crucial

part of using FRET that should be mentioned here is to meticulously check if the signal is indeed valid especially when spectroscopic data is not available. This can be done by using negative controls, dynamic FRET or applying more than one FRET technique.

Materials

The dyes 7-(diethylamino)coumarin-3-carbohydrazide (DCCH, Purity 95%, CAS: 100343-98-4) and fluorescein-5-thiosemicarbazide (FTSC, Purity 99%, CAS: 76863-28-0) were bought from Santacruz Biotechnology. Solvents N,N-dimethylformamide (DMF), Tetrahydrofuran (THF), and Acetonitril were purchased from VWR. All chemicals were used without further purification. Poly(2-hydroxyethyl methacrylate) (pHEMA) for manufacturing of thin films was purchased from Sigma Aldrich. The model films were deposited on PET foils. The pulp used was an unbleached softwood Kraft pulp from industrial production.

Sample preparation

For investigating pulp fibers [bleached Kraft wood, ratio spruce/pine (90/10)], the samples were prepared as described by Thomson et al. (2007). Fibers were dyed in 15 mL of a solution of either dye in DMF (1 mmol/L and 0.2 mmol/L) overnight at a pH of 5, adjusted by adding HCl. The dyes form a meta-stable bond with the reducing end of the cellulose molecule and by adding HCl this equilibrium is shifted towards the meta-stable bond species side. After the dyeing, sodium borohydrate NaBH_4 (0.02 mmol NaBH_4 per 0.5 g fibers) was added immediately to the solution and allowed to react for 1 h. The sodium borohydrate leads to a reductive amination of the dyes with the cellulose which results in a covalent bond between the reagents. After this reductive amination the samples were first washed in DMF and again washed by Soxhlet extraction with acetonitrile for at least 4 h to remove any non-covalently bonded dye. Subsequently the dyed fibers were stored in an aqueous pH 9 buffer solution using 0.4 g/L borax. The fiber bonds were prepared by crossing one DCCH dyed and one FTSC dyed fiber in a droplet of water (pH 9) and subsequently drying them in a Rapid Köthen sheet former. For microscopy the fiber bonds were then transferred to microscopy slides. Fiber

Crossings (negative control for FRET) were prepared by simply crossing two fibers and covering them with a microscopy cover slip.

The model films were prepared by doctorblading 500 μL of a 10% pHema in a 95/5 EtOH/H₂O solution mixed with dyes dissolved in THF onto PET foils. This resulted in an approx. 1.5 μm thick film. To ensure alkaline conditions a volume of 12 μL triethylamine was added to the solution. The PET foils were cleaned with acetone before the doctorblading. FRET was investigated in two different model systems. In the first trial (Mixture sample) the dyes were added to the film as follows. Donor in pHema, Acceptor in pHema and Donor + Acceptor in pHema. The interaction of molecules within this film was investigated. In a second step (Bonds and Crossings) two films (Donor in pHema, Acceptor in pHema) were prepared, stacked together and left at 1 bar pressure at 93 °C for 3 h to form contact. The concentrations and applied measurement methods for the samples can be seen in Table 1.

FRET from spectrophotometry

Fluorescence spectra were recorded on a RF-5301PC, spectrofluorophotometer from Shimadzu. FRET experiments were performed with concentrations of molecules seen in Table 1. Also care was taken to

minimize the exposure of any of the samples to ambient light to avoid photo bleaching. The model films were on the one hand investigated using this fluorometry setup and on the other hand they were investigated using a wide field microscope with the filter sets seen in Table 2. The spectra of the pHema films were recorded using the setup seen in Fig. 3. The samples were investigated under an angle that avoids the detection of the directly reflected light and only measures the fluorescence coming from the sample.

The efficiency of the FRET energy transfer is calculated from the measured spectra and is being explained in Fig. 4. Due to the energy transfer the donor emission is quenched (I_{DA}) with respect to the normal emission of the donor (I_D). The energy not emitted by the donor is then transferred to the acceptor and increases (or sensitizes) the emission (I_{AD}) compared to the normal acceptor sensitization (I_A). The spectral overlap seen in Fig. 4 is a necessary requirement for FRET and determines to a large extent the distance range of the effect as can be seen in Eq. 2.

$$R_0 = \left(\frac{9 \ln(10)}{128 \pi^5 N_A} (k^2 n^{-4} Q_D J) \right)^{1/6} \quad (2)$$

R_0 is the Förster radius, k is the orientation factor, n the refractive index, (Q_D) the quantum yield of the donor and J the overlap integral. The Förster radius determines the distance of the energy transfer as it is known

Table 1 Concentrations and parameters for the FRET measurements

Sample	Conc. donor (mmol/L)	Conc. acceptor (mmol/L)	FRET investigation	Instrument
pHema film	3	3	Mixture films	SP + WM
pHema bond/crossing	3	3	Between films	SP + WM
Fiber bonds	0.2	0.2	Between fibers	WM
Fiber crossings	0.2	0.2	Between Fibers	WM

WM wide field microscopy, SP spectroscopy

Table 2 Filter sets used for the Fluorescence Microscopy

Filter set	Excitation (nm)	Dichroic mirror (nm)	Emission
Donor (D)	436 \pm 10	455 long pass	480 \pm 20
Acceptor (A)	500 \pm 10	515 long pass	520 l. pass
FRET (F)	436 \pm 10	515 long pass	520 l. pass

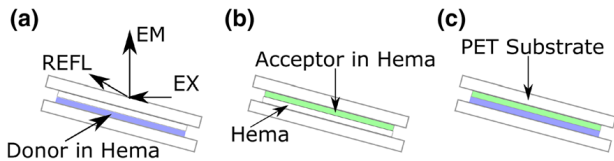


Fig. 3 Measurement setup of the pHema films in the fluorometry. In **a** the setup is explained in more detail. It was chosen such that the reflected (REFL) beam following the excitation (EX) of the sample does not hit the detector and only the fluorescence signal emitted (EM) directly from the sample will be detected. **a–c** The Donor, Acceptor and Donor-Acceptor samples as they were investigated

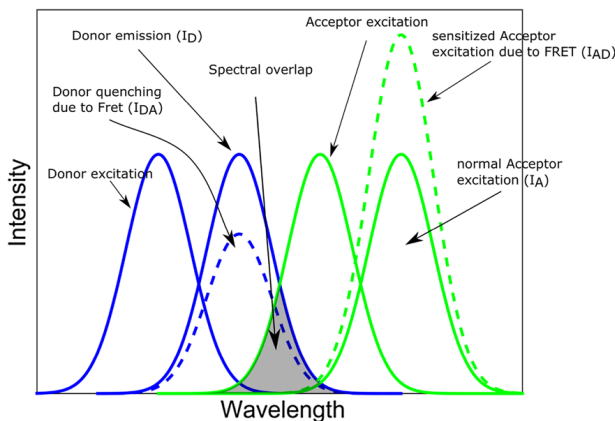


Fig. 4 Excitation and Emission spectra of a generic donor-acceptor pair. FRET affects the donor emission intensity (donor quenching) and the acceptor emission intensity (acceptor sensitization). Also the spectral overlap of the donor emission and the acceptor excitation spectrum is shown.

that quantification of FRET is only possible within distances ranging from $(\frac{1}{2} - 2)R_0$ as also depicted in Fig. 2. A detailed description on how to determine the Förster radius can be found in FRET—Förster Resonance Energy Transfer by Medintz and Hildebrandt (Meer 2013).

The fluorescence emission spectra of DCCH and FTSC overlap to a certain extent as seen in Fig. 7. Therefore, to get an accurate measurement of the FRET efficiency the spectra need to be spectrally unmixed. To do this in the spectrometer we fitted the emission peaks and used the area under the peaks as the intensity of the fitted signal. Practically this was done by fitting Gaussian peaks to the recorded emission spectra of a pure donor sample (resulted in I_D), a pure acceptor sample (resulted in I_A) and a sample of interest (resulted in I_{DA} and I_{AD}) such as in Fig. 11. The full fitting parameters can be found in the

supplementary information (Figure S3 and Table S2). The resulting intensity information was used with Eqs. 3 and 4 to get the FRET efficiency. For the donor quenching (Eq. 3) and acceptor sensitization (Eq. 4) the following equations were used.

$$\eta_{FRET} = 1 - \frac{I_{DA}}{I_D} \quad (3)$$

$$\eta_{FRET} = \left(\frac{I_{AD}}{I_A} - 1 \right) \frac{\epsilon_A}{\epsilon_D} \quad (4)$$

ϵ_A and ϵ_D are the extinction coefficients of the acceptor and donor at the excitation wavelength (Meer 2013; Clegg 1992, 1995). The ratio of $\frac{\epsilon_A}{\epsilon_D}$ was determined to be 0.02 and can be found in the supplementary information (Table S1). Acceptor sensitization and donor emission are sketched in Fig. 4.

FRET from optical microscopy

The paper fibers were investigated using a wide field microscopy (WM) setup equipped with the filter sets seen in Table 2. The WM was operated with a 50 W halogen lamp and a CMOS detector from QI Imaging (Optimos).

Both the intensity of the lamp and the detector sensitivity show a dependency of the wavelength and were corrected by calculating correction factors from the lamps emission spectrum folded with the excitation filters and the extinction coefficient and the detector sensitivity folded with the emission filters and the emission spectra. These correction factors were applied to the recorded images to get a true representation of the measured intensity.

A schematic of the dyed fibers and pHema films can be seen in Fig. 5. The images are false colored to emphasize the differences in the fibers/films. The samples were investigated using a 400× magnification

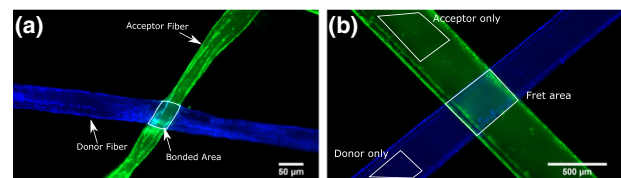


Fig. 5 False color images of **a** a fiber bond and **b** a pHema crossing measured in a wide field fluorescence microscope. In **b** also typical regions of interest for the Xia algorithms are shown. The regions are chosen to minimize scattered light from the other fiber/film

in the case of fibers and $50\times$ magnification for the case of films. To minimize background noise, the microscope was used in a box surrounded by black fabric.

When using the microscope one trades the spectral for spatial information and one loses the advantage to apply this simple fitting method described above. Here, a sophisticated algorithm that results in a fully corrected measure of the FRET efficiency has been developed by Gordon et al. (1998). The method makes use of images recorded with the three different filter sets from Table 2 of three different samples. Usually this would result in a total of nine images but with the arrangement seen in Fig. 5 it is possible to get the same information from only three images instead as in every image there is automatically a pure donor, a pure acceptor and the FRET area included. For a detailed description of the algorithm please refer to the original paper (Gordon et al. 1998). In brief this method calculates the FRET intensity corrected for all possible spectral bleed-through scenarios according to the following equations.

$$\overline{Afa} = \frac{Af - \left(\frac{Ad}{Fd}\right)Ff}{1 - \left(\frac{Fa}{Aa}\right)\left(\frac{Ad}{Fd}\right)} \quad (5)$$

$$FRET1 = \frac{\left(Ff - \left(\frac{Fd}{Dd}\right)Df - \overline{Afa}\left[\left(\frac{Fa}{Aa}\right) - \left(\frac{Fd}{Dd}\right)\left(\frac{Da}{Aa}\right)\right]\right)}{G\left[1 - \left(\frac{Da}{Fa}\right)\left(\frac{Fd}{Dd}\right)\right]} \quad (6)$$

$$\overline{Dfd} = Df + FRET1\left[1 - G\left(\frac{Da}{Aa}\right)\right] - \overline{Afa}\left(\frac{Da}{Aa}\right) \quad (7)$$

$$FRETN = \frac{FRET1}{\overline{Afa} * \overline{Dfd}} \quad (8)$$

The equations consist of variables with 2 letters. The first letter stands for the used filter set as seen in Table 2, the second letter for the investigated sample (d = donor only, a = acceptor only, f = FRET area). E.g. Af therefore stands for the FRET region (bonded area) investigated with the acceptor filter set. The variables represent the measured light intensities from the aforementioned microscope images recorded as 16 bit gray values. \overline{Afa} refers to the acceptor signal that would have been if no donor were present and therefore no FRET occurred. Similarly, \overline{Dfd} refers to the donor signal that would have been if no acceptor were present and therefore no FRET occurred.

Regions of interest were chosen in the images as depicted in Fig. 5b. The evaluation was performed pixelwise. G is a factor relating the loss of the donor signal to the increase of the acceptor signal (see Supplementary information Table S3). In this work we used the slightly different algorithm by Xia et al. which differs solely in the normalization of the N_{FRET} value but is otherwise equivalent to the Gordon algorithm (Xia and Liu 2001).

$$N_{FRET} = \frac{FRET1}{\sqrt{\overline{Afa} * \overline{Dfd}}} [-] \quad (9)$$

For being able to reproduce the area in molecular contact a method was developed to always choose the appropriate area. The method consisted of manually drawing an ROI (region of interest) capturing the “optically-bonded” area in Fig. 6. Subsequently we applied image erosion to avoid the edges and thus obtain the Eroded ROI (Fig. 6, bottom images) which was then used for evaluation of FRET intensity. Avoiding the edges was necessary because regions of extreme intensity appear to give a false positive FRET signal. Additionally, false positives were also detected on areas that are impossible to exhibit FRET such as the area seen in Fig. 6a that is not in the bonded region.

Other FRET experiments

It should be mentioned here that other FRET experiments were also employed. A confocal laser scanning microscope (CLSM, Leica TCS SPE) with a photomultiplier tube from Hamamatsu was used to investigate acceptor photobleaching and sensitized emission of the acceptor in fiber–fiber bonds. The idea was that due to the superior setup a better signal to noise ratio will be achieved.

Results and discussion

Excitation (EX) and emission (EM) spectra

To check that the combination of dyes can be used as a FRET system on the chosen substrates and the chosen pH value the excitation and emission spectra of the dyes on both substrates at a pH of 9 were

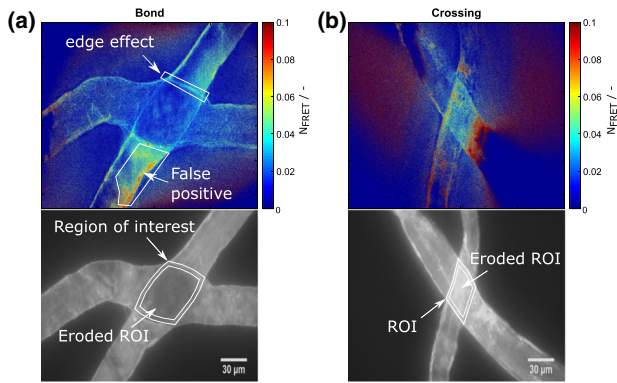


Fig. 6 Demonstration of the FRET analysis of **a** a fiber bond and **b** a fiber crossing. In **a** two typical problems with the analysis can be seen. First a high FRET signal was often detected on the edges of both, the bonded area and also the fibers. Secondly, a strong false positive FRET signal can be seen on an area that is clearly not possible to exhibit FRET. In the microscopy image the erosion technique used for analysis can be seen

investigated. An optimal setup would have a significant spectral overlap between the donor emission spectrum and the acceptor excitation spectrum (Overlap Integral, necessary condition for FRET) while having as little spectral bleed-through as possible. The resulting spectra can be seen in Fig. 7. As can be seen the donor emission and the acceptor excitation spectra show significant overlap. However also there is partial spectral overlap of the donor emission and the acceptor emission and vice versa. Also the acceptor excitation spectrum overlaps with the donor excitation spectrum. This spectral bleed through in the fluorescence microscopy is the reason for the necessity of the Xia algorithm in the optical microscopy and the spectral unmixing in the spectrophotometry to correct the signal. When comparing the dyes in the different substrates one can see some changes. First one can see that the excitation spectra of both dyes change at approx. 400 nm when comparing the fibers and

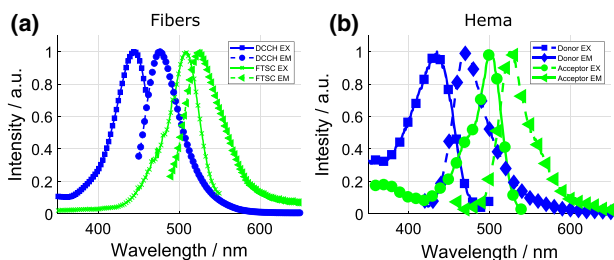


Fig. 7 Excitation and emission spectra of DCCHEX and FTSC on **a** paper fibers and **b** in pHema. Spectra are normalized to their peak value

pHema. Additionally, the FTSC spectra slightly shift in wavelength. These changes are attributed to the covalent linking and therefore chemical modification of the dye molecules. That the covalent bonding has an effect on the dyes can also be seen in the quantum yield reported in the supplementary information (Table S1). The changes are low enough to be able to compare the two systems with each other.

Investigation of FRET between paper fibers

Paper fiber bonds and crossings were investigated to see if it is possible to measure the area in molecular contact between two paper fibers using FRET fluorescence microscopy. When investigating fiber bonds one would expect a FRET signal between the fiber surfaces because the two surfaces and therefore also the dye molecules come very close. To check the plausibility of the signal, unbonded fiber crossings were investigated as a reference. As can be seen in Fig. 8 for both dye concentrations (0.2 mmol/L and 1 mmol/L) it is not possible to detect a significant difference between the bond and the crossing. For illustration also refer to Fig. 6b where a considerable false FRET signal can be seen in the overlapping (but unbonded) regions of the fiber crossing. A possible concentration dependence of the FRET signal was also investigated but did not show any improvement. These results show that it is not possible to measure the interaction of two paper fiber surfaces by using the employed method.

One reason for not being able to detect a difference in the fibers could be a low signal to noise ratio. If the dyes stay only at the surface of the fibers the signals can only originate from a thin layer of interaction. If, however the complete bulk is dyed it would likely lead

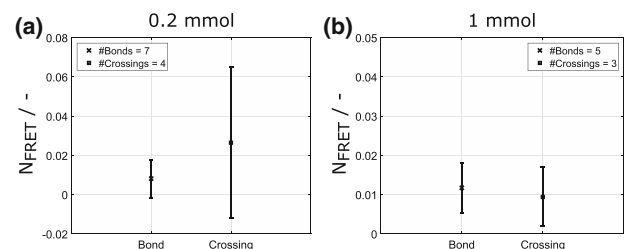


Fig. 8 Results from the analysis of 12 bonds and 7 not bonded crossings. **a** The fibers were dyed with a concentration of 0.2 mmol/L. **b** The concentration was increased to 1 mmol/L. In both cases the fiber bonds do not show a higher FRET signal than the crossings. Error bars are 95% confidence limits

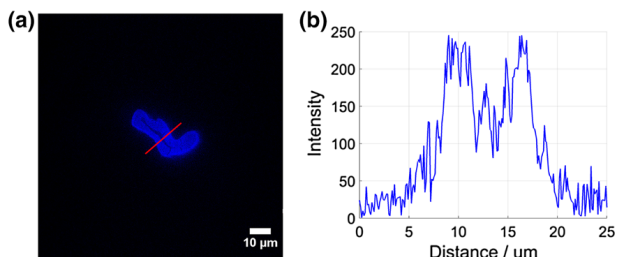


Fig. 9 **a** Cross section of a dyed paper fiber in false color. **b** Intensity Profile of the Line indicated in **a**. The cross section as well as the profile shows that the complete bulk of the fiber was dyed

to a disadvantageous signal to noise ratio. To investigate this the cross sections of the fibers were looked at by using a confocal laser scanning microscope. The results of this investigation seen in Fig. 9 show that the complete bulk of the paper fibers with a thickness of up to 10 μm was dyed by the employed method. This continuous dyeing of a 10 μm thick bulk will lead to a very low signal to noise ratio as the following argumentation shows. The energy transfer due to FRET is only possible up to 2 times the Förster distance. In our case the Förster distance was measured to be about 6 nm. (supplementary information Table S1) This means that a minimum distance of 12 nm is needed to get a FRET signal. In other words this means that when our paper fibers are bonded a thickness layer of approx. 10 nm is interacting. Comparing this to a fiber thickness of up to 10 μm this results in a signal to noise ratio of 1:1000. Therefore, if there is even only little spectral bleed-through it will strongly interfere with the FRET signal. This argumentation shows that if one wants to measure a FRET signal between two surfaces it is necessary to maximize the signal to noise ratio either by using thinner substrates or by confining the dyes to the region of interaction.

Dynamic FRET experiments

Another way to see whether a FRET experiment is successful or not is to investigate the dynamic development of the FRET signal. In our case we tried to replicate the experiments done by Thomson et al. (2007) in which the drying of a fiber bond was monitored. During paper drying the capillary forces of the retracting water are pressing the fiber surfaces together, thus creating the molecular contact area that

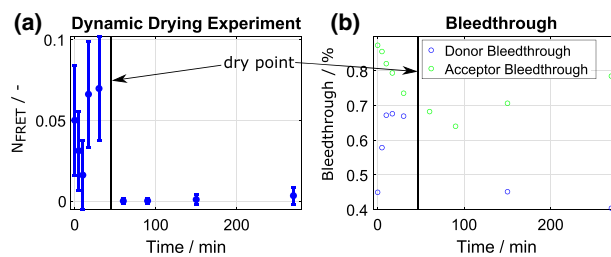


Fig. 10 In **a** one can see the development of the N_{FRET} value as determined with the Xia algorithm. Initially it decreases before it increases again and subsequently finally drops to almost zero. In **b** one can see the donor and acceptor bleed-through as it develops during drying

facilitates adhesion between the fiber surfaces (Persson et al. 2012). In this investigation 6 fiber bonds were investigated that all show a similar behavior as to the one seen in Fig. 10. The collected measurements can be found in the supplementary information (Figure S2). As can be seen in Fig. 10a the FRET intensity is largest below the “dry point”. The dry point is the time at which no water could be detected in the microscopy images. After this point the N_{FRET} drops to almost zero and stays there. Hence, we were observing the opposite of what one would expect. In the wet state where the fibers are certainly not bonded the FRET signal is the strongest and decreases to zero during the drying where the signal should increase. In Fig. 10b one can see that the spectroscopic bleed-through between the filter sets changes over the drying period which is a partial reason for the unexpected development of the N_{FRET} characteristic. Since the bleed-through values are a measure of the spectroscopic properties of the dyes this means that as the water is reduced the excitation and emission spectra of the dyes bound to the fibers appear to be changing. In other words, this means that during drying the properties of the dyes are changing as well which makes a comparable analysis between measurements difficult. The reason for this change could be the change in pH when the amount of water is going down and thus the chemicals concentration is changing. Another reason for the trend could be the worse signal to noise ratio when investigating structures in water due to the stronger scattering of the light.

In summary both experiments aiming to validate the FRET system at hand did not show an increase in FRET signal between bonded and unbonded fibers. Thus the investigated FRET technique seems not suited to provide qualitative or quantitative

information on the molecular contact area related to the adhesion between the fibers. The possible reasons for this is firstly and most likely the poor signal to noise ratio but also reflection and scattering of light on the fibers proves to be a difficult obstacle to overcome as it apparently leads to artifacts in the FRET signal.

FRET in pHema model films using spectroscopy

Our next step was to see whether it is possible to measure a FRET signal using the two dyes mixed together within one film. This measurement serves as a proof of concept that the employed dye system is in fact applicable as a FRET pair. The results are

presented in Fig. 11a. There one can see the clear behavior of a FRET system. In the presence of the acceptor the donor decreases (donor quenching I_D to I_{DA}) in magnitude and transfers its energy to the acceptor (acceptor sensitisation I_A to I_{AD}) which shows a strong increase. The curves in Fig. 11 were fitted with Gaussian peaks and the values for I_D , I_A , I_{DA} and I_{AD} were extracted and used for the calculation of the FRET efficiencies, Eqs. 3 and 4, results are seen in Table 3, line 1. As presented a clear FRET response was measured using the spectrofluorometry.

In another experiment we wanted to see if we can measure a FRET interaction between two initially separated films as depicted in Fig. 2c. To achieve this,

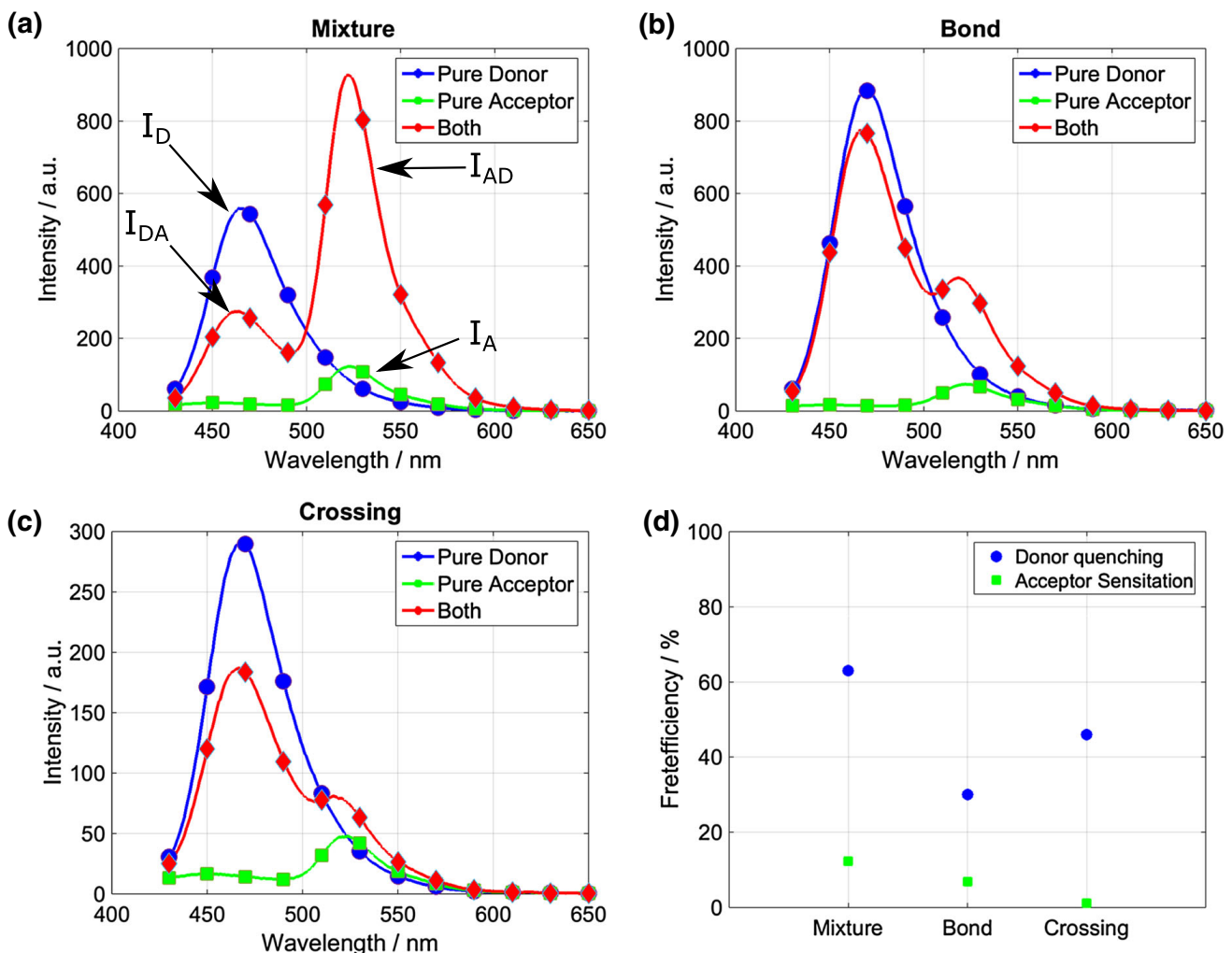


Fig. 11 Comparison of the FRET measurements between 3 types of systems in the spectrofluorometer. **a** Strong FRET signal stemming from the interaction of dyes mixed together within one film. **b** Weaker FRET signal coming from two separate pHema films bonded (bond) together. **c** No FRET

signal in the case of unbonded (crossing). **d** FRET efficiency of the three systems calculated via the acceptor sensitization and donor quenching. The values for the calculation of the FRET efficiency can be found in Table 3

Table 3 Calculation of the FRET efficiency according to Eqs. 3 and 4

Sample	I_D (a.u.)	I_{DA} (a.u.)	I_A (a.u.)	I_{AD} (a.u.)	DQ (%)	AS (%)
Mixture	30,891	11,415	5468	39,337	63	12.4
Bond	46,750	32,693	3534	17,236	30	7.8
Crossing	16,239	8868	2179	3459	45	1.2

The areas under the peaks were determined by fitting Gaussian peaks. The exact procedures and the determination of the ratio ϵ_A/ϵ_D (0.02) can be found in the supplementary information (Figure S1). I_D ... Intensity of the donor peak in the absence of acceptor I_{DA} ... Intensity of the donor peak in the presence of acceptor I_A ... Intensity of the acceptor peak in the absence of donor I_{AD} ... Intensity of the acceptor peak in the presence of donor DQ... Donor quenching according to Eq. 3 AS... Acceptor sensitisation according to Eq. 4

pHema films dyed with either FTSC or DCCH were produced. In a next step these films were subjected to the bonding procedure described in the experimental section. Similar to the fibers we produced bonds and crossings as a reference. If the system works the bonds should exhibit a significantly higher FRET signal than the crossings but should not exceed the mixture as this is the maximum signal that one should be able to achieve at a constant concentration of dyes in the films. In Fig. 11b one can see the results for the bonded films. As expected, the FRET signal is stronger than the FRET response in Fig. 11c but weaker than in the case of the mixed film. In Fig. 11c one can see the spectroscopy measurement of the crossed but not bonded thin films. This measurement serves as a reference for unbonded surfaces as in this case the dyes are not capable of interacting with each other. This result is a good example on why it is not sufficient and reliable to only use donor quenching as an indication for FRET. As can be seen in Fig. 11d the result from the donor quenching indicates a higher FRET signal for the crossings while the FRET efficiency from the acceptor sensitisation correctly shows a lower signal than the bonded films. The reason for the lower reliability of donor quenching is because a reduction in the donor signal can come from other reasons than energy transfer such as environmental quenching (Meer 2013). Here the lower donor signal is likely due to the gap of air between the thin films that only exists in the crossed but unbonded samples. Although measured with the same instrument settings, the overall intensity of the crossed films is much lower than in the within and bonded samples as seen in Fig. 11. Therefore, it is necessary to use the acceptor sensitisation as a more reliable measure for FRET.

One reason why the pHema system works could be the increased concentration of dye molecules in the

films compared to the fibers. The concentrations of dye molecules in the pHema film can be seen in Table 1. The concentration of the fibers was estimated by measuring the intensity of the dyed fibers and comparing it to the thin films with a known concentration. Using the measured quantum yield and thickness of the systems the concentrations in Table 2 were calculated. As can be seen the concentrations differs by a factor of approx. 15. An increased concentration means that the potential of dyes to be much closer increases and also the amount of interacting dyes increases. Both leads to an increase in the FRET efficiency.

Another reason could be the increased signal to noise ratio. First the films (1.5 μm) are thinner than the paper fibers (10 μm). But also due to the temperature initiated bonding procedure very close to the melting point of pHema it is likely that the dyes within the films were diffusing into the other film. Both the decreased thickness and the diffusion of the dyes lead to an increased signal to noise ratio.

In summary the experiments with the pHema thin films permit two important conclusions. With the film with the mixed dyes it is demonstrated that the dyes DCCH and FTSC provide a working FRET system. The experiments with the bonded and unbonded films demonstrate that this FRET system, while it has not been able to indicate bonding between fiber surfaces, is able to indicate the bonding between the pHema thin films.

FRET in pHema model films using fluorescence wide field microscopy

In this final experiment we wanted to see if it is possible to replicate the FRET results obtained by the photo spectroscopy setup using widefield fluorescence microscopy. The reason why this is more difficult is

that for widefield microscopy the camera only provides intensity data instead of the full spectral information. Of course on the other hand one gains spatial information on where in the sample the signal stems from and one might even be able to detect local intensity differences and differentiate between the strength of interaction. Therefore, we again produced pHema bonds (11 bonds) and crossings (10 crossings) and also investigated a film with a mixture of dyes in it. Figure 12 shows the same kind of samples as investigated by the spectrofluorometer. In Fig. 13 the average values of the N_{FRET} intensity can be seen and show the same trend as in Fig. 11d. The N_{FRET} of the mixture is the highest as there, almost all the DCCH and FTSC molecules interact due to the homogeneous distribution of molecules. But also the bonds exhibit a 3 times higher FRET signal than the crossings as seen in Fig. 13 (subfigure). These results highlight that it is possible to measure a FRET signal between substrates using widefield microscopy.

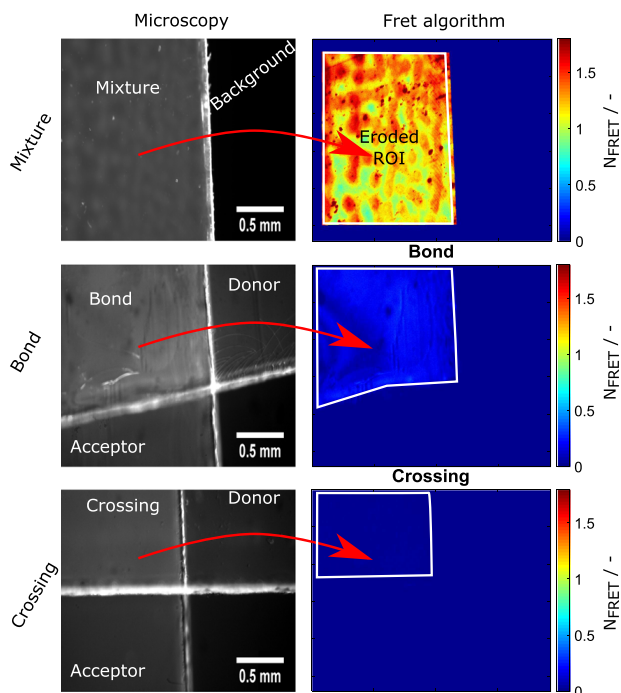


Fig. 12 Comparison of the FRET measurements between 3 types of systems using fluorescence microscopy. **a** Strong FRET signal stemming from the interaction of dyes mixed (Mixture) together within one film. Here also the image erosion technique used to analyze the images can be seen. **b** Weaker FRET signal coming from two separate films bonded (bond) together. **c** No FRET signal in the case of unbonded (crossing) films

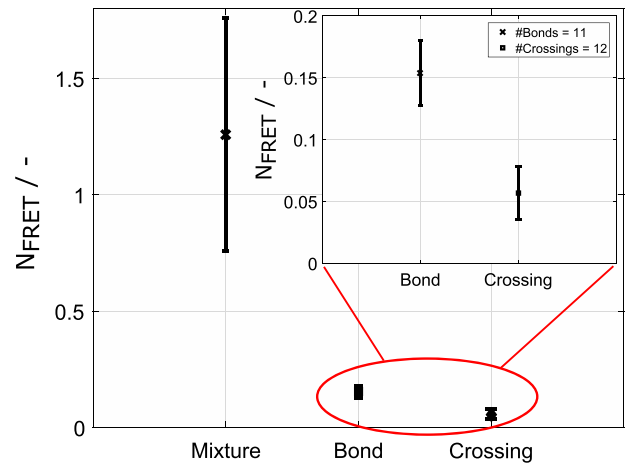


Fig. 13 Statistical analysis of the thin film models seen in Fig. 12. As expected the mixture shows the highest FRET response. The signal from bonds is about 3 times larger than from crossings. Error bars are 95% confidence limits

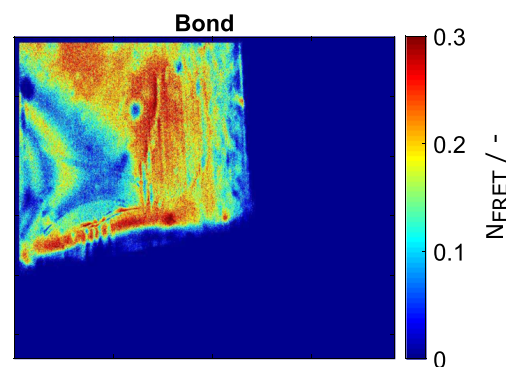


Fig. 14 Enlarged image of the N_{FRET} response of the pHema bond seen in Fig. 11. Here the scale was changed to emphasize the differences in the FRET signal at different positions in the film. The higher signal comes from a stronger interaction of the dyes

We also looked at the images in more detail to see if it is possible to see local variations in the FRET signals of the bonded film. Figure 14 shows the enlarged and rescaled pHema bond from Fig. 12. The higher the N_{FRET} value the stronger is the interaction. In the image there are regions with considerably higher FRET signals than in others. Since the dyes are not covalently linked and the bonds were formed using increased temperature it is not possible at the moment to say whether this increased signal comes from a stronger bonding (as molecules get closer the N_{FRET}

increases) or interdiffusion (as more molecules interact with each other the N_{FRET} increases). However, in either case it is a sign for local variations in bonding intensity between the surfaces.

Other FRET experiments

As briefly mentioned in the experimental Sect. 2.6 we also tried acceptor photobleaching and sensitized emission, using a CLSM. From literature we found that acceptor photobleaching promises to be a rather simple but reliable FRET experiment (Jares-Erijman and Jovin 2003) and by using a CLSM we were hoping that due to the improved microscopy setup with greater focus and sensitivity a solution to the problems stated above would be found. However also with the CSLM it was not possible to detect a FRET signal when investigating the fiber-fiber bonds.

Conclusions

In this work we investigate the possibility of measuring molecular interactions between two bonded surfaces using the effect of Förster Resonance Energy Transfer. We measured the degree of molecular contact for paper fibers and pHema model films dyed with DCCH and FTSC. In bonded paper fibers we were unable to detect a significant FRET intensity which is likely due to the poor signal to noise ratio of the system, as the bulk of the fibers is fully dyed and only the bonded surface gives a FRET signal. Thus we recommend only surface active dyeing when investigating molecular interaction between surfaces with FRET. Another reason for the poor FRET signal could be that the concentrations of dye in the paper fibers is approximately a factor of 15 smaller than in the pHema films.

Using the pHema model films we were able to validate the FRET approach. Three types of pHema systems were investigated, one that consisted of a mixture of dyes within one film, two separately dyed films subsequently bonded together and separately dyed films crossed but not bonded. Molecular contact and FRET transfer was detected by both, spectroscopy and fluorescence microscopy, in the case of mixed dyes and bonded thin films. For fluorescence microscopy, the difference between the signals was smaller due to various obstacles such as focus, bleed through

or the necessary image corrections, all affecting the signal to noise ratio. Therefore, we conclude that in principle it is possible to quantify the degree of contact on the nanometer scale between two surfaces with the FRET system we have used. However, we have not been able to reproduce FRET between paper fibers as published elsewhere (Thomson et al. 2007, 2008a, b).

Acknowledgments The authors thank the Austrian Federal Ministry of Economy, Family and Youth and the Austrian National Foundation for Research, Technology and Development for their financial support. Also the industrial partners Mondi, Océ, SIG Combibloc and Kelheim Fibres are acknowledged. Furthermore this research has received funding from the EU Horizon 2020 program under Marie Skłodowska-Curie Grant Agreement No. 764713, ITN Project FibreNet. Finally the authors thank Christoph Staudinger for valuable discussions and help with some of the experiments. Funding was provided by Christian Doppler Forschungsgesellschaft. Open access funding provided by Graz University of Technology.

Open Access This article is distributed under the terms of the Creative Commons Attribution 4.0 International License (<http://creativecommons.org/licenses/by/4.0/>), which permits unrestricted use, distribution, and reproduction in any medium, provided you give appropriate credit to the original author(s) and the source, provide a link to the Creative Commons license, and indicate if changes were made.

References

- Asunaa S, Steenberg B (1958) Beaten pulps and the fibre-to-fibre bond in paper. *Svensk Papperstidning* 61:686–695
- Broussard JA, Rappaz B, Webb DJ, Brown CM (2013) Fluorescence resonance energy transfer microscopy as demonstrated by measuring the activation of the serine/threonine kinase Akt. *Nat Protoc* 8(2):265–281
- Clegg RM (1992) [18] Fluorescence resonance energy transfer and nucleic acids. In: *Methods in enzymology*, vol 211. Elsevier, pp 353–388
- Clegg RM (1995) Fluorescence resonance energy transfer. *Curr Opin Biotechnol* 6(1):103–110
- Förster T (1948) Zwischenmolekulare Energiewanderung und Fluoreszenz. *Ann Phys* 437(1–2):55–75
- Gordon GW, Berry G, Liang XH, Levine B, Herman B (1998) Quantitative fluorescence resonance energy transfer measurements using fluorescence microscopy. *Biophys J* 74(5):2702–2713
- Haselton WR (1954) Gas adsorption by wood, pulp, and paper. *Tappi J* 37:404–412
- Hirn U, Schennach R (2015) Comprehensive analysis of individual pulp fiber bonds quantifies the mechanisms of fiber bonding in paper. *Sci Rep* 5:10503
- Hirn U, Schennach R (2017) Fiber-fiber bond formation and failure: mechanisms and analytical techniques. In: *Trans.*

- of the 16th Fundamental Research Symposium, Oxford, pp 839–863
- Hirn U, Schennach R, Ganser C, Magnusson M, Teichert C, Östlund S (2013) The area in molecular contact in fiber-fiber bonds. In: *Trans. of the 15th fundamental research symposium*, Cambridge, pp 201–226
- Jares-Erijman EA, Jovin TM (2003) FRET imaging. *Nat Biotechnol* 21(11):1387
- Kappel L, Hirn U, Bauer W, Gilli E, Schennach R (2010) Revisiting polarized light microscopy for fiber-fiber bond area measurement—part I: theoretical fundamentals. *Nordic Pulp Paper Res J* 25(1):65–70
- Lindström T, Wågberg L, Larsson T (2005) On the nature of joint strength in paper—a review of dry and wet strength resins used in paper manufacturing. p 111
- Meer BWVD (2013) Förster theory. In: *FRET – Förster resonance energy transfer*. Wiley-Blackwell, pp 23–62
- Persson BN, Ganser C, Schmied F, Teichert C, Schennach R, Gilli E, Hirn U (2012) Adhesion of cellulose fibers in paper. *J Phys Condens Matter* 25(4):045002
- Persson BNJ (2003) On the mechanism of adhesion in biological systems. *J Chem Phys* 118(16):7614–7621
- Persson BNJ, Albohr O, Tartaglino U, Volokitin AI, Tosatti E (2004) On the nature of surface roughness with application to contact mechanics, sealing, rubber friction and adhesion. *J Phys Condens Matter* 17(1):R1–R62
- Sormunen T, Ketola A, Miettinen A, Parkkonen J, Retulainen E (2019) X-ray nanotomography of individual pulp fibre bonds reveals the effect of wall thickness on contact area. *Sci Rep* 9(1):4258
- Thomson C, Lowe R, Page D, Ragauskas A (2008a) Exploring fibre-fibre interfaces via FRET and fluorescence microscopy. *J Pulp Paper Sci* 34(2):113–120
- Thomson CI, Lowe RM, Ragauskas AJ (2007) Imaging cellulose fibre interfaces with fluorescence microscopy and resonance energy transfer. *Carbohydr Polym* 69(4):799–804
- Thomson CI, Lowe RM, Ragauskas AJ (2008b) First characterization of the development of bleached kraft softwood pulp fiber interfaces during drying and rewetting using FRET microscopy. *Holzforschung* 62(4):383–388
- Torgnysdotter A, Kulachenko A, Gradin P, Wågberg L (2007) The link between the fiber contact zone and the physical properties of paper: a way to control paper properties. *J Compos Mater* 41(13):1619–1633
- Xia Z, Liu Y (2001) Reliable and global measurement of fluorescence resonance energy transfer using fluorescence microscopes. *Biophys J* 81(4):2395–2402
- Yang C, Persson BNJ, Israelachvili J, Rosenberg K (2008) Contact mechanics with adhesion: interfacial separation and contact area. *EPL* 84(4):46004

Publisher's Note Springer Nature remains neutral with regard to jurisdictional claims in published maps and institutional affiliations.

4. Part II: Using Brillouin Spectroscopy to investigate cellulosic fibers

4.1. Introduction

The investigation of cellulosic fibers regarding their mechanical properties is of great interest as they are the bulk material that make up so many of the products used in our everyday lives. The products range from ordinary paper to highly functional clothing. In all the cases the mechanical properties of the fibers are partly responsible for the functionality of the product. Therefore, the investigation of the mechanical properties is a necessary step for the further improvement of the products originating from the fibers.

Mechanical testing of fibers has been employed for a long time. Due to the orthotropic nature of most natural fibers the investigation of the materials need to be done along the fiber axis which we call longitudinal properties and transverse to the fiber axis which we call transversal properties. The longitudinal properties have been investigated first by many researches as it poses less experimental obstacles. A detailed summary of the work done on single fibers in longitudinal direction can be found in (Fischer, 2013; Jajcinovic, 2017).

The transverse properties are harder to investigate as simple tensile tests cannot be used to investigate this direction. Different approaches with similar underlying principles were used to investigate this direction. Mainly nanoindentation (NI) and Atomic Force Microscopy - Nanoindentation (AFM-NI) were used to probe this direction of the fibers. A comprehensive

4. Part II: Brillouin Spectroscopy

literature list has been established in the introduction of the appended paper. Although these methods provide valuable information they have severe shortcomings. Simple NI lacks the information on what part of the investigated fiber is being measured. And while AFM-NI can provide valuable information on the complete fiber the measurement itself takes a long time and statistics are usually poor.

Here in this work we used Brillouin Light Scattering Microscopy (BLS) to my knowledge for the first time to investigate the viscoelastic material constants of softwood and viscose fibers. It has been shown by others that BLS can be used to measure the material properties of different natural fibers and biological tissues. I believe that this technique will provide a valuable addition to the already existing techniques that will lead to a deeper understanding on the mechanics in products made from natural fibers.

4.2. Brillouin Spectroscopy

Brillouin spectroscopy is a technique that measures the response of light interacting with matter. The principle is based on Brillouin scattering which is the general term of the inelastic scattering of light and some sort of material wave. In the context of this work Brillouin Light Scattering Microscopy (BLS) investigates the propagation of phonons in the material. The interaction can give insights in the viscoelastic properties such as storage and loss modulus. This is due to the relation of the phonon group velocity (speed of sound) and the mechanical moduli of the system. So therefore it is worth to say a few sentences about phonons in general.

4.2.1. Phonons

A phonon is the quantum mechanical representation of a vibrational motion in which a lattice of atoms or molecules uniformly oscillates at a single frequency. (Simon, 2013) In classical terms phonons represent vibrations in the material. The following classic mechanical approach to oscillations of

4. Part II: Brillouin Spectroscopy

a one-dimensional linear chain of atoms connected by springs was taken from Simon, 2013.

Consider a system as in Figure 4.1. A one-dimensional chain of atoms with mass m that are connected by springs with a spring constant of κ . At rest the distance between the atoms is a . Newton's equation of motion for this system can thus be written as

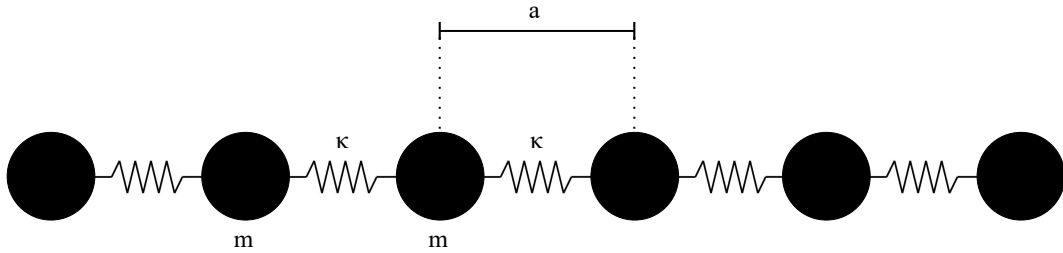


Figure 4.1.: One-dimensional monoatomic chain. The atoms with mass m are connected by springs with a spring constant κ . The distance between the atoms at rest is a .

$$m(\delta\ddot{x}_n) = \kappa(\delta x_{n+1} - \delta x_n) + \kappa(\delta x_{n-1} - \delta x_n). \quad (4.1)$$

This can be rewritten as

$$m(\delta\ddot{x}_n) = \kappa(\delta x_{n+1} + \delta x_{n-1} - 2\delta x_n). \quad (4.2)$$

For the solution of equation 4.2 we use an ansatz that describes the normal modes of the system as waves

$$\delta x_n = A e^{i(\omega t - k n a)} \quad (4.3)$$

with A being the amplitude, ω the frequency and k the wavevector of the proposed wave. Please note that I use the symbol k for the wavevector and κ for the spring constant as it is customary in solid state physics.

Plugging the ansatz of Eq. 4.3 into Eq.4.2 we find

$$m \omega^2 A e^{i(\omega t - k n a)} = \kappa A e^{i\omega t} (e^{-i k a (n+1)} + e^{-i k a (n-1)} - 2 e^{-i k a n}) \quad (4.4)$$

4. Part II: Brillouin Spectroscopy

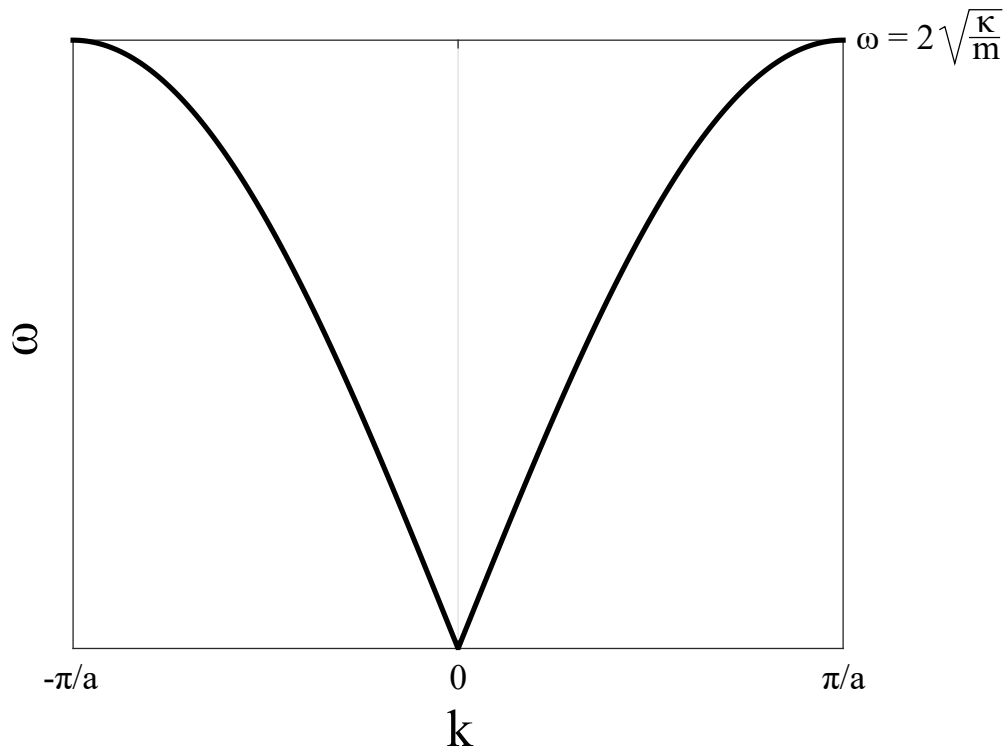


Figure 4.2.: Phonon dispersion relation for a monoatomic linear chain connected by springs. At low k (high wavelength limit) it can be seen that the dispersion is linear.

which can be rewritten using Eulers identity as

$$m \omega^2 = 2 \kappa [1 - \cos(ka)] = 4 \kappa \sin^2(ka/2) \quad (4.5)$$

A relationship between a frequency (energy) and a wavevector (momentum) is known as a dispersion relation and in our problem we therefore arrive at the following result

$$\omega = 2 \sqrt{\frac{\kappa}{m}} |\sin(ka/2)|. \quad (4.6)$$

When we plot Equation 4.6 we obtain the graph seen in Figure 4.2.

4. Part II: Brillouin Spectroscopy

In the long wavelength limit (which corresponds to low k values) the sine can be approximated as $\sin(x) \approx x$ and the dispersion relation is linear with the wavevector which is also evident from Figure 4.2. Hence Equation 4.6 reduces to

$$\omega = 2 \sqrt{\frac{\kappa}{m}} \frac{a}{2} k = v_{sound} k \quad (4.7)$$

For us we arrive at the important result that the speed of sound in a linear monoatomic chain follows the simple form.

$$v_{sound} = a \sqrt{\frac{\kappa}{m}}. \quad (4.8)$$

This is the simplest model to understand that the speed of sound in a material depends on the structure (a), the spring constant (κ) and the mass of the atoms. This linear chain can be expanded in 2 or 3 dimensions however the basic concepts still hold in higher dimensions. By this I mean (although it might be obvious) that the speed of sound depends also in higher dimensions always on the aforementioned constants of a material.

Here I want to mention that to fully understand every detail of phonons it is worth reading a solid state physics textbook as almost all of them will cover the topic of phonons. The textbooks also dive further into the subjects such as Brillouin zones, crystal momentum or the reciprocal lattice that were intentionally left out here as it is beyond the scope of this thesis.

4.2.2. Material Constants of Fibers

The derivation of the following equations stems from (Mavko et al., 2009). In a linear elastic solid Hook's law states that the stress σ_{ij} is linearly proportional to the strain ϵ_{ij} . The relation can be written as

$$\sigma_{ij} = C_{ijkl} \epsilon_{kl} \quad (4.9)$$

4. Part II: Brillouin Spectroscopy

with C_{ijkl} being the elastic stiffness tensor. This general fourth-rank tensor has 81 individual components. However, the symmetry of stresses and strains and the existence of a unique strain energy potential reduces the number of independent constants to a maximum of 21.

Fibers are commonly seen as a transversely isotropic medium. For such a material the elastic stiffness tensor reduces to the following form

$$\begin{bmatrix} c_{11} & c_{12} & c_{13} & 0 & 0 & 0 \\ c_{12} & c_{11} & c_{13} & 0 & 0 & 0 \\ c_{13} & c_{13} & c_{33} & 0 & 0 & 0 \\ 0 & 0 & 0 & c_{44} & 0 & 0 \\ 0 & 0 & 0 & 0 & c_{44} & 0 \\ 0 & 0 & 0 & 0 & 0 & c_{66} \end{bmatrix}$$

with $c_{66} = \frac{1}{2}(c_{11} - c_{12})$. This tensor has five independent constants. For waves propagating in such an anisotropic material, equations for the velocity of such a wave can be given. The equations for the velocities of the three orthogonally polarized modes of propagation in any plane containing the symmetry axis are given as

$$v_P = (c_{11} \sin^2(\theta) + c_{33} \cos^2(\theta) + c_{44} + \sqrt{M})^{1/2} (2\rho)^{-1/2} \quad (4.10)$$

$$v_{SV} = (c_{11} \sin^2(\theta) + c_{33} \cos^2(\theta) + c_{44} - \sqrt{M})^{1/2} (2\rho)^{-1/2} \quad (4.11)$$

$$v_{SH} = \left(\frac{c_{66} \sin^2(\theta) + c_{44} \cos^2(\theta)}{\rho} \right)^{1/2} \quad (4.12)$$

with

$$M = [(c_{11} - c_{44}) \sin^2(\theta) - (c_{33} - c_{44}) \cos^2(\theta)]^2 + (c_{13} + c_{44})^2 \sin^2(2\theta) \quad (4.13)$$

4. Part II: Brillouin Spectroscopy

and θ being the angle between the wave vector and the symmetry axis and ρ the density of the material. v_P is the velocity of the quasi-longitudinal mode, v_{SV} that of the quasi-shear mode and v_{SH} that of the pure shear mode. The five independent components of the stiffness tensor can be obtained by five independent measurements of the velocity namely $v_P(0^\circ)$, $v_P(90^\circ)$, $v_P(45^\circ)$, $v_{SH}(90^\circ)$ and $v_{SH}(0^\circ) = v_{SV}(0^\circ)$. The components can be calculated by the following expressions.

$$c_{11} = \rho V_P^2(90^\circ) \quad (4.14)$$

$$c_{12} = c_{11} - 2\rho V_{SH}^2(90^\circ) \quad (4.15)$$

$$c_{33} = \rho V_P^2(0^\circ) \quad (4.16)$$

$$c_{44} = \rho V_{SH}^2(0^\circ) \quad (4.17)$$

$$c_{13} = -c_{44} + \sqrt{4\rho^2 V_P^4(45^\circ) - 2\rho V_P^2(45^\circ)(c_{11} + c_{33} + 2c_{44}) + (c_{11} + c_{44})(c_{33} + c_{44})} \quad (4.18)$$

Equations 4.10 - 4.12 are obtained by solving the Christoffel Equation. In Geophysics these equations are used for the ab-initio calculation of sound velocities from the stiffness components of the Christoffel matrix. A thorough description on how the equation is solved was published by Jaeken and Cottenier. (Jaeken & Cottenier, 2016)

4.2.3. Measuring the speed of sound

A Brillouin experiment can very simplified be sketched as in Figure 4.3. The derivation of the following equations was conducted with the help of the book (Berne & Pecora, 2000). Incoming photons (k_0, ω_0) scatter inelastically from phonons (q, Ω) in the thin film at an angle θ . The scattered photon (k_1, ω_1) is subsequently detected. The whole process must conserve energy and momentum which leads to the following equations

$$\omega_0 - \omega_1 = \Omega \quad (4.19)$$

4. Part II: Brillouin Spectroscopy

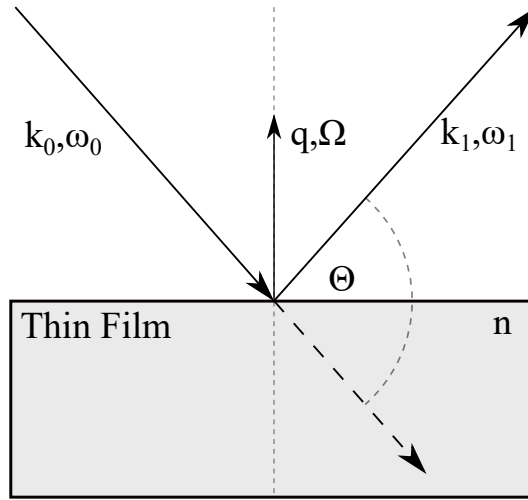


Figure 4.3.: Schematic of the inelastic scattering process of light with the phonons of a thin film.

$$k_0 - k_1 = q \quad (4.20)$$

From the expression for the conservation of momentum (Eq. 4.20) it follows that

$$|q|^2 = |k_0 - k_1|^2 = |k_0|^2 + |k_1|^2 - 2 |k_0| |k_1| \cos(\theta) \quad (4.21)$$

Using the binomial formula $(a - b)^2 = a^2 - 2ab + b^2$ and $\sin\left(\frac{\theta}{2}\right) = \sqrt{\frac{1 - \cos(\theta)}{2}}$ Eq. 4.21 can be rewritten as

$$|q|^2 = (|k_0| - |k_1|)^2 + 4 |k_0| |k_1| \sin^2\left(\frac{\theta}{2}\right) \quad (4.22)$$

Since the momentum change of the photon will be very small the term $(|k_0| - |k_1|)^2$ will be small and hence it is a legitimate approximation to

4. Part II: Brillouin Spectroscopy

neglect the term which leads to

$$|q| = 2 |k| \sin\left(\frac{\theta}{2}\right) \quad (4.23)$$

Using Eq. 4.7 and $k = \frac{n\omega}{c}$ we finally arrive at a familiar equation to connect the frequency shift during a Brillouin experiment to the speed of sound in the sample.

$$\Omega = v_{sound} \frac{2 n \omega_0}{c} \sin\left(\frac{\theta}{2}\right) \quad (4.24)$$

with ω_0 being the angular frequency of the incident light, n the refractive index of the material, c the speed of light, v_{sound} the velocity of the acoustic waves and θ the angle under which the incident light is scattered. Therefore, if the refractive index of the material is known the speed of sound can be calculated.

Using Equation 4.24 together with the knowledge of Section 4.2.2 we know the theoretically optimal setup to measure the elastic constants of our material.

4.2.4. Brillouin Light Scattering Experiment

This section will briefly cover how a Brillouin Spectra looks and how the necessary information for the calculation of the speed of sound will be obtained. For this purpose I constructed a generic Brillouin spectrum as seen in Figure 4.4. The figure shows the intensity of the light scattered from the sample over the frequency shift of this detected light.

A frequency shift occurs due to the interaction of the photons from the incident light with the phonons of the material. First one can see that the obtained spectra are symmetric. This occurs due to the excitation (Anti-Stokes) and relaxation (Stokes) of phonons due to the interaction with the incident beam. Likewise will the light scattered from the sample have higher (Stokes) and lower (Anti-Stokes) energy compared to the incident light

4. Part II: Brillouin Spectroscopy

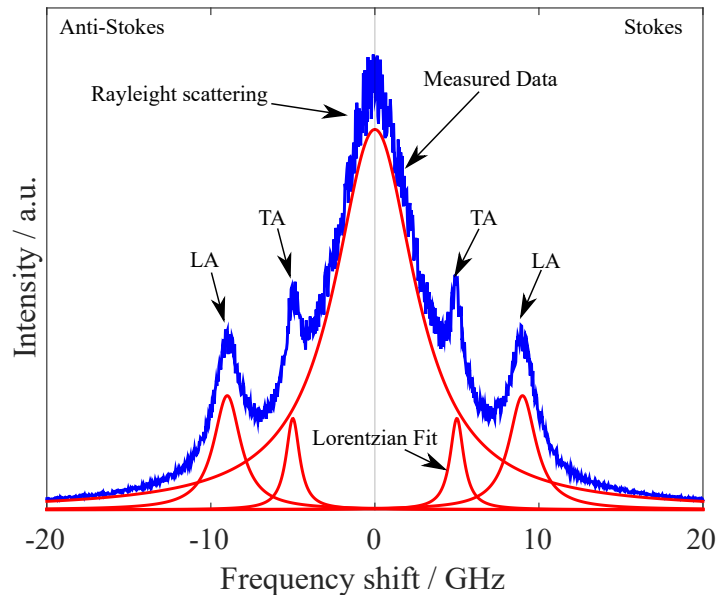


Figure 4.4.: Schematic of a possible Brillouin Spectroscopy measurement (generic). The large center peak is also known as Rayleigh peak and stems from the elastic scattering of the incident light. As can be seen the measurements are symmetric around this center because the incident light can excite phonons and thereby lose some energy (Stokes branch) or the light can gain energy from the phonons (Anti-Stokes branch). Also it can be seen that due to the strong Rayleigh peak the measurement needs to be unmixed which is in spectroscopy usually done by Lorentzian distributions. The Brillouin peaks labelled as TA and LA correspond to the transverse acoustic and the longitudinal acoustic mode of the excitation.

beam. The strong center peak of the spectrum comes from elastic (Rayleigh) scattering of the incident beam with the sample. As this sort of interaction is usually the strongest in all materials the center peak will be very strong compared to the Brillouin scattering peaks.

In the case of our generic spectrum there are two Brillouin peaks. One labelled TA for transverse acoustic and one LA for longitudinal acoustic. This will certainly not occur in every sample or under every direction of investigation as it depends on the material (symmetry of the material) and the measurement geometry if two peaks will be observed. Once such a spectrum is obtained the peaks are fitted. In spectroscopic experiments

4. Part II: Brillouin Spectroscopy

often Lorentzian fits (Cauchy distributions) are used to properly describe the signals. (Mayerhöfer & Popp, 2019) Then the position of the peak can be used in Equation 4.24 to determine the speed of sound. Additionally as it is shown in the publication the full width at half maximum (FWHM) can be related to the corresponding loss modulus. Hence it is possible to investigate the viscoelastic material parameters using this technique. In the published paper a spectrum such as the one seen in Figure 4.4 was recorded and evaluated for every pixel. In such a way it is possible to map the response of the Brillouin experiment to obtain a map (microscopy image) of the investigated structures.


Bibliography

- Berne, B. J., & Pecora, R. (2000). *Dynamic Light Scattering: With Applications to Chemistry, Biology, and Physics* [Google-Books-ID: vBB54ABhmuEC]. Courier Corporation. (Cit. on p. 68).
- Fischer, W. J. (2013). *A novel direct method for mechanical testing of individual fibers and fiber to fiber joints* (Doctoral dissertation). Technische Universität Graz. Graz. (Cit. on p. 62).
- Jaeken, J. W., & Cottenier, S. (2016). Solving the Christoffel equation: Phase and group velocities. *Computer Physics Communications*, 207, 445–451. <https://doi.org/10.1016/j.cpc.2016.06.014> (cit. on p. 68)
- Jajcinovic, M. (2017). *Strength of individual fibres and fibre to fibre joints - influence of the pulp type, environmental conditions and the degree of refining* (Doctoral dissertation). Technische Universität Graz. Graz. (Cit. on p. 62).
- Mavko, G., Mukerji, T., & Dvorkin, J. (2009). *The Rock Physics Handbook: Tools for Seismic Analysis of Porous Media* [Google-Books-ID: 2yzcyUqEqsC]. Cambridge University Press. (Cit. on p. 66).
- Mayerhöfer, T. G., & Popp, J. (2019). Quantitative Evaluation of Infrared Absorbance Spectra – Lorentz Profile versus Lorentz Oscillator. *ChemPhysChem*, 20(1), 31–36. <https://doi.org/10.1002/cphc.201800961> (cit. on p. 72)
- Simon, S. H. (2013). *The Oxford Solid State Basics*. Oxford, New York, Oxford University Press. (Cit. on pp. 63, 64).

5. Paper C



Mechanical Properties of cellulose fibers measured by Brillouin spectroscopy

Kareem Elsayad · Georg Urstöger · Caterina Czibula · Christian Teichert · Jaromir Gumulec · Jan Balvan · Michael Pohl · Ulrich Hirn 

Received: 13 September 2019 / Accepted: 19 February 2020
© The Author(s) 2020

Abstract We investigate the potential of Brillouin Light Scattering (BLS) Microspectroscopy for fast non-invasive all-optical assessment of the mechanical properties of viscose fibers and bleached softwood pulp. Using an optimized Brillouin spectrometer, we demonstrate fast spatial mapping of the complex longitudinal modulus over extended areas ($> 100 \mu\text{m}$). Our results reveal that while the softwood pulp has a relatively uniform moduli, the viscous fibers have significant spatial heterogeneous in the moduli. Specifically, the viscose fibers exhibited a regular pattern of increasing and decreasing modulus normal to the fiber axis. The potential influence of a locally changing refractive index is investigated by holographic phase microscopy and ruled out. We

discuss our results in light of the anisotropic mechanical properties of the fibers and are able to estimate the relative difference between the modulus along the fiber axis and that perpendicular to it. Results are presented alongside reference measurements of the quasi-static mechanical properties transverse to the fiber axes obtained using AFM-nanoindentation which reveal a similar trend, hinting at the potential usefulness of BLS for mechanical characterization applications. However, more detailed investigations are called for to uncover all the factors influencing the measured high-frequency BLS modulus and its significance in relation to physical properties of the fiber that may be of practical interest.

Electronic supplementary material The online version of this article (<https://doi.org/10.1007/s10570-020-03075-z>) contains supplementary material, which is available to authorized users.

Keywords Storage modulus · Young's modulus · Loss modulus · Brillouin spectroscopy · Viscoelasticity · Cellulose fiber

K. Elsayad
Advanced Microscopy, Vienna Biocenter Core Facilities,
Vienna Biocenter, Dr. Bohr-Gasse 3, Vienna 1030,
Austria

C. Czibula · C. Teichert
Institute of Physics, Montanuniversität Leoben, Leoben,
Austria

G. Urstöger · U. Hirn (✉)
Institute of Bioproducts and Paper Technology, Graz
University of Technology, Graz, Austria
e-mail: ulrich.hirn@tugraz.at

J. Gumulec · J. Balvan
Department of Pathophysiology, Masarykova Univerzita,
Brno, Czech Republic

M. Pohl
Canon Production Printing, Poing, Germany

G. Urstöger · C. Czibula · C. Teichert · U. Hirn
Christian Doppler Laboratory for Fiber Swelling and
Paper Performance, Vienna, Austria

Introduction

The mechanical properties of pulp fibers have been investigated using numerous different approaches. Longitudinal (i.e. along the fiber axis) measurements of fiber properties like the E-modulus and the breaking strength are usually studied using fiber tensile testing (Kompella and Lambros 2002; Burgert et al. 2005; Fischer et al. 2012; Jajcinovic et al. 2018) [see also Fischer (2013) and Jajcinovic (2017) for extensive reviews]. In contrast the transverse properties of fibers (i.e. perpendicular to the fiber axis) were initially investigated via compressive measurements on wet fibers (Hartler and Nyren 1970; Dunford and Wild 2002; Wild et al. 2005). Bergander et al. carried out tests on radial double-wall cut wood strips in an environmental scanning electron microscope (Bergander and Salmen 2000). Atomic Force Microscopy (AFM) based methods have also been used to investigate fiber properties such as flexibility and conformability (Nilsson et al. 2000; Pettersson et al. 2017) as well as transverse mechanical properties (Ganser et al. 2013; Ganser and Teichert 2017). A comprehensive list of literature on the topic can be found in Czibula et al. (2019).

While the viscoelastic nature of cellulosic fibers has been known for a long time, earlier studies focused predominantly on the creep behaviour of fibers in the longitudinal direction (Stanzl-Tschegg and Navi 2008; Cisse et al. 2015). The viscoelastic behaviour of wood has been characterized for pine specimens along the grain direction (Penneru et al. 2006) and for green wood in the transverse direction (Bardet and Gril 2002). However, only recently has fiber viscoelasticity in the transverse direction been addressed using an AFM-Nano-Indentation (NI) based method (Ganser et al. 2018) at varying levels of relative humidity (RH) (Czibula et al. 2019).

In this work spontaneous Brillouin Light Scattering (BLS) Microspectroscopy is applied to probe the mechanical properties of cellulosic fibers. Spontaneous BLS is based on the inelastic scattering of light from acoustic phonons that are inherently present in the probed material. Acoustic phonons are collective molecular excitations, which unlike optical phonons, have a significantly lower energy (in the GHz range) and will extend over many molecules. BLS measures the effective velocity of these excitations, by measuring the frequency shift of the so-called BLS peaks

relative to the probing laser. In a typical BLS microspectroscopy experiment when one couples to a single acoustic phonon mode, one observes *two* Brillouin scattering peaks on either side of the probing laser frequency, which correspond to the “creation” and “annihilation” of a phonon. The shift of these peaks relative to the elastic scattering peak (i.e. frequency of the probing laser) is directly proportional to the hypersonic velocity of the phonons via Eq. (1). The velocity can in turn be used to calculate the elastic storage modulus at the corresponding frequency via the Christoffel equation [Eq. (2)].

Key advantages of BLS microscopy are that it is a completely non-invasive, non-contact method that can measure mechanical properties in short acquisition times (~ 100 ms or less per position). This is particularly useful for investigation of pulp fibers, as their small size (length 0.6–3 mm, width 15–40 μm) require elaborate sample preparation and intricate micromachinery for mechanical testing. Another potentially promising aspect of BLS microscopy is that it can be used to evaluate the full elastic tensor of anisotropic materials. Due to the fibril orientation in the S2 wall and the misalignment between the fibril orientation angle and the fiber axis, the fiber should be described by an orthotropic material model of the fiber wall, explicitly taking into account also the fibril orientation angle (Magnusson and Östlund 2013). As thus the fibers can be characterized by either performing mechanical measurements in the longitudinal and the transverse direction—i.e. two tensile plus two shear moduli—together with the fibril angle, or, by performing direct orthogonal measurements of the three tensile moduli plus the three shear moduli. Measurement of pulp fiber shear moduli is even more complicated than tensile moduli, and to the best of our knowledge has not been done. BLS has routinely been used to measure mechanical properties and even the complete elastic tensor of biological fibers such as for spider silk (Koski et al. 2013), proteins (Randall et al. 1979; Speziale et al. 2003), collagens (Harley et al. 1977; Cusack and Miller 1979; Edginton et al. 2016), muscle fibers (Berovic et al. 1989), or recently bamboo wood splinters (Williams et al. 2019). Being a non-contact method able to measure the full elastic tensor (i.e. the elastic moduli and shear moduli in all three spatial directions) BLS has the potential to provide substantial progress for mechanical testing of cellulosic fibers and, at the same time, resolve the

laborious and complicated issues in fiber handling during mechanical testing.

In this work we demonstrate the applicability of the method for cellulosic fibers by analyzing the BLS-measured mechanical properties of pulp- and viscose fibers. Specifically, the elastic modulus (storage modulus) representing the elastic behavior and the loss modulus (dampening coefficient) representing the viscous behavior are evaluated. By adjusting the effective solid angle over which we are probing and detecting (via the effective numerical aperture of the objective lens) we are able to transition between coupling to predominantly acoustic phonon modes perpendicular to the fiber axis and acoustic phonon modes both perpendicular and parallel to the fiber axis. We note that because of the employed back-scattering geometry and polarization of detection we are exclusively measuring *longitudinal acoustic phonons*, which in turn yield the so-called *longitudinal moduli*. In this brief communication we also for the first time to our knowledge demonstrate the feasibility of using a Virtual Imaged Phase Array (VIPA)-based imaging spectrometer for studying such fibers. While having a lower spectral resolution and finesse than the traditionally employed multi-pass Fabry–Perot spectrometers (Sandercock 1970), it also has some advantages in regard to required acquisition time and illumination intensity, as well as affordability, which would be important for wider research and potentially also industrial applications.

Materials and methods

Fibers

The two different fibers investigated were hand ribbon shaped viscose fibers (Leonardo fiber from Kelheim Fibers) and fully bleached softwood kraft pulp fiber from industrial production (Sappi). For the BLS measurements two viscose fibers and two softwood fibers were investigated. Reference measurements, by AFM-NI, were carried out on fully bleached Canadian softwood kraft pulp (Canfor) at about 50% RH. AFM-NI data of round shaped viscose fibers from Kelheim were used as the second reference.

Calculation of elastic modulus from BLS measurements

The measured BLS frequency shift ν_B (GHz) is in general related to the speed of the probed acoustic phonons $V_{\hat{q}}$ for a given scattering wavevector \hat{q} via:

$$\nu_B = \pm 2\mathbf{n} \cdot \hat{q} c^{-1} \nu_0 V_{\hat{q}} \quad (1)$$

where \mathbf{n} is the refractive index (written here as a tensor for the general anisotropic case), ν_0 is the frequency of the probing laser, and c is the vacuum speed of light. (In the backscattering geometry this reduces to $\nu_B = \pm 2nc^{-1}\nu_0 V$). The propagation of phonons in the \hat{x}_i direction is described by (Berne and Pecora 2000):

$$\rho \frac{\partial^2 u_i}{\partial t^2} = c_{ijkl} \frac{\partial}{\partial x_j} \left(\frac{\partial u_l}{\partial x_k} \right) \quad (2)$$

where ρ is the mass density and c_{ijkl} is the *stiffness tensor*. It follows that the components of the latter can be calculated from the measured acoustic velocity (Eq. 1) via (Berne and Pecora 2000):

$$\left| (\hat{x}_k \cdot \hat{q})(\hat{x}_l \cdot \hat{q})c_{ijkl} - \rho V_{\hat{q}}^2 \right| = 0 \quad (3)$$

For the case of an isotropic material in the back-scattering geometry one would probe the first three diagonal components ($c_{1111} = c_{2222} = c_{3333}$), such that the position of the BLS peaks directly yield the longitudinal storage modulus M' :

$$M' = \rho V^2 \quad (4)$$

The corresponding loss modulus (M'') can be obtained from the lifetime of the phonons—which is manifested in the homogeneous broadening of the BLS peak Γ_B —via (Carroll and Patterson 1984; Floudas et al. 1991)

$$M'' = \rho V^2 \frac{\Gamma_B}{\nu_B} \quad (5)$$

The case of anisotropic samples—as is the case with the studied fibers—is more subtle, given the distinct elastic moduli in different directions. For the studied fibers we may assume a transverse anisotropic symmetry such that measurements will yield a linear combination of the modulus parallel and perpendicular to the fiber axis (M_{\parallel} and M_{\perp} , respectively). The respective contribution of these can be calculated from

Eqs. 1 and 3 by considering the projection of the scattering wavevector on the stiffness tensor.

Finite numerical aperture

In order to achieve a high lateral spatial resolution, one needs to probe with a correspondingly large numerical aperture (NA). Finite NA measurements will in the studied case result in two modifications to the measured spectrum. Firstly, one would observe an inherent effective broadening and slight shift in the peak position of the BLS signal resulting from the frequency dependence of the scattering wavevector (Eq. 1) (Antonacci et al. 2013). This can readily be calculated by integrating Eq. 1 over the probed solid angles. Secondly, one may observe an effective broadening due to the anisotropy of the sample, namely that the phonon speed is dependent on direction. To illustrate the latter for the samples studied here, let us assume the fibers are orientated in the \hat{x}_1 direction and we probe along the perpendicular \hat{x}_3 -axis, such that $c_{1111}(=M_{\parallel}) \neq c_{2222} = c_{3333}(=M_{\perp})$. By increasing the effective probing NA from ≈ 0 one will thus transition from probing exclusively M_{\perp} to probing a linear combination of M_{\perp} and M_{\parallel} . Given that $M_{\parallel} \neq M_{\perp}$ this will result in an effective broadening with increasing NA and a shift in the measured v_B to lower (higher) frequencies if $M_{\parallel} < M_{\perp}$ ($M_{\parallel} > M_{\perp}$). The exact dependence can again be obtained by integrating Eq. 1 over the probed solid angles, this time taking these symmetry conditions into account and noting that there will also likely be an associated anisotropy in the refractive index (i.e. $n_{\parallel} \neq n_{\perp}$). Since we do not have access to the latter, in this study we calculate an *effective* elastic modulus (\bar{M}). This is obtained by calculating a single effective acoustic velocity ($V_{\hat{q}} = V$) from Eq. 1 assuming the back-scattering geometry and an effective refractive index ($\mathbf{n} \cdot \hat{q} = n$), and subsequently calculating the complex modulus from Eqs. 4 and 5. Prior to fitting the BLS spectra to obtain v_B and Γ_B the results are deconvolved with the elastic scattering peak and corrected for broadening exclusively due to the finite NA as described below. The effective refractive index (1.3–1.4) was taken from holographic phase microscopy measurements (see below) on the same samples, and a density of 1500 kg/m^3 was assumed throughout.

Measurements on the same samples using a very small NA (< 0.01) were used to estimate the contribution of M_{\perp} to the total high-NA measured Modulus, since the former can be assumed to exclusively probe in the direction transverse to the fiber axis. The ratio of the elastic modulus along the fiber axis to that perpendicular to the fiber axis was also estimated via:

$$\frac{M'_{\perp}}{M'_{\parallel}} = \left[1 + 2n \left[\left(\frac{v_B}{v_B^{\perp}} \right)^2 - 1 \right] \right]^{-1} \quad (6)$$

where v_B is measured BLS-shift with NA = 1, and v_B^{\perp} is that measured for NA < 0.01 .

An effective loss tangent is also calculated from the measured effective storage and loss moduli as $\tan(\delta) = \bar{M}''/\bar{M}'$ for each of the measured samples.

BLS setup

The employed setup consists of a self-built confocal sample scanning Brillouin microscope as described in e.g. Elsayad et al. (2016). In particular this consisted of an inverted microscope frame (iX73 by Olympus, Japan) with the laser and spectrometer coupled to the lower right port. Samples were mounted on standard microscopy slides and imaged through standard $170 \mu\text{m}$ glass coverslips. An objective (numerical aperture (NA) = 1.3, 60 \times , Si-immersion oil, Olympus, Japan) was employed for all BLSM measurements. The aperture of which was only partially filled yielded an effective NA ~ 1.0 . The measured (optical) lateral and axial resolution (corresponding to the probing volume) were 290 nm and $650\text{--}700 \text{ nm}$ as determined from the Full Width Half Maximum of the Point Spread Function. To assure optimum confocality the physical pinhole was fixed at $100 \mu\text{m}$, corresponding to just over one Airy unit with the employed tube lens. Excitation was performed via a solid state single-mode 532 nm laser (Torus by Quantum Laser, Germany), passed through an optical isolator, expanded, and coupled into the optical path via a 90:10 non-polarizing beam splitter. The sample was scanned using a long travel range 3-axis piezo stage (Physik Instrumente, Germany) and for each position one spectrum was acquired. Average laser power at the sample was kept low and measured to be below 3 mW . The dwell time per scanned point was fixed at 100 ms . After the pinhole the beam passed through a polarizer and 2 nm narrow band pass filter centered at 532 nm .

The Brillouin spectrometer consisted of a cross dispersion Virtual Imaged Phased Array (VIPA) spectrometer similar to the one described in Scarcelli et al. (2015) with the elastic scattering peaks blocked by masks at intermediate imaging planes. The employed VIPAs (Light Machinery, Canada) each had a free spectral range of 30 GHz. Also employed were self-fabricated gradient apodization filters prior to each VIPA. The resulting spectral projection was subsequently Fourier filtered using a Lyot stop (Edrei et al. 2017) and magnified. Finally, the Brillouin spectra consisting of only the Brillouin peaks, was imaged on a cooled EM-CCD camera (ImageEM II, Hamamatsu, Japan) which was read out for each scan point. Measurements on distilled water and spectroscopic grade ethanol before and after each scan were used for scaling the dispersion axis of the spectral projection. All spectra were fitted with Lorentzian functions with a quadratic background correction term, using a standard least-squares fitting algorithm in Matlab as described in Elsayad et al. (2016).

To account for the instrumental spectral response as well as the contribution from multiple-scattering in the sample, the spectra was deconvolved with a measurement of the elastic Rayleigh scattering peak measured in each respective sample. This was performed by optically attenuating the laser and opening the slits of the spatial masks in the spectrometer. Since our laser line has a line-width (kHz–MHz) that is orders of magnitude smaller than the spectral resolution, a straight forward deconvolution can be assumed to accurately capture the spectral response of our setup. This however will not account for the spectral broadening induced by the finite NA (see below).

To account for this, measurements were performed at different effective NAs by placing a ring-actuated iris diaphragm (Thorlabs, Germany) immediately behind the objective lens. By closing the iris (which could be done with an accuracy of several hundred microns) we could tune the effective NA from < 0.01 up to the maximum of the objective lens. We note that this would equally affect the probing and detection NA. The effective NA (NA_{eff}) was calculated from the radius (R) of the iris aperture via: $NA_{\text{eff}} = nR(w^2 + R^2)^{-1/2}$, where w is the working distance of the objective lens. The results on distilled water showed an increase in the line width by a factor of $1.9(\pm 0.1)$ from $NA \sim 0$ to $NA = 1.0$, with a small

shift in the peak position to lower frequencies of 310 MHz ($\sim 4\%$).

The effect of changing the effective NA from ~ 0 to 1.0 was also measured on each of the samples using the same approach. To determine the contribution from the anisotropy to the observed broadening, the measured frequency shift and line width at each NA was corrected in the sample measurements by a multiplicative factor corresponding to the effective modification in the peak position and linewidth (see above) measured in distilled water for the same corresponding NA relative to the low-NA limit.

BLS measurement time

The total time consumed by the sample preparation and the BLSM measurements amounted to approx. 3–4 h. During this time calibration measurements were performed and multiple areas of approx. $100 \times 100 \mu\text{m}$ were measured, each of which were divided into 21×5 measurement spots.

Testing conditions

It is important to note that BLSM measurements are very sensitive to the level of hydration (Wu et al. 2018) as well as temperature. Also, cellulose fiber mechanical properties are strongly affected by relative humidity under ambient conditions (Jajcinovic et al. 2018). Special care was thus taken that these were kept at the same level (25 °C, 30–50% RH) for all measured samples.

Holographic phase microscopy

Refractive index tomograms were acquired on a commercial holographic phase microscope with rotating scanner (3D Cell Explorer, Nanolive SA, Lausanne, Switzerland) with a Nikon BE Plan 60 \times NA 0.8 objective lens. The size of acquired tomogram was $93.1 \times 93.1 \times 35.7 \mu\text{m}$ (XYZ). Water was used as the reference refractive index (1.330) in all measurements. The software “Steve 1.6.3496” (Nanolive SA) was used for image acquisition and reconstruction, and maximum intensity projections were plotted using FIJI/ImageJ.

AFM nanoindentation

All AFM measurements were performed with an Asylum Research MFP-3D AFM. The instrument is equipped with a closed-loop planar x–y-scanner with a scanning range of $85 \times 85 \mu\text{m}^2$ and a z-range of about $15 \mu\text{m}$. For the experiments, four-sided pyramidal, full diamond probes (ND-DYIRS, Advanced Diamond Technology) with a tip apex radius of about 50 nm have been used. The spring constant of the cantilever was about 60 N/m and calibration of the cantilever was performed according to Hutter and Bechhoefer (1993). In AFM-NI, the sample surface is plastically deformed and according to the Oliver–Pharr method (Oliver and Pharr 1992) the reduced modulus E_r and the hardness H can be obtained. The method has been successfully established for pulp and viscose fibers before and is thoroughly described in Ganser et al. (2013) and Ganser and Teichert (2017).

Results and discussion

Figure 1 shows spatial maps of the measured BLS frequency shift ν_B of the viscose and bleached softwood Kraft fibers and the calculated effective transversal storage modulus (\bar{M}) and widefield transmitted light pictures of each fiber. While the pulp fibers seem to have a quite uniform elastic modulus the viscose fibers exhibit a regular longitudinal stripe pattern. Along the fiber axis there are elongated regions with lower (low region, 4.2 GPa) and higher (high region, 5.4 GPa) effective transversal moduli.

Figure 2 shows the effect of increasing the effective numerical aperture ($\text{NA} = 0.01\text{--}1$) for the viscose (high region and low region separately) and bleached softwood Kraft fibers. The plotted storage and loss modulus have in each case been corrected for the effect of finite NA excitation/detection by a linear coefficient determined from measuring distilled water with the corresponding NA (see above). As such the observed changes with NA can be attributed to the anisotropy of the sample. In all cases one sees an increase in both the loss modulus (line width) and the storage modulus (frequency shift) with increasing NA. The latter suggests that the component of the storage modulus along the fiber axis is larger than that perpendicular to the fiber axis. This corresponds to

the anisotropic nature of both, viscose (strong orientation of cellulose due to stretching during the spinning process) and wood fibers (strong orientation of fibrils in S2 wall). The loss modulus as well as the loss tangent also show an increasing trend with increasing NA, however the errors on the measurements are quite high.

As the BLS frequency shift scales linearly with the refractive index (Eq. 1) we used holographic phase microscopy to investigate whether there are any significant differences in n (between and within samples) which could account for any observed variations in the frequency shift. Maximum intensity projections of the reconstructed refractive index holograms are shown for two different representative sample types in Fig. 3. The local variation of the refractive index is in each case rather low and therefore cannot in itself explain the differences in the calculated longitudinal modulus (see above). Interestingly similar longitudinal patterns in the viscose fiber can be observed for the refractive index maps (Fig. 3a) as for the storage modulus (Fig. 2c, e), which might be the result of the drawing of the filaments during the spinning process.

Table 1 summarizes the results for the refractive index n , BLS frequency shift ν_B , the measured effective longitudinal storage and loss moduli (\bar{M}' and \bar{M}'') and the loss tangent for the two fiber types. Also shown is the derived ratio of the storage modulus perpendicular and along the fiber axis ($M'_{\perp}/M'_{\parallel}$), calculated from the point measurements at different NA's (see above). We note that for this calculation an isotropic refractive index is assumed for each of the sample regions (as referenced in table), which is likely not the case. The calculations for all NA's can be found in the ESI.

As also evident from the spatial maps (Fig. 1) the low region of the viscose fibers and the softwood pulp have comparable values for \bar{M}' while the (longitudinal) “stripes” in the viscose fiber (high region) have a significantly larger \bar{M}' . We suspect the differences may be related to either a local densification of the material or a local hardening of the structure.

Table 1 also shows reference data for the reduced modulus in the transverse fiber direction obtained from AFM-NI of viscose and bleached softwood pulp fibers. In comparison the measurements from AFM-NI are higher for the viscose and lower for softwood pulp.

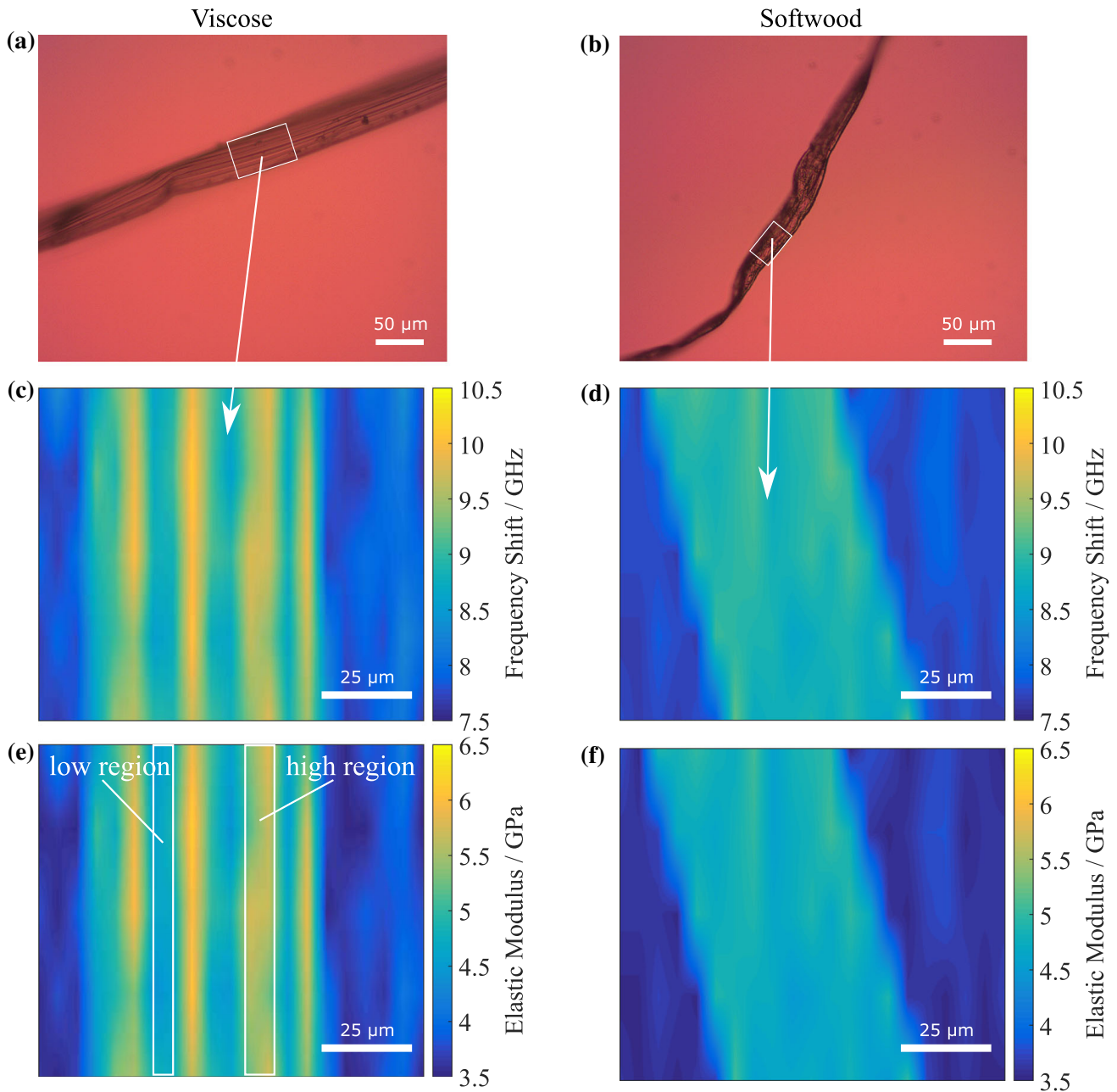
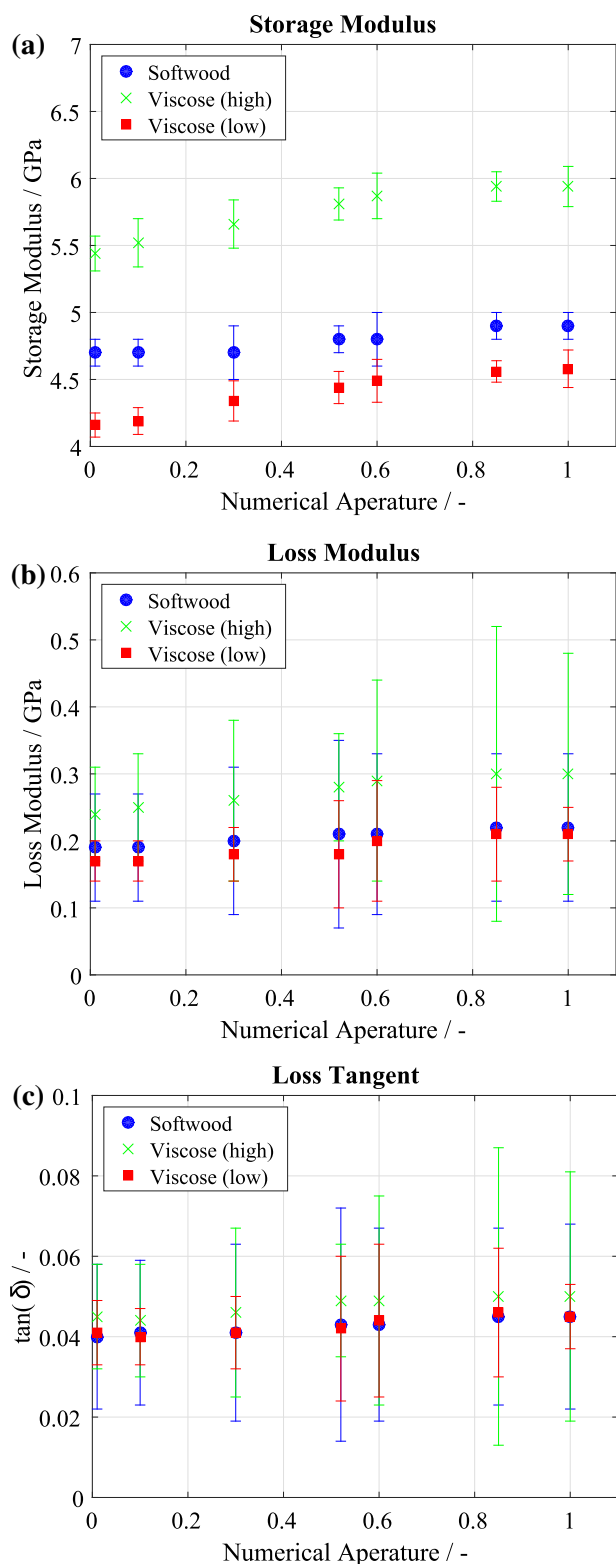


Fig. 1 **a, b** Transmitted light widefield microscopy images of the viscose and bleached softwood Kraft fibers respectively. **c, d** confocal spatial maps of the BLS-frequency shift. **e, f** the calculated effective transversal storage modulus (see main text)

While these show a similar trend to the average effective longitudinal storage moduli measured with BLS, the percentage difference is significantly larger between the two types of fiber. It is often the case when attempting to perform correlative AFM and BLS studies that relatively large changes in the AFM measured (Young's) moduli will correspond to only subtle changes in the BLS-measured (longitudinal)

from **a, b**. *Note* The widefield pictures in **a, b** were taken through a different microscope port and with a different magnification, and are thus not spatially aligned with the confocal BLS-maps in **c–f**

moduli—in many cases scaling in a roughly semi-logarithmic fashion (e.g. Scarcelli et al. 2015). It should be noted though that currently such relations are empirical and lacking theoretical foundation, given the different boundary conditions of the measured moduli and the vastly different frequency regimes probed (quasi-static vs. GHz) which will be sensitive to distinct mechanical relaxation processes.



It is also understood that under high hydration levels (> 90%) the solvent can dominate the contribution to the modulus measured with BLS and such an apparent correlation breaks down (Wu et al. 2018).

◀ **Fig. 2** Measurements of the properties over a changing NA. The storage modulus **a** shows a consistent trend to higher moduli at higher NA. These results show that, as expected, the storage modulus along the fiber axis is higher than perpendicular to it. The loss modulus **(b)** and the loss tangent **(c)** also appear to show a similar trend but the associated uncertainties are too large to draw any definitive conclusions

In the context of the current study it is also necessary to emphasize that the references were not measured on the same fibers. The counterintuitive result that the quasi-static AFM measurements yield an effectively lower modulus may possibly be due to the effective length scales probed with BLS. Since the probed phonons have a wavelength of approximately 100–200 nm with decay lengths on the order of 1 μm , they probe an effective collective response. Aside from more detailed knowledge of molecular level interactions, interpretation of the BLS spectra would for the case of heterogeneous media also require (ultra-)structural considerations on these scales especially for the viscous fibers.

The loss tangent ($\tan(\delta)$) relates the storage and the loss modulus and is a measure of how well energy is dissipated in the material. A $\tan(\delta) = 0$ would mean that the material is fully elastic while a number > 1 means that more energy is dissipated than stored. Importantly in the case of BLS measurements the loss tangent will be independent of the density and refractive index (which cancel out—Eqs. 4 and 5) which means that a change in loss modulus indicates a “true” change in the moduli of the structure. Within experimental uncertainties the loss tangent was similar between the two fiber types, with the values being in the same range than quasi-static measurements (Zhou et al. 2001; Csóka et al. 2012).

Given the frequency of the probed phonons in BLS, the most relevant mechanical relaxation times probed will be on the scale of picoseconds. It is possible to extract effective mechanical relaxation times (τ) from BLS measurements by driving the sample across a thermodynamic phase transition (at which $v_B \tau \sim 1$), e.g. Carroll and Patterson (1984). It is however in general challenging to obtain the relaxation times from the BLS measurements, as they will also depend to a large degree on the distribution (model) of relaxation times (Floudas et al. 1991). A detailed investigation of this would also benefit from complementary lower

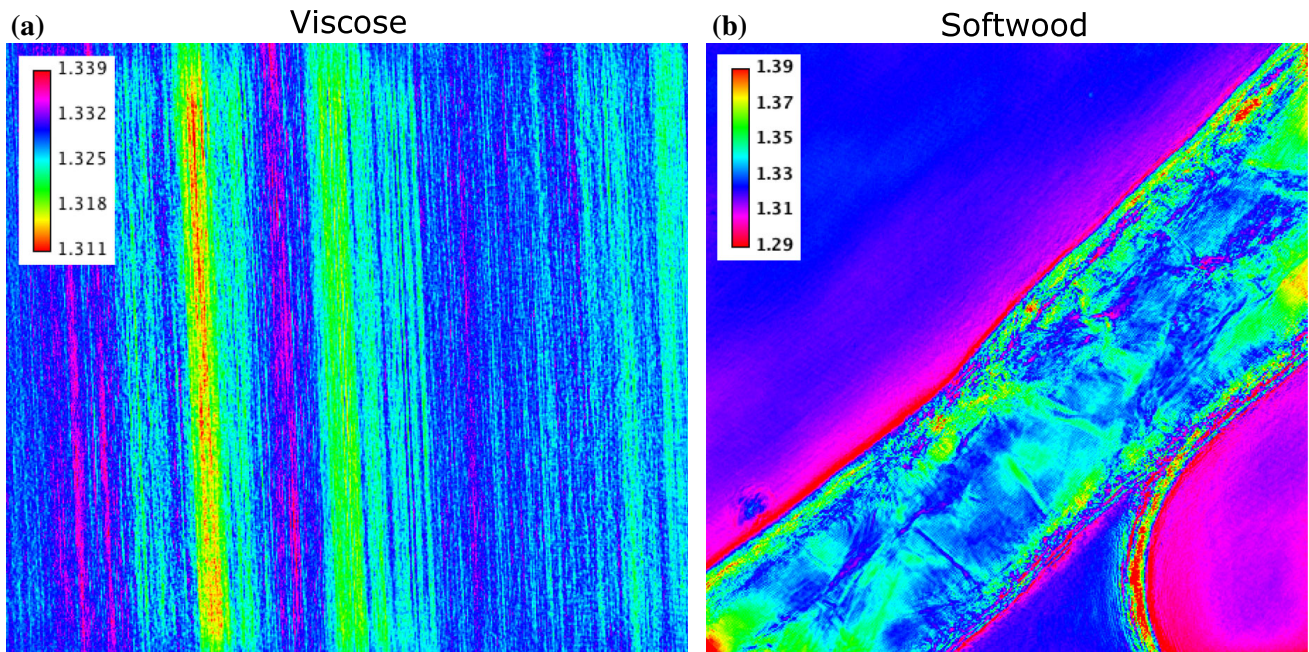


Fig. 3 Refractive index n of the Viscose (a) and bleached softwood Kraft (b) fibers (colorbar = n), suggesting only relatively small variations between and within the samples

frequency broader-bandwidth techniques (such as photon correlation spectroscopy), which is beyond the scope of the current study.

Conclusions

We have demonstrated spatial mapping of the high-frequency effective transversal storage and loss modulus for viscose and softwood pulp fibers using a VIPA based Brillouin Microscope. Reference measurements with AFM-NI revealed a similar trend—namely a larger elastic modulus for viscous than softwood pulp fibers, although a direct comparison between the two moduli is at this point unjustified given the different mechanical relaxation processes probed.

Our results suggest that Brillouin microscopy can serve as a fast and reliable technique to investigate the high-frequency mechanical properties of cellulosic fibers. One demonstrated advantage is the ability to map the properties in different directions (longitudinal and transverse to the fiber axis). In addition it has the ability to rapidly and all-optically map properties over larger areas using a VIPA based spectrometer such as was employed here. In this regard we see much potential for BLS microscopy for understanding and testing the mechanical properties of cellulose fibers as

it is also less cumbersome and a lot faster than direct mechanical testing. Extensions of the technique to e.g. consecutively probing at different angles (scattering wavevectors) can also be used to investigate the full elastic (stiffness) tensor of the fiber material, i.e. tension stiffness and shear stiffness in all three spatial directions, as has been demonstrated for other natural fiber materials (Koski et al. 2013; Edginton et al. 2016). It is however important to note that the measured properties with BLS are by construction different than those probed with most other mechanical testing techniques. This will be due to the high-frequency regime probed (where coupling of constituents/solutes to liquids will be much stronger and the latter will have a high modulus) and the different boundary conditions associated with deriving the elastic modulus from the speed of acoustic phonons. While there is ongoing active research in the direction of both empirically and theoretically relating the BLS measured moduli to more familiar structural and physical parameters and shedding light on their relevance in assessing otherwise relevant chemical/physical properties, the current study demonstrates the practical feasibility and potential of Brillouin microscopy for studying the anisotropic mechanical properties of cellulosic fibers.

Table 1 Data obtained from the measurements presented in Figs. 1 and 2

Sample	Refractive index: n	Frequency shift ν_B (GHz)	Measured effective storage modulus: \bar{M}' (GPa)	Measured effective loss modulus: \bar{M}'' (GPa)	Tan(δ)	Estimated ratio of storage modulus transverse to fiber axes and storage modulus along fiber axis: $M'_{\perp}/M'_{\parallel}$	Reduced modulus (GPa)
Viscose (region high)	1.31	9.4 ± 0.1	5.4 ± 0.13	0.24 ± 0.07	0.045 ± 0.013	0.81 ± 0.16	5.6–7.3 ^a (50–30) %RH
Viscose (region low)	1.34	8.40 ± 0.1	4.2 ± 0.1	0.17 ± 0.03	0.041 ± 0.008	0.79 ± 0.04	
Bleached softwood Kraft	1.34 ± 0.02	8.7 ± 0.1	4.5 ± 0.1	0.18 ± 0.08	0.040 ± 0.018	0.88 ± 0.17	1.3 ± 0.7 (50) %RH N = 3

Values were calculated as described in the main text

^aData from Ganser (2014)

Acknowledgments Open access funding provided by Graz University of Technology. The financial support by the Austrian Federal Ministry for Digital and Economic Affairs and the National Foundation for Research Technology and Development is gratefully acknowledged. Furthermore, the authors want to thank Canon Production Printing, Mondi, Kelheim Fibres and SIG Combibloc for their financial support. The authors thank Lisa-Marie Weniger for assistance with the AFM-NI measurements. KE acknowledges support from the Austrian Ministry of Science and the City of Vienna (Vision 2020). Georg Urstöger and Kareem Elsayad contributed equally to the publication and share first authorship.

Open Access This article is licensed under a Creative Commons Attribution 4.0 International License, which permits use, sharing, adaptation, distribution and reproduction in any medium or format, as long as you give appropriate credit to the original author(s) and the source, provide a link to the Creative Commons licence, and indicate if changes were made. The images or other third party material in this article are included in the article's Creative Commons licence, unless indicated otherwise in a credit line to the material. If material is not included in the article's Creative Commons licence and your intended use is not permitted by statutory regulation or exceeds the permitted use, you will need to obtain permission directly from the copyright holder. To view a copy of this licence, visit <http://creativecommons.org/licenses/by/4.0/>.

Funding Funding was provided by Christian Doppler Forschungsgesellschaft (Grant: CD Laboratory for Fiber Swelling and Paper Performance).

References

- Antonacci G, Foreman MR, Paterson C, Török P (2013) Spectral broadening in Brillouin imaging. *Appl Phys Lett* 103:221105. <https://doi.org/10.1063/1.4836477>
- Bardet S, Gril J (2002) Modelling the transverse viscoelasticity of green wood using a combination of two parabolic elements. *Comptes Rendus Mécanique* 330:549–556. [https://doi.org/10.1016/S1631-0721\(02\)01503-6](https://doi.org/10.1016/S1631-0721(02)01503-6)
- Bergander A, Salmen L (2000) The transverse elastic modulus of the native wood fibre wall. *J Pulp Pap Sci* 26:234
- Berne BJ, Pecora R (2000) *Dynamic light scattering: with applications to chemistry, biology, and physics*. Courier Corporation, North Chelmsford
- Berovic N, Thomas N, Thornhill RA, Vaughan JM (1989) Observation of Brillouin scattering from single muscle fibres. *Eur Biophys J* 17:69–74. <https://doi.org/10.1007/BF00257104>
- Burgert I, Frühmann K, Keckes J et al (2005) Microtensile testing of wood fibers combined with video extensometry for efficient strain detection. *Holzforschung* 57:661–664. <https://doi.org/10.1515/HF.2003.099>
- Carroll PJ, Patterson GD (1984) Rayleigh–Brillouin spectroscopy of simple viscoelastic liquids. *J Chem Phys* 81:1666–1675. <https://doi.org/10.1063/1.447892>

- Cisse O, Placet V, Guicheret-Retel V et al (2015) Creep behaviour of single hemp fibres. Part I: viscoelastic properties and their scattering under constant climate. *J Mater Sci* 50:1996–2006. <https://doi.org/10.1007/s10853-014-8767-1>
- Csóka L, Božanić DK, Nagy V et al (2012) Viscoelastic properties and antimicrobial activity of cellulose fiber sheets impregnated with Ag nanoparticles. *Carbohydr Polym* 90:1139–1146. <https://doi.org/10.1016/j.carbpol.2012.06.065>
- Cusack S, Miller A (1979) Determination of the elastic constants of collagen by Brillouin light scattering. *J Mol Biol* 135:39–51. [https://doi.org/10.1016/0022-2836\(79\)90339-5](https://doi.org/10.1016/0022-2836(79)90339-5)
- Czibula C, Ganser C, Seidlhofer T et al (2019) Transverse viscoelastic properties of pulp fibers investigated with an atomic force microscopy method. *J Mater Sci* 54:11448. <https://doi.org/10.1007/s10853-019-03707-1>
- Dunford J, Wild P (2002) Cyclic transverse compression of single wood-pulp fibres. *J Pulp Pap Sci* 28:136–141
- Edginton RS, Mattana S, Caponi S et al (2016) Preparation of extracellular matrix protein fibers for Brillouin spectroscopy. *J Vis Exp*. <https://doi.org/10.3791/54648>
- Edrei E, Gather MC, Scarcelli G (2017) Integration of spectral coronagraphy within VIPA-based spectrometers for high extinction Brillouin imaging. *Opt Express* 25:6895–6903. <https://doi.org/10.1364/OE.25.006895>
- Elsayad K, Werner S, Gallemí M et al (2016) Mapping the subcellular mechanical properties of live cells in tissues with fluorescence emission–Brillouin imaging. *Sci Signal* 9:rs5. <https://doi.org/10.1126/scisignal.aaf6326>
- Fischer WJ (2013) A novel direct method for mechanical testing of individual fibers and fiber to fiber joints. Technische Universität Graz, Graz
- Fischer WJ, Hirn U, Bauer W, Schennach R (2012) Testing of individual fiber–fiber joints under biaxial load and simultaneous analysis of deformation. *Nord Pulp Pap Res J* 27:237–244. <https://doi.org/10.3183/npprj-2012-27-02-p237-244>
- Floudas G, Fytas G, Alig I (1991) Brillouin scattering from bulk polybutadiene: distribution of relaxation times versus single relaxation time approach. *Polymer* 32:2307–2311. [https://doi.org/10.1016/0032-3861\(91\)90065-Q](https://doi.org/10.1016/0032-3861(91)90065-Q)
- Ganser C (2014) Influence of water on mechanical properties of cellulosic materials studied by AFM based methods. University of Leoben, Leoben
- Ganser C, Teichert C (2017) AFM-based Nanoindentation of cellulosic fibers. In: Tiwari A, Natarajan S (eds) *Applied nanoindentation in advanced materials*. Wiley, New York, pp 247–267
- Ganser C, Hirn U, Rohm S et al (2013) AFM nanoindentation of pulp fibers and thin cellulose films at varying relative humidity. *Holzforschung* 68:53–60. <https://doi.org/10.1515/hf-2013-0014>
- Ganser C, Czibula C, Tscharnuter D et al (2018) Combining adhesive contact mechanics with a viscoelastic material model to probe local material properties by AFM. *Soft Matter* 14:140–150. <https://doi.org/10.1039/C7SM02057K>
- Harley R, James D, Miller A, White JW (1977) Phonons and the elastic moduli of collagen and muscle. *Nature* 267:285–287. <https://doi.org/10.1038/267285a0>
- Hartler N, Nyren J (1970) Transverse compressibility of pulp fibers. 2. Influence of cooking method, yield, beating, and drying. *Tappi* 53:820
- Hutter JL, Bechhoefer J (1993) Calibration of atomic-force microscope tips. *Rev Sci Instrum* 64:1868–1873. <https://doi.org/10.1063/1.1143970>
- Jajcinovic M (2017) Strength of individual fibres and fibre to fibre joints—influence of the pulp type, environmental conditions and the degree of refining. Technische Universität Graz, Graz
- Jajcinovic M, Fischer WJ, Mautner A et al (2018) Influence of relative humidity on the strength of hardwood and softwood pulp fibres and fibre to fibre joints. *Cellulose* 25:2681–2690. <https://doi.org/10.1007/s10570-018-1720-8>
- Kompella MK, Lambros J (2002) Micromechanical characterization of cellulose fibers. *Polym Test* 21:523–530. [https://doi.org/10.1016/S0142-9418\(01\)00119-2](https://doi.org/10.1016/S0142-9418(01)00119-2)
- Koski KJ, Akhenblit P, McKiernan K, Yarger JL (2013) Non-invasive determination of the complete elastic moduli of spider silks. *Nat Mater* 12:262–267. <https://doi.org/10.1038/nmat3549>
- Magnusson MS, Östlund S (2013) Numerical evaluation of interfibre joint strength measurements in terms of three-dimensional resultant forces and moments. *Cellulose* 20:1691–1710. <https://doi.org/10.1007/s10570-013-9939-x>
- Nilsson B, Wågberg L, Gray D (2000) Conformability of wet pulp fibres at small length scales. FSCN, Mitthögskolan, Sundsvall
- Oliver WC, Pharr GM (1992) An improved technique for determining hardness and elastic modulus using load and displacement sensing indentation experiments. *J Mater Res* 7:1564–1583. <https://doi.org/10.1557/JMR.1992.1564>
- Penneru AP, Jayaraman K, Bhattacharyya D (2006) Viscoelastic behaviour of solid wood under compressive loading. *Holzforschung* 60:294–298. <https://doi.org/10.1515/HF.2006.047>
- Pettersson T, Hellwig J, Gustafsson P-J, Stenström S (2017) Measurement of the flexibility of wet cellulose fibres using atomic force microscopy. *Cellulose* 24:4139–4149. <https://doi.org/10.1007/s10570-017-1407-6>
- Randall JT, Vaughan JM, Buckingham AD et al (1979) Brillouin scattering in systems of biological significance. *Philos Trans R Soc Lond Ser A Math Phys Sci* 293:341–348. <https://doi.org/10.1098/rsta.1979.0101>
- Sandercock JR (1970) Brillouin scattering study of SbSI using a double-passed, stabilised scanning interferometer. *Opt Commun* 2:73–76. [https://doi.org/10.1016/0030-4018\(70\)90047-7](https://doi.org/10.1016/0030-4018(70)90047-7)
- Scarcelli G, Polacheck WJ, Nia HT et al (2015) Noncontact three-dimensional mapping of intracellular hydro-mechanical properties by Brillouin microscopy. *Nat Methods* 12:1132–1134. <https://doi.org/10.1038/nmeth.3616>
- Speziale S, Jiang F, Caylor CL et al (2003) Sound velocity and elasticity of tetragonal lysozyme crystals by Brillouin spectroscopy. *Biophys J* 85:3202–3213. [https://doi.org/10.1016/S0006-3495\(03\)74738-9](https://doi.org/10.1016/S0006-3495(03)74738-9)
- Stanzl-Tschegg SE, Navi P (2008) Fracture behaviour of wood and its composites. A review COST action E35 2004–2008: wood machining—micromechanics and

- fracture. *Holzforschung* 63:139–149. <https://doi.org/10.1515/HF.2009.012>
- Wild P, Omholt I, Steinke D, Schuetze A (2005) Experimental characterization of the behaviour of wet single wood-pulp fibres under transverse compression. *J Pulp Pap Sci* 31:116–120
- Williams DR, Nurco DJ, Rahbar N, Koski KJ (2019) Elasticity of bamboo fiber variants from Brillouin spectroscopy. *Materialia* 5:100240. <https://doi.org/10.1016/j.mtla.2019.100240>
- Wu P-J, Kabakova IV, Ruberti JW et al (2018) Water content, not stiffness, dominates Brillouin spectroscopy measurements in hydrated materials. *Nat Methods* 15:561–562. <https://doi.org/10.1038/s41592-018-0076-1>
- Zhou Tashiro K, Hongo T et al (2001) Influence of water on structure and mechanical properties of regenerated cellulose studied by an organized combination of infrared spectra, X-ray diffraction, and dynamic viscoelastic data measured as functions of temperature and humidity. *Macromolecules* 34:1274–1280. <https://doi.org/10.1021/ma001507x>

Publisher's Note Springer Nature remains neutral with regard to jurisdictional claims in published maps and institutional affiliations.

Appendix

Appendix A.

Matlab Code for Image Analysis

A.1. Script for Figure Import

```
clear all
close all
clc

% Choose and load input images for FRET
disp('Choose Donor Image')
[d,path_donor] = uigetfile('C:\*.*','Choose donor image');
disp('Choose Acceptor Image')
[a,path_acceptor] = uigetfile('C:\*.*','Choose acceptor image');
disp('Choose FRET Image')
[f,path_fret] = uigetfile('C:\*.*','Choose Fret image');

% Choose a clear image for processing
[p,path_p] = uigetfile('C:\*.*',...
'Choose a clear image jpeg');

filename2 = inputdlg('Enter filename',...
'Specify filename to save data', [1 60]);
filename = cell2mat(filename2);

global filename
```

Appendix A. Matlab Code for Image Analysis

```
donor = imread([path_donor,d]);
acceptor = imread([path_acceptor,a]);
fret = imread([path_fret,f]);
```

A.2. Function drawroi

```
function [varargout] = drawroi(numberofROIs,fretimage,...
saveimage)

% With this function it is possible to analyse as many
% regions of interest as specified by the input parameters.

% Input Parameters:
% - numberOfROIs: positive integer that specifies how
%   many ROIs one wants to investigate in the image.
% - fretimage: Image of the fretintensity or a different
%   image in which the image under investigation is
%   clearly visible
% - saveas: Logical variable. If 1 then the images are
%   saved as a figure

% Output Parameters:
% - varargout: Logical matrices the size of fretimage
%   that contain the individual ROIs.

% Example: [I1,I2,I3] = drawroi(3,FRETN_gordon,15,1)
%   I am interested in comparing and investigating 3
%   ROI of the image FRETN_gordon. It will be figure 15
%   and I want to save the image.

global filename

ROIfigure = figure();
```


Appendix A. Matlab Code for Image Analysis

```
imagesc(fretimage)

for i = 1:numberofROIs
    uiwait(msgbox('Define area'));
    area_f = impoly(gca);
    api_f = iptgetapi(area_f);
    position_f = api_f.getPosition();

    %Create a matrix with which has ones at the coordinates of
    %the polygon
    y = 1:1:length(fretimage(:,1,1));
    figurenumber = 1:1:length(fretimage(1,:,1));
    xvalues = repmat(figurenumber,length(fretimage(:,1,1)),1);
    yvalues = repmat(y',1,length(fretimage(1,:,1)));

    varargout{i} = inpolygon(xvalues,yvalues,position_f(:,1),...
    position_f(:,2));
end

if saveimage
    saveas(ROIfigure,[filename,'_ROIs.png'])
    saveas(ROIfigure,[filename,'_ROIs.epsc'])
end
end
```

A.3. Function drawpolygons

```
function [I_d,I_a,I_f] = drawpolygons(donorimage,...
acceptorimage,fretimage,x)

% This function lets you draw three polygons into the donor,
% acceptor and FRET images and returns three logical matrices
% with the size of the image and ones at the indexes where
```

Appendix A. Matlab Code for Image Analysis

```
% the polygons are.

% Display images and define the areas that need to be
% analysed. The polygons are defined only in one image
% because the areas should be the same in every picture.
% It doesn't matter in which image they are defined so
% I chose the donor.

%Get positions of the polygons

figure(x)
imagesc(donorimage);
uiwait(msgbox('Define area on donor fibre'));
area_d = impoly(gca);
api_d = iptgetapi(area_d);
position_d = api_d.getPosition();

figure(x)
imagesc(acceptorimage);
uiwait(msgbox('Define area on acceptor fibre'));
area_a = impoly(gca);
api_a = iptgetapi(area_a);
position_a = api_a.getPosition();

figure(x)
imagesc(fretimage);
uiwait(msgbox('Define area on bonded area'));
area_f = impoly(gca);
api_f = iptgetapi(area_f);
position_f = api_f.getPosition();

% Create a matrix with which has ones at the coordinates of
% the polygon
y = 1:1:length(acceptorimage(:,1,1));
x = 1:1:length(acceptorimage(1,:,1));
xvalues = repmat(x,length(acceptorimage(:,1,1)),1);
yvalues = repmat(y',1,length(acceptorimage(1,:,1)));
```

Appendix A. Matlab Code for Image Analysis

```
I_d = inpolygon(xvalues,yvalues,position_d(:,1),position_d(:,2));
I_a = inpolygon(xvalues,yvalues,position_a(:,1),position_a(:,2));
I_f = inpolygon(xvalues,yvalues,position_f(:,1),position_f(:,2));

end
```

A.4. FRET Evaluation Script

```
clc

%% Background subtraction and image corrections
global filename

picture = imread([path_p,p]);

uiwait(msgbox('Subtract Background from images'));

[I_b] = drawroi(1,fret,0);

donor = (donor - mean(donor(I_b)));
acceptor = acceptor - mean(acceptor(I_b));
fret = fret - mean(fret(I_b));

donor_grey = double(donor(:,:,1));
acceptor_grey = double(acceptor(:,:,1));
fret_grey = double(fret(:,:,1));

close(1)

%% Correction factors

donor_grey = donor_grey./0.4407./0.472;
```

Appendix A. Matlab Code for Image Analysis

```
acceptor_grey = acceptor_grey./0.9769./0.534;
fret_grey = fret_grey./0.4407./0.534;

%% Ratio control
donor_bt = fret_grey./donor_grey;
acceptor_bt = fret_grey./acceptor_grey;

donor_bt(donor_bt < 0 | donor_bt > 4) = 0;
acceptor_bt(acceptor_bt < 0 | acceptor_bt > 4) = 0;

figure()
imagesc(donor_bt)
title('Donor BT (FRET/Donor)')
colormap jet
colorbar
caxis([0,1])

figure()
imagesc(fret_grey)
title('Acceptor BT (FRET/Acceptor)')
colormap jet
colorbar
caxis([0,1])

uiwait(msgbox('Check the ratios and choose desired ratio
(best case uniform ratio over whole fiber')));

%% The logical matrices of drawpolygons are used to analyze
%% the images

figure()
[I_d,I_a,I_f] = drawpolygons(donor_grey,acceptor_grey,...
fret_grey,6);

Ddm = mean(donor_grey(I_d));
err_Ddm = std(donor_grey(I_d));
```

Appendix A. Matlab Code for Image Analysis

```
Fdm = mean(fret_grey(I_d));
err_Fdm = std(fret_grey(I_d));
Adm = mean(acceptor_grey(I_d));
err_Adm = std(acceptor_grey(I_d));

Dam = mean(donor_grey(I_a));
err_Dam = std(donor_grey(I_a));
Fam = mean(fret_grey(I_a));
err_Fam = std(fret_grey(I_a));
Aam = mean(acceptor_grey(I_a));
err_Aam = std(acceptor_grey(I_a));

close all

%% Equations to calculate normalized Fret signal from
%% Gordon et al. and Xia algorithm
G = 1.57;
cutoff = 1;

Af2 = imgaussfilt(acceptor_grey);
Df2 = imgaussfilt(donor_grey);
Ff2 = imgaussfilt(fret_grey);

figure(1)
imagesc(Ff2)

% optional
% numberofROIs = inputdlg('How many ROIs will be investigated?');
% numberofROIs = numberofROIs{1};
% numberofROIs = str2num(numberofROIs);

close(1)
numberofROIs = 1;

[I1] = drawroi(numberofROIs,Ff2,0);
```

Appendix A. Matlab Code for Image Analysis

```
SE = strel('square',40);
I_eroded = imerode(I1,SE);

F2 = figure()
imagesc(Ff2)
hold on
% imagesc(I1)
imagesc(I_eroded*10000,'AlphaData',0.5)
hold off
colormap jet

% saveas(F2,'Erosion_R0Iinfigure.png')
% saveas(F2,'Erosion_R0Iinfigure.eps')

I1 = I_eroded;

%% Xia algorithm

afa_numerator = Af2 - (Adm/Fdm).*Ff2;
afa_denominator = 1-(Fam/Aam)*(Adm/Fdm);

afa = afa_numerator./afa_denominator;

figure()
imagesc(afa)
title('afa')
colormap jet
colorbar
figure()
histogram(afa)
title('afa')

fret_numerator = Ff2 - (Fdm/Ddm).*Df2 - ...
afa.*((Fam/Aam) - (Fdm/Ddm)*(Dam/Aam));
fret_denominator = G*(1-(Dam/Fam)*(Fdm/Ddm));

fret1 = fret_numerator./fret_denominator;
```

Appendix A. Matlab Code for Image Analysis

```
figure()
imagesc(fret1)
title('fret1')
colormap jet
colorbar
figure()
histogram(fret1)
title('fret1')

fret1(fret1<0) = 0;
dfd = Df2 + fret1.*(1 - G*(Dam/Aam)) - afa.*(Dam/Aam);

figure()
imagesc(dfd)
title('normalization of Bond (dfd)')
colormap jet
colorbar
figure()
histogram(dfd)
title('histogram of normalization (dfd)')

afa(afa < 0) = 0;
dfd(dfd < 0) = 0;

normalization = sqrt(afa.*dfd);

figure()
imagesc(normalization)
title('normalization of Bond (afa.*dfd)')
colormap jet
colorbar
figure()
histogram(normalization)
title('histogram of normalization (afa.*dfd)')

% Depending on how many ROIs are investigated the following
```

Appendix A. Matlab Code for Image Analysis

```
% line can give an error. The cutoff can be used for manual
% adjustment. Per default it is defined above as 1.

normalization(normalization < min(normalization(I1))*cutoff)...
    = inf;

F2 = figure();
subplot(2,1,1)
imagesc(normalization)
title('FRETn normalization')
colormap jet
colorbar
subplot(2,1,2)
histogram(normalization)
title('FRETn normalization')

FRETn_xia = fret1./normalization;

figure()
imagesc(dfd)
title('normalization of Bond (dfd)')
colormap jet
colorbar
figure()
histogram(dfd)
title('histogram of normalization (dfd)')

dfd(dfd < min(dfd(I1))*cutoff) = inf;

F3 = figure();
subplot(2,1,1)
imagesc(dfd)
title('Fret efficiency normalization')
colormap jet
colorbar
subplot(2,1,2)
histogram(dfd)
```


Appendix A. Matlab Code for Image Analysis

```
title('Fret efficiency normalization')

Fret_efficiency_xia = (fret1./dfd).*100;

disp(['Gordon Adm/Fdm = ', num2str(Adm/Fdm)]);
disp(['Gordon Fdm/Ddm = ', num2str(Fdm/Ddm)]);
disp(['Gordon Fam/Aam = ', num2str(Fam/Aam)]);

%% Sensitized Emission Method
%Fret = Ff - A*Af - B*Df /// A = Fa/Aa, B = Fd/Dd

Af2(Af2<0) = 0;
Df2(Df2<0) = 0;

A = Fam/Aam;
err_A = sqrt((1/Aam*err_Fam)^2 + ((Fam/Aam^2)*err_Aam)^2);

B = Fdm/Ddm;
err_B = sqrt((1/Ddm*err_Fdm)^2 + ((Fdm/Ddm^2)*err_Ddm)^2);

disp(['Sensitized D = ', num2str(Fdm/Ddm), setstr(177), ...
num2str(err_A)]);
disp(['Sensitized A = ', num2str(Fam/Aam), setstr(177), ...
num2str(err_B)]);

FRETN_sensitized = (Ff2 - A.*Af2 - B.*Df2);

% figure()
% imagesc(FRETN_sensitized)
% title('Sen Emission')
% colormap jet
% colorbar
% figure()
% histogram(FRETN_sensitized)
% title('Sen Emission')

FRETN_sensitized(FRETN_sensitized<0)=0;
```

Appendix A. Matlab Code for Image Analysis

```
normalization_sensitized = sqrt(Af2.*Df2);

% figure()
% imagesc(normalization_sensitized)
% title('normalization of Bond (Af2.*Df2)')
% colormap jet
% colorbar
% figure()
% histogram(normalization_sensitized)
% title('histogram of normalization (Af2.*Df2)')

% Here the same as above applies.
normalization_sensitized(normalization_sensitized ...
< min(normalization_sensitized(I1)*cutoff)) = inf;

FRETN_sensitized_norm = FRETN_sensitized./...
normalization_sensitized;

quenched_donor = Df2;
unquenched_donor = quenched_donor + FRETN_sensitized*G;

% figure()
% imagesc(unquenched_donor)
% title('unquenched donor')
% colormap jet
% colorbar
% figure()
% histogram(unquenched_donor)
% title('unquenched donor')

%Numbers need to be adjusted
unquenched_donor(unquenched_donor < 8000) = inf;

Fretefficiency_sensitized = 100*(1-quenched_donor./...
unquenched_donor);
Fretefficiency_sensitized(Fretefficiency_sensitized...
```

Appendix A. Matlab Code for Image Analysis

```
==100) = 0;

%% Plotting

%Sensitized Emission
% F2 = figure('units','normalized','outerposition',[0 0 1 1]);
% subplot(2,1,1)
% imagesc(FRETN_sensitized_norm)
% title('Sensitized Emission Method','FontSize',12)
% colormap jet
% colorbar
% % if maximum > 0
%     caxis([0,0.1])
% % end
% subplot(2,1,2)
% imagesc(Fretefficiency_sensitized)
% title('FRET efficiency (Sensitized)','FontSize',12)
% colormap jet
% colorbar

% Xia Algorithm
F1 = figure('units','normalized','outerposition',[0 0 1 1]);
subplot(2,1,1)
imagesc(FRETN_xia)
title('FRETN Xia algorithm','FontSize',12)
colormap jet
colorbar
set(gca,'FontSize',20,'XTickLabel','','YTickLabel','')
% if maximum > 0
%     caxis([0,0.1])
% end
subplot(2,1,2)
imagesc(Fretefficiency_xia)
title('FRET efficiency (Xia algorithm)','FontSize',12)
colormap jet
colorbar
caxis([0,100])
```

Appendix A. Matlab Code for Image Analysis

```
title('Fretefficiency')
set(gca,'FontSize',20,'XTickLabel','','YTickLabel','')
% set(gca,'FontSize',20,'XTickLabel','','YTickLabel','')
% caxis([0,100])
% hold off

%% Saving of figures and workspace

S = struct('ROI',I1,'FRETN_Xia',{FRETN_xia},...
'Xia_efficiency (Donor_quenching)',...
    Fretefficiency_xia,'sensitized_emission',...
FRETN_sensitized_norm,...
    'fretefficiency_sensitized',...
Fretefficiency_sensitized,'A',A,'D',B);

save([filename,'.mat'],'S')

filename_Xia = strcat(filename,'_Xia');
print(F1,filename_Xia,'-depsc','-r300')
print(F1,filename_Xia,'-dpng')

print(F2,[filename_Xia,'_colocalization_FRETN'],'-depsc','-r300')
print(F2,[filename_Xia,'_colocalization_FRETN'],'-dpng')

print(F3,[filename_Xia,'_colocalization_Eff'],'-depsc','-r300')
print(F3,[filename_Xia,'_colocalization_Eff'],'-dpng')
```